KU LEUVEN

FACULTEIT BIO-INGENIEURSWETENSCHAPPEN

Thin Film Nanocomposite Membranes: control over the position of the filler

Dunne Film Nanocomposiet Membranen: controle over de positie van de vuller

Promotor:
Prof. Ivo Vankelecom
Departement Microbiële en Moleculaire Systemen
Centrum voor Oppervlaktechemie en Katalyse

Masterproef voorgedragen
tot het behalen van het diploma van
Master of science in de bio-ingenieurswetenschappen:
katalytische technologie

Rhea Verbeke

juni 2015

KU LEUVEN

FACULTEIT BIO-INGENIEURSWETENSCHAPPEN

Thin Film Nanocomposite Membranes: control over the position of the filler

Dunne Film Nanocomposiet Membranen: controle over de positie van de vuller

Promotor:
Prof. Ivo Vankelecom
Departement Microbiële en Moleculaire Systemen
Centrum voor Oppervlaktechemie en Katalyse

Masterproef voorgedragen
tot het behalen van het diploma van
Master of science in de bio-ingenieurswetenschappen:
katalytische technologie

Rhea Verbeke

juni 2015

Preface

Het leven zoals het is: het labo.

Ik heb veel bijgeleerd dit thesisjaar, op wetenschappelijk vlak, maar vooral ook op menselijk vlak. Ik zie een labo als een samenleving op zich, een maatschappij op kleine schaal. En zoals in elke samenleving heerst er tevredenheid en ontevredenheid, volgzaamheid en revolte, hoop en wanhoop, macht en onmacht, bezieling en onverschilligheid. Als ik er nog niet van overtuigd was, dan ben ik het nu alleszins wel: onverschilligheid doodt. Harde woorden voor een harde werkelijkheid, die onze huidige maatschappij, op eender welk niveau, pijnlijk goed markeren. Gelukkig zijn onbehagen en onvrede het begin van alle verandering!

Dank u wel Papa en Mama om me zo hard te steunen gedurende deze hobbelige reis. Jullie ruimdenkendheid en kritische blik brengen me meer bij dan eender welk wetenschappelijk boek ooit zal kunnen. Time to spread out my wings now.

“When mom and dad don’t understand, a sister always will.” Moet ik hier nog iets aan toevoegen? Ik denk van niet. Danku Zussiemonster om mijn anker te zijn waar ik me al te graag aan vastklamp.

Stijntje, ben ik blij dat de IR-machine op Chemie staat en dat je ondertussen bent gepromoveerd van kotbroer naar schoonbroer.

Laurent, mijn favoriet wandelend woordenboek, bedankt om onze vriendschap oneindig te maken.

Renate, until we die!

LBK-vriendjes, wat waren het vijf geweldige jaren. Free en Michiel, my little ones, bedankt om mijn gezaag, geklaag en gelach altijd aan te horen. Michiel, special thanks for all the compliments, they lightened up my day! Tim, Smollie & Giel, merci om mij immuun te maken voor steekjes en opmerkingen. Lotte & Cleo, membraan-buddies, bedankt voor de happy labo-moments!

Sanne & Hanne, dé interfaciale polymerisatie encyclopedieën, dank jullie wel voor alle hulp!. Veysi & Remi, my favourite internationals, I am so glad to have met you. Thank you very much for the elucidating and supporting talks. Take care! Maxim, in the end werkt uw positivisme toch aanstekelijk. Blijf vooral meezingen! Matthias & Annelies, het schattige membraankoppeltje, merci voor de lachwekkende gesprekken – it’s all in the small things!

Cédric, dank u wel voor alle hulp en steun die je mij geboden hebt dit jaar. Ondanks alle tegenslagen, ups and downs, was het fijn samenwerken met u! Bedankt om er steeds voor me te staan met een berg vol rust en begrip.

And last but not least, Professor Vankelecom. Dank u wel om mij de kans te hebben gegeven om me te verdiepen in de wondere membraanwereld en om me de liefde voor membranen bij te dragen. Mijn fascinatie en enthousiasme zullen niet snel gestild worden.

Nederlandstalige samenvatting

Dunne film nanocomposiet membranen bevatten nanopartikels in de dunne toplaag, waardoor een sterk verhoogde permeabiliteit, zonder verlies in retentie, wordt waargenomen. Het mechanisme achter deze verhoogde water flux is echter ongekend. De algemeen aanvaarde hypothese stelt dat versneld water transport plaatsvindt door de poriën van de poreuze vuller. Andere hypotheses beweren dat er een structuurverandering optreedt in de polyamide (PA) toplaag. Momenteel is er niet genoeg experimenteel bewijs om de hypotheses te staven. Het doel van deze thesis is te onderzoeken wat de invloed is van de grootte, de locatie en de hoeveelheid van de geïncorporeerde vuller op de membraan performantie en morfologie. TFN membranen werden gesynthetiseerd met het oog op het controleren van de positie van de vuller, ZIF-8, in de toplaag. Dit werd gerealiseerd door twee nieuwe methoden.

De *evaporation controlled filler positioning* (ECFP) methode werd ontwikkeld om de nanopartikels te pre-positioneren op de steunlaag. De optimum performantie werd bereikt bij een partikelconcentratie van 0.005 wt% voor beide partikel groottes (80 nm en 155 nm), wat resulteerde in een verhoging van de permeabiliteit met 200 %. Deze membranen behaalden een hogere performantie bij lagere vuller concentratie, in vergelijking met de traditionele (TRAD) synthese methode. Daarenboven werd een hogere incorporatiegraad behaald, alsook een betere positionering op de steunlaag. Desondanks werden slechts enkele nanopartikels werkelijk geïncorporeerd in de toplaag. De morfologie van de traditionele TFN en ECFP toplagen verschilt sterk en de PA cross-linking graad verandert eveneens. Deze resultaten suggereren dat de hoeveelheid en locatie van de vuller de toplaag structuur beïnvloeden.

De *chemically modified polyimide* (CMPI) methode werd ontwikkeld om nanopartikels coördinatief vast te zetten op de PA/steunlaag interfase. Ookal waren de gemodificeerde PI membranen in staat om ZIF-8 te binden, de performantie van de resulterende TFN membranen was ondermaats. Dit is hoogstwaarschijnlijke te wijten aan slechte adhesie van de PA aan de gemodificeerd PI steunlaag. Optimalisering van de CMPI methode is dus vereist.

De behaalde resultaten in dit onderzoeksproject tonen aan dat de ECFP membranen een grote verbetering zijn op een groot aantal dunne film (nano)composiet membranen, beschreven in de literatuur. Daarenboven suggereren ze dat veranderingen in de PA structuur door de vuller een grote rol spelen in de verhoogde permeabiliteit van het TFN membraan De hoeveelheid van de geïncorporeerde poreuze vuller is te klein om de grootste bijdrage te kunnen leveren aan de verhoogde water flux, zoals wordt beweerd in de algemeen aanvaarde hypothese.

English summary

Thin film nanocomposite (TFN) membranes consist of incorporated nanoparticles in the thin toplayer, resulting in a tremendous increase in permeance, without compromising rejection. The exact mechanism behind the increased water flux however, remains unknown. The hypothesis that is most widely accepted implies that fast water transport occurs through the pores of the incorporated filler. However, other theories suggest that the filler alters the toplayer's structure, thereby enhancing performance. No direct evidence to substantiate both hypotheses is found in literature. Therefore, the aim of this thesis was to investigate how the size, position and the amount of incorporated filler influences the membrane performance and morphology. TFN membranes were also synthesized to control the position of the incorporated filler, being ZIF-8, in the polyamide (PA) toplayer via two new methods.

The *evaporation controlled filler positioning* (ECFP) method was invented to pre-position the filler on the support. The optimum performance was achieved at a loading of 0.005 wt%, for both filler sizes (80 nm and 155 nm), resulting in an increase in permeance of around 200%, compared to the unfilled membrane. The membranes resulting from the ECFP method attained a higher performance at a lower filler concentration, compared to the membranes synthesized via the traditional way. In addition, a higher incorporation degree was achieved, along with a better positioning towards the porous support. Nevertheless, only a few nanoparticles were truly incorporated in the thin layer. The PA morphology of the TRAD and ECFP toplayers differed substantially and the PA cross-linking degree also varied when incorporating nanoparticles. The obtained results suggest that the amount and location of the filler influence the structure of the selective layer.

The *chemically modified polyimide* (CMPI) method was developed to coordinatively affix the nanoparticles to the PA/support interface. Although the membrane was able to bind ZIF-8, the resulting TFN membranes were not performant. This was presumed to be caused by bad adhesion of the toplayer on the modified PI. Optimization of this method is required.

The obtained results in this Master thesis show that the ECFP membranes are a huge improvement on the conventional thin film (nano)composite membranes. Additionally, they suggest that changes in PA, caused by the presence of the filler, play a major role in the enhanced permeance of a TFN membrane. The amount of truly incorporated porous filler is too low to contribute solely to the increased water flux, as claimed in the most widely accepted hypothesis.

List of abbreviations and symbols

4-ABA	4-amino benzoicacid
6-AHA	6-amino hexanoicacid
AFM	atomic force microscopy
ATR-FTIR	attenuated total reflectance – Fourier transform infrared
BTC	benzene tricarboxylate
CAIP	co-solvent assisted interfacial polymerization
DLS	dynamic light scattering
DMF	N,N'-dimethyl formamide
DMSO	dimethyl sulfoxide
ECFP	evaporation controlled filler positioning
EDX	energy-dispersive X-ray spectroscopy
ELM	emulsion liquid membrane
EtOH	ethanol
f-MWCNT	functionalized – multi-walled carbon nanotube
H-OMC	hydrophilized – ordered mesoporous carbon
ICP	inductively coupled plasma
ILM	immobilized liquid membrane
Im	imidazolate
IR	infrared
M	metal
MeOH	methanol
MF	microfiltration
MMM	mixed matrix membrane
MOF	metal organic framework
MPD	*meta*-phenylenediamine
MQ-water	milli-Q water
MW	molecular weight
MWCO	molecular weight cut-off
NF	nanofiltration
NMP	N-methylpyrrolidone
PA	polyamide
PALS	positron annihilation light spectroscopy
PAN	polyacrylonitrile
PCP	porous coordination polymers
PE	polyethylene
PEG	polyethylene glycol
PES	polyether sulfone
PI	polyimide
PIP	piperazine
PO	phosphate oxide
PP	polypropylene
PS	polystyrene
PSf	polysulfone
RB	rose Bengal
RO	reverse osmosis
SAPO	silicoaluminophosphates
SDS	sodium dodecylsulphate
SEM	scanning electron microscopy

SIM	simplified
SRNF	solvent resistant nanofiltration
TEA	triethylamine
TEM	transmission electron microscopy
TFC	thin film composite
TFC PA	thin film composite polyamide
TFC SRNF	thin film composite solvent resistant nanofiltration
TFN RO	thin film composite reverse osmosis
TGA	thermo-gravimetric analysis
TMC	trimesoyl chloride
UF	ultrafiltration
UV	ultraviolet
UV-Vis	ultraviolet - visible
XPS	X-ray photoelectron scattering
XRD	X-ray diffraction
ZIF	zeolitic imidazolate framework

ΔP	pressure gradient
μ	viscosity
A	membrane surface
$C_{f,p}$	concentration in feed or permeate
J	flux
P	effective permeability of species in MMM
Pd	permeability of species in the dispersed phase
Pm	permeability of species in the continues matrix
Pr	relative permeability of species
R	rejection
r_p	pore radius
t	time
V	volume
$x_{A,B}$	concentration of component A or B in feed
$y_{A,B}$	concentration of component A or B in permeate
$\alpha_{A/B}$	separation factor
δm	membrane thickness
ε	membrane porosity
λdm	permeability ratio P_d/P_m
Φ	volume fraction of filler particles
Φd	volume fraction of the dispersed phase

List of Tables and Figures

Table of contents

Context and targets

Membrane technology has become a reputable separation technology over the past decades as it holds several advantages compared to conventional separation techniques, such as distillation. Membrane filtrations work with a relatively low energy use and without the addition of chemicals. Hence, membrane processes are currently implemented in industry. A wide range of polymeric and inorganic (and hybrid) membranes are used, depending on the application. As an illustration, thin film composite (TFC) membranes hold about 90% of the total desalination market.[1] This research project focusses on a new class of membranes that are closely related to these TFC membranes and also currently industrialized for water purification purposes.

TFC membranes are prepared by placing very thin selective layers over the surface of finely porous support layers. This is in this case done via the well-known interfacial polymerization technique. The established thin toplayer acts as the actual selective barrier and permits high permeances as well as high rejections. Nevertheless, the performance of the current generation membranes leaves room for improvement. Therefore, a recent category of membranes, called thin film nanocomposite (TFN) membranes, received a lot of attention lately. Nanoparticles are incorporated in the thin toplayer, resulting in an increase in permeance without observing a loss in rejection. A 50 to 200 % increase in permeance is obtained, compared to the TFC analogue. However, little or no evidence is found over the exact function of the filler in the toplayer nor over its exact location. Also, the influence of the embedded nanoparticles on the toplayer morphology is barely understood, although the altered morphology is presumed to contribute to the increased permeance.

The aim of this research thesis consisted of two parts; (i) to control the location of the nanoparticles in the toplayer and (ii) to elucidate the influence of the filler on the toplayer morphology and on the membrane performance. The primary effect of introducing porous particles to the selective layer is the creation of preferential flow paths for the solvent molecules, hence enhancing the permeance. Incorporation of nanoparticles in the toplayer also alters and influences the structure of the selective layer (e.g. thickness, cross-linking degree, homogeneity, morphology), which can likewise contribute to the enhanced permeance. These effects are called the secondary effect of the filler on the membrane performance. Both effects, primary and secondary, were investigated in detail, in order to see which of them dominates. In addition, research was done on controlling the location of the filler in the toplayer. This is actually impossible in the conventional method of synthesizing TFN membranes, but can probably result in better performing membranes. Two new methods were invented to attain this, based on

different concepts. In one method, called the *evaporation controlled filler positioning* (ECFP) method, the filler is deposited on the porous support layer, prior to the interfacial polymerization reaction. This was done to attain a higher amount of embedded nanoparticles, as well as a better incorporation in the thin film. The other method, called the *chemically functionalised PI* (CMPI) method, consists of chemically modifying the support, in order to establish a coordinative bond with the filler. As a result, the filler is affixed to the substrate, resulting in a likely better positioning in the toplayer compared to the traditional method. The traditional (TRAD) method for making TFN membranes, as described in literature, was used as reference for the ECFP and CMPI methods. All three methods are illustrated in the figure below. As filler, the well-studied metal organic framework ZIF-8 was used.

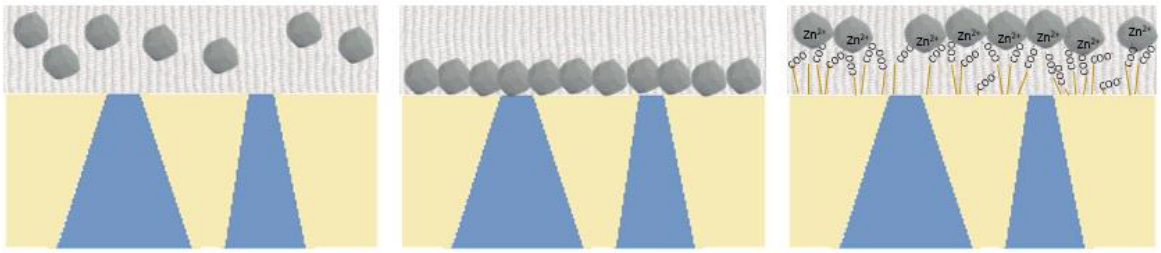

Illustration of the three methods used to synthesize TFN membranes. (left) TRAD method, where no control over the filler is possible; (middle) ECFP method, where the filler is located in the bottom part of the toplayer via deposition of the filler on the substrate; (right) CMPI method, where the filler is affixed to the porous support via the carboxyl groups present on the surface. ZIF-8 is represented as a grey particle. The porous PI Structure is showed in grey, while the toplayer is represented by the light brown striped rectangle.

In the first part of this thesis, synthesis and characterization of the filler is performed. As it is believed that the size of the incorporated filler influences the membrane performance, ZIF-8 particles of different diameter are synthesized via two well-established protocols. Characterization of the nanoparticles via different methods is executed.

The second part of this thesis was mainly devoted to the synthesis methods of TFN membranes via the TRAD and ECFP method. In a first stage, the ECFP method was compared with the TRAD method, in order to see which method produced the best performing TFN membranes. Different amounts of filler were incorporated in the membrane in the hope to attain a certain optimum concentration. In addition, changes in toplayer morphology as function of the amount and size of incorporated filler were investigated. The contribution of the primary and secondary effects to the enhanced membrane permeance was examined in order to determine which one plays a decisive role. Different techniques to quantify the amount of incorporated ZIF are explored as well. Special attention was paid to the stability of the filler during the interfacial polymerization conditions.

The CMPI method was explored in the third part of this research project. Optimum conditions to chemically modify the support were determined. The thin toplayer was deposited on the functionalized support via the ECFP as well as via the TRAD method. The performance of these membranes was investigated and both methods were again compared.

PART I: Literature review

1. Membranes and membrane processes

1.1. Introduction

Separation processes account for 40-70 % of both the capital and operating costs in industry.[2] In membrane separations, the aim is to retain one (or more) component(s) of a mixture, while other components can freely permeate through the membrane under a driving force that can be a pressure, concentration or potential gradient. According to Mulder, the general macroscopic definition of a membrane is the following: 'A selective barrier between two phases, through which some components can pass more readily than others'.[3] Figure 1 illustrates this basic principle. The permeate consists of the components which can pass through the membrane, via the membrane pores. The retentate is composed of the solutes, retained by the membrane.

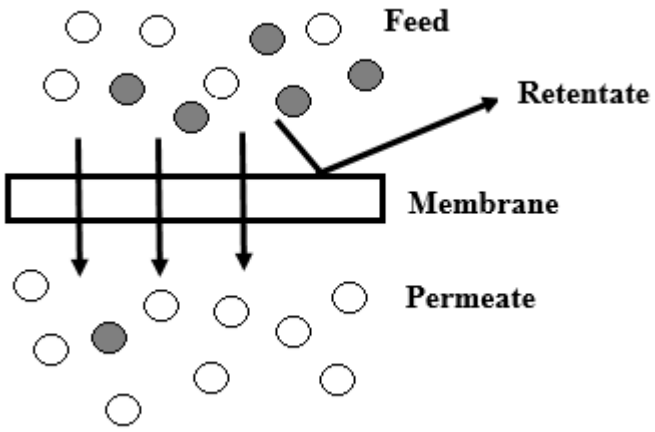

Figure 1: Basic scheme of a membrane separation process.

1.2. Advantages and disadvantages

Membrane technology is currently an emerging field of science thanks to the many advantages it has to offer compared to the traditional separation processes, such as distillation, adsorption, absorption or solvent extraction. The benefits include continuous operation, lower energy consumption, possibility of integration with other separation processes, mild conditions and thus more environment friendly, easy but linear up-scaling, feasibility of making tailor-made membranes and less requirement of additives.[3] The drawbacks are the low flux, concentration polarization and the low membrane lifetime due to fouling. Fouling consists of the partially irreversible deposition of suspended or dissolved particles in or on the membrane. Concentration polarisation is a reversible phenomenon, caused by an accumulation of retained

molecules near the membrane surface resulting in a highly concentrated layer.[3] The low selectivity in some cases is another important disadvantage of membrane separation processes.

1.3. Classification

According to Mulder and Duval, membranes and membrane processes can be classified either by their nature, by their structure or by their separation principle.[3,4]

1.3.1. Nature

The first distinction is made by nature, i.e. biological or synthetic membranes. Biological membranes can be further divided into living and non-living membranes, while synthetic membranes are subdivided into organic and inorganic membranes. The vast majority of membranes used in industry are polymer-based organic membranes.[4] Inorganic membranes are generally thermally and chemically more stable but are much more expensive and more difficult to prepare compared to organic membranes.[3]

1.3.2. Structure

Classifying membranes by their structure results in following categories:[3]

-symmetric: 1) (cylindrical) porous
2) dense/homogeneous

-asymmetric: 1) porous
2) porous with dense toplayer (integrally skinned)
3) composite (toplayer of a different material from the porous support)

Symmetric membranes consist of a polymer or a polymer blend. The total membrane thickness, which generally varies from 10 to 200 µm[3], is the most important parameter determining the overall hydrodynamic resistance of the membrane. The membrane's properties are not altered throughout its cross-section. Symmetric membranes can be sub-divided, based on their porosity, into cylindrical porous, porous or dense membranes (Figure 2).

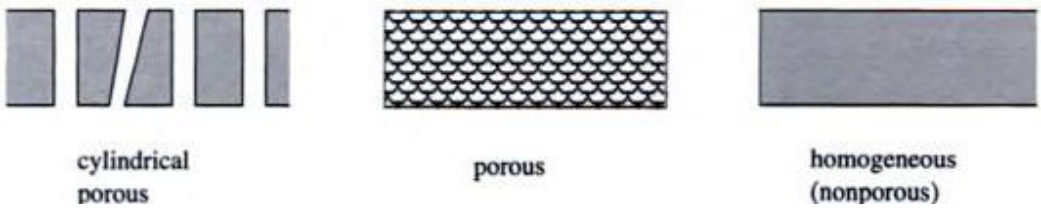

Figure 2: Schematic representation of different types of symmetric membrane.[3]

Asymmetric membranes, invented by Loeb and Sourirajan in 1962, lead to a major breakthrough in membrane processes.[5] Asymmetric membranes consist of different layers,

which are built up from one or different polymers (Figure 3). The first layer often consists of a 'non-woven' fabric upon which the asymmetric membrane is synthesized. The non-woven support provides mechanical strength and easy handling of the membrane. In integrally skinned membranes, the dense toplayer (0.1 to 0.5 µm) is made up of the same polymer as the support (thickness of 50 to 150 µm), being an integral part of the membrane.[3] When the polymer of the toplayer differs from the polymer used in the support layer, the membrane is called *composite*. Nevertheless, composite membranes can also refer to mixed matrix membranes, in which a filler is dispersed in the polymeric matrix. The big advantage of asymmetric membranes is that the thin toplayer performs the actual separation, while the support only provides mechanical strength. As the flux is mainly determined by the thickness of the active layer, asymmetric membrane have a higher efficiency than symmetric ones.

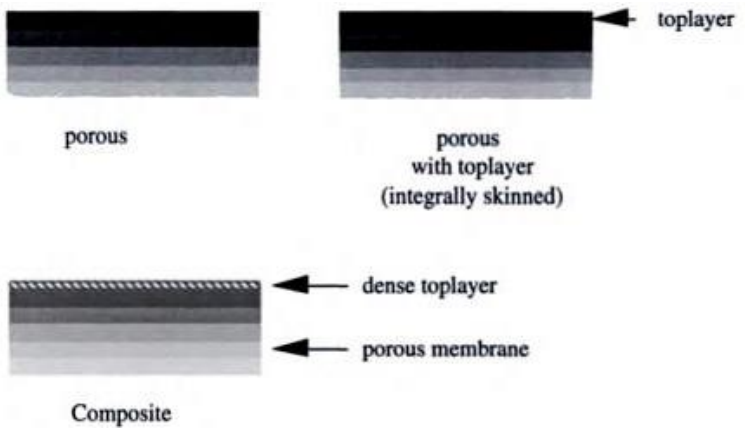

Figure 3: Schematic representation of different types of asymmetric membranes.[3]

1.3.3. Separation principle

The third classification is provided by the separation principle.[6] The separation principle of porous membranes, used for ultra and microfiltration, is size-based sieving. The pore size of the membrane relative to the size of the solutes, which have to be separated, will determine the membrane performance. The polymer itself has impact on fouling and on the chemical and thermal stability of the membrane. On the other hand, the separation process of dense membranes is based on differences in affinity of the solutes for the membranes and on differences in diffusion rates. Another class of membranes consists of liquid membranes, which can be divided into two subclasses. The first group are immobilised liquid membranes (ILM) where the (organic) liquid is immobilised in the pores of a porous framework. The second type of liquid membranes is the emulsion liquid membrane (ELM), where 2 immiscible phases are mixed to form an emulsion.[3] Increasing the selectivities of these membranes can be achieved

by incorporating carrier molecules, such as crown ethers and calixarenes, which have high affinities for a specific solute.[3]

1.4. Membrane processes

Membrane processes are sub-divided into different groups, according to the driving force, responsible for the transport across the membrane. Membrane processes can be driven thermally, electrically, by a pressure or by a concentration gradient. If pressure acts as the driving force, membranes and membrane processes are divided in the following classes: micro (MF), ultra (UF), and nanofiltration (NF), and reverse osmosis (RO). Their specifications are given in Table 1.

Table 1: Summary of pressure driven membrane processes.[3,7]

	Pressure range (bar)	Flux range L/(m².h.bar)	Pore sizes (nm)	Separation principle
Microfiltration	0.1-2.0	>50	50-10000	Sieving
Ultrafiltration	1.0-5.0	10-50	1-100	Sieving
Nanofiltration	5.0-20	1.4-12	<2	Solution diffusion
Reverse Osmosis	10-100	0.05-1.4	<1.5	Solution diffusion

1.5. Performance characterization

1.5.1. Flux

Membrane separation performance (or efficiency) is determined by two parameters: the selectivity and the solvent flux.[3] The flux can be defined as the volume flowing through the membrane per unit area and per unit time and is given by Equation (1),

$$J = \frac{V}{A * t} \quad (1)$$

where J is the solvent flux (L/m²s), V the volume of the permeate (L), A the unit area (m²) and t the time (s).

1.5.2. Permeance

Membrane permeance is calculated via Equation (2) , where ΔP is the applied pressure (bar), V the volume of the permeate (L), A the unit area (m²) and t the time (s).

$$L_p = \frac{V}{A * t * \Delta P} \quad (2)$$

The permeability, expressed in L.m/m².h.bar, equals the multiplication of the permeance, in L/m².h.bar, and the thickness of the membrane, in meters. The permeation rate is expressed in

L/m².h. In general, the permeance and the selectivity are inversely related: when the permeance increases, a decrease in rejection is observed. A trade-off between those two parameters should be taken into account when considering membrane performance. In principle, solvent and solute permeability are intrinsic properties of the membrane, while flux and rejection are not. Flux and rejection are also influenced by mass transfer properties and operating conditions.

1.5.3. Selectivity

The selectivity of a membrane towards one component in a mixture can be expressed by the separation factor α (Equation (3)) and the rejection R (Equation (4)), both dimensionless numbers.

$$\alpha_{A/B} = \frac{y_A/y_B}{x_A/x_B} \tag{3}$$

The separation factor $\alpha_{A/B}$, where y_A and y_B are the concentrations of components A and B in the permeate and x_A and x_B are the concentrations in the feed, denotes that the permeation rate of A is bigger than that of B. When $\alpha_{A/B} = \alpha_{B/A} = 1$, no separation is achieved. The rejection is given by the following formula:

$$R = \left(\frac{C_f - C_p}{C_f}\right) * 100\% = \left(1 - \frac{C_p}{C_f}\right) * 100\% \tag{4}$$

C_f and C_p are the solute concentrations in the feed and in the permeate, respectively. When the rejection equals 100%, all solutes are retained. When the rejection is 0%, no separation is achieved: the solvent as well as the solute pass through the membrane.

1.5.4. Molecular weight cut-off value

In addition, membrane separation efficiency can also be evaluated via the 'molecular weight cut-off' (MWCO) value, which is most often determined by a MWCO-curve, indicating the membrane's rejection with increasing solute molecular weight (MW). The MWCO value represents the MW corresponding to a reference compound (e.g. styrene, polyethylene glycol) that is typically retained for 90%.[4] In Figure 4, this value corresponds to 83 kDa.

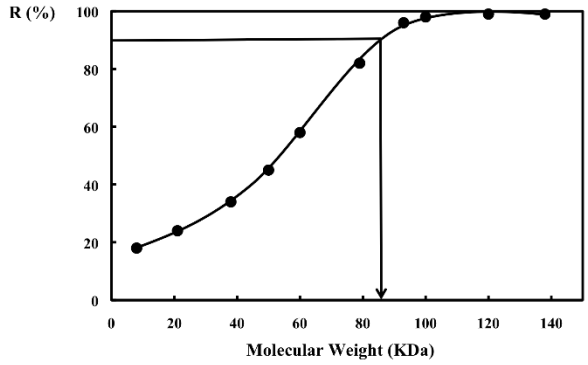

Figure 4: A typical molecular weight cut-off curve, with a MWCO-value of 83 kDa for 90 % rejection.[8]

2. Composite Membranes

2.1. Thin film composite membranes

2.1.1. Introduction

Composite membranes, also called thin-film composite (TFC) membranes, first developed by Cadotte in 1985[9], possess a tri-layered asymmetric structure. A thin dense toplayer is located upon a porous support, which is on its turn supported by a 'non-woven fabric' (Figure 5). The latter provides mechanical strength and easy handling of the membrane, while the porous support mainly allows a defect-free toplayer formation. The toplayer itself is the actual selective barrier. Each layer consists of a different polymer. The first composite membrane was made by spreading a polymer on a liquid phase. By letting evaporate the solvent, a polymer film was formed and transferred to a porous support, resulting in a membrane with low mechanical stability.[4] Nowadays, the support is made by phase inversion and does not contribute to the actual separation process. The toplayer can be established by several techniques from which interfacial polymerization (IP) is the most prevalent one (section 2.1.4).

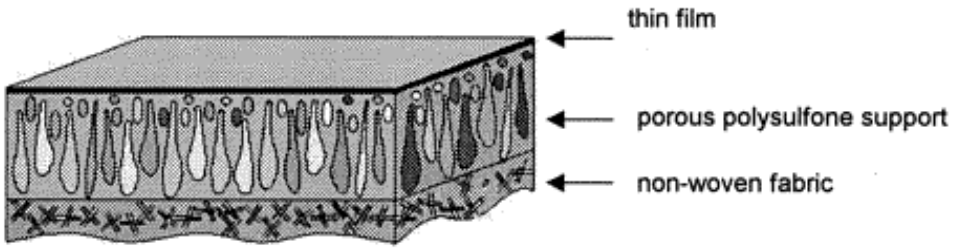

Figure 5: Structure of a composite membrane.[10]

2.1.2. Advantages

The biggest advantage of these hybrid membranes is the possibility to control and optimise each layer individually for its own function. The thin active layer can be optimised for a high solvent flux without allowing a decrease in the solute rejection.[11] Maximum strength and minimum resistance are desired features of the support layer. Additionally, both linear and cross-linked polymers can be used in TFC membranes, whereas in asymmetric membranes, linear, soluble polymers are most commonly used.[11]

2.1.3. Support layer

The support layer is usually an asymmetric ultrafiltration membrane, synthesized via phase inversion. A routine polymer for this purpose is polysulfone (PSf) (Figure 6). PSf is widely available and easy to process[12] but its hydrophobic nature and solvent sensitivity set limits on possible applications.[11] Due to its hydrophobicity, impregnation with the aqueous amine

solution is sometimes insufficient, increasing the risk of pinhole defects, which are detrimental for the membrane performance.[13] The use of TFC membranes in solvent streams is limited due to the poor solvent-resistance of PSf.[1] This low solvent stability also restricts the choice of the organic phase during IP.

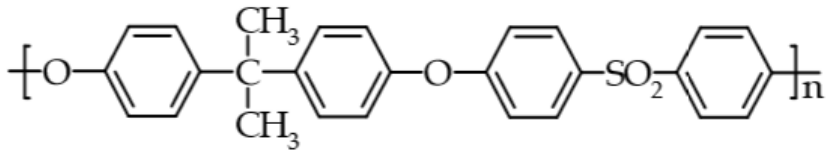

Figure 6: Chemical structure of a polysulfone.[3]

Other polymers which can form the support layer are for example polyimide (PI), polyvinylfluoride, poly(phthalazinone ether amide), polyacrylonitrile (PAN), polypropylene (PP) and polyethersulfone (PES).[12] In general, less attention is paid to the support layer compared to the toplayer because the substrate does not play a fundamental role in fouling and solute separation. Nevertheless, research on the substrate and on the interaction between it and the toplayer is important and is slowly but surely expanding.[14]

2.1.4. Interfacial polymerization

a) Concept

Interfacial polymerization (IP) is one of the techniques to deposit a thin layer upon a support and proceeds by a simple mechanism, based on a condensation reaction between two monomers. The majority of TFC membranes made by IP consists of a polyamide (PA) toplayer, but synthesis methods of poly(amide imide), poly(ether amide), polyuria and poly(urea amide) toplayers have been reported as well.[11] Interfacially polymerized films can also be employed as sensors [15] and for the encapsulation of drugs, e.g. peptides.[16]

b) Preparation technique of TFC PA membranes

IP of a toplayer can be established in two ways, by the traditional method and by the simplified (SIM) method.[17] The traditional method consists of separately dissolving a difunctional amine and a trifunctional acid halide (in the case of a PA toplayer) in respectively a water and an organic phase, often hexane. Water and hexane are immiscible liquids, which is a requirement for the choice of both solvents. The support membrane, typically a PSf flat sheet, made by phase inversion, is immersed in the aqueous solution, containing the amine monomer. Once saturated, the membrane is transferred to the organic solution, containing an acid halide (Figure 7). A polymerization reaction between both monomers occurs at the interface, resulting in a thin film.

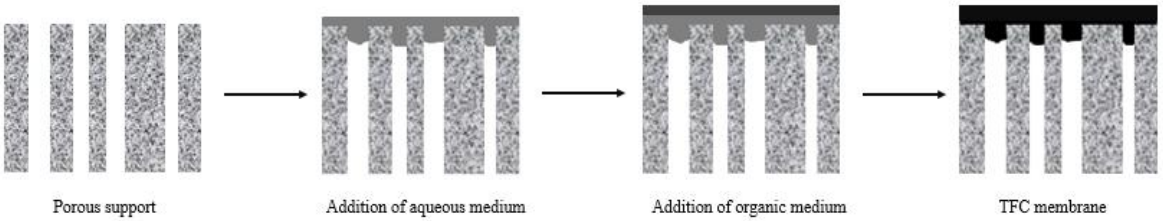

Figure 7:Schematic drawing of the IP procedure (= aqueous solution, = organic solution, = toplayer).

In the SIM method, the coagulation bath, used during phase inversion of the support membrane, already contains the amine. Hence, only the hexane solution is poured over the membrane. This is in contrast with the traditional method. As a result, incomplete wetting of the support layer during solvent and/or reagent exchanges can be avoided, resulting in a more homogeneous toplayer, with less chance of defects.[17] Hermans *et al.* concluded that the SIM method is an alternative, simplified, more efficient, time and material saving way to obtain TFC membranes.[17]

It is commonly believed that the film formation takes place in the organic phase.[11,18,19] This implicates that the diffusion of the amine into the organic phase is the limiting factor at first. As the acid chloride is negligible soluble in the water phase, the main driving force of this process is the concentration gradient of the amine, as it is relatively soluble in the hexane phase. Secondly, when the toplayer is formed, the amine has to diffuse from the aqueous phase, through this newly formed layer, to finally react with the acid chloride, present at the other side. The new layer forms a barrier and the supply of reactants becomes the rate-limiting step, causing this technique to be self-inhibiting.[1,14] By this self-healing and self-terminating mechanism, very thin toplayers of roughly 150 nm originate.[20]

c) Reaction mechanism of the polyamide formation

The reaction mechanism of the PA formation is shown in Figure 8, based on the Schotten-Baumann reaction.[21] The first step is an addition reaction, consisting of a nucleophilic attack from the lone electron pair of the nitrogen atom of the amine on the partially positively carbon atom. The second step is an elimination reaction. The carbon-oxygen bond reforms and the chloride ion is eliminated. The hydrogen atom from the nitrogen can be removed either by the chloride ion, resulting in the formation of hydrogen chloride, or by another amine group, often triethyl amine (TEA) (not shown in this scheme).

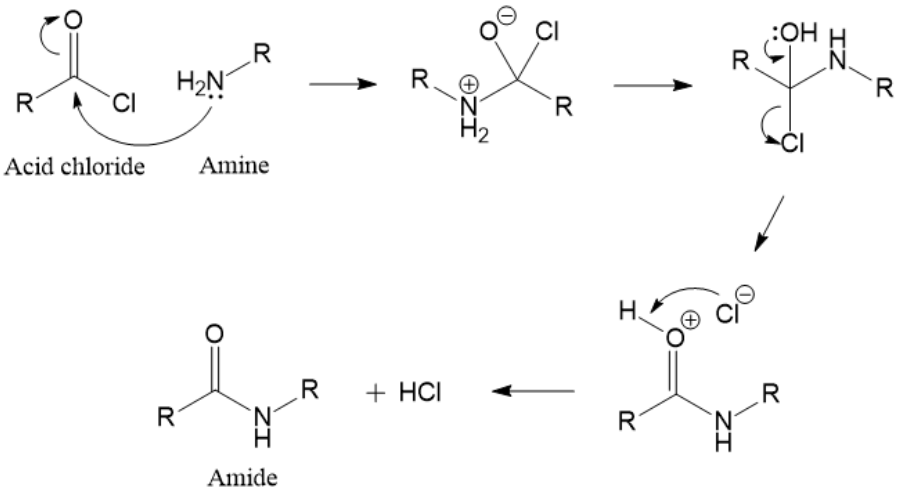

Figure 8: Mechanism of polyamide formation, starting from an acid chloride and an amine. HCl is released during the reaction.

d) Structure of the PA film

IP results in a TFC membrane with an active layer of thickness within the 150 nm range, in the case of polyamide formation.[22] The active layer has a rough appearance, resulting in the so-called 'ridge-and-valley' morphology. Pacheco *et al.* concluded that the rugose thin film consists of two distinct polyamide layers.[23] Firstly, "a dense base of nodular polyamide that forms a relatively smooth interface with the PSf support" is observed. Secondly, "a more open structure of loose polyamide extending outward from the nodular base comprising the ridge-and-valley structure." It is the dense base that is mainly responsible for the actual separation. Recent work from Ghosh and Hoek showed that the support has an influence on the PA morphology, as well as on the performance properties of the film.[12] Large, hydrophobic pores of the support layer produce more permeable and rough membranes, compared to hydrophilic pores. The reason for this finding is believed to lie in the differences in location of PA formation. In supports with hydrophilic pores, more PA is formed deeper within the pores, whereas for hydrophobic pores, more PA is formed above the pore mouth.[12]

e) Parameters

The structure of the resulting PA film is influenced and affected by a whole range of parameters, which can by varied during and after the membrane preparation. Choice of monomers, choice of solvent, reaction temperature, addition of additives, choice of support and curing temperature are examples of factors that can be varied and examined. The diffusivity and solubility of the monomers have also a big impact on the resulting membrane and consequently also on the separation performance and interfacial properties.

Amine

The most successful membranes formed by IP are formed with monomeric amines.[19] A widely researched amine for this purpose is piperazine (PIP), which reacts with trimesoyl chloride (TMC), the acyl chloride in a hexane solution. The IP reaction is given in Figure 9 (top) and results in the formation of poly(piperazine amide). The carboxylic acid functional group often arises due to the partial hydrolysis of the acyl chloride unit of TMC[24], making the membrane more hydrophilic.

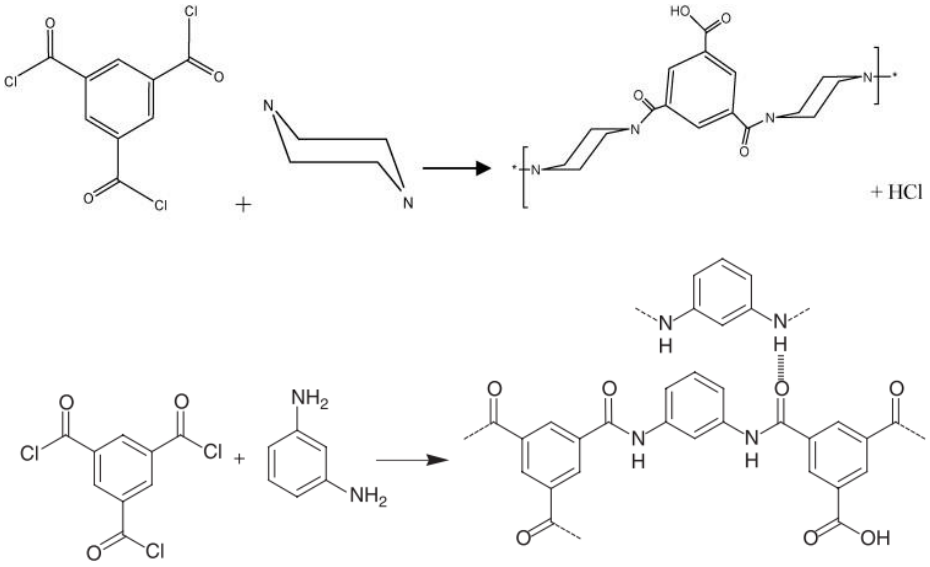

Figure 9: (top) IP reaction between TMC and PIP resulting in poly(piperazineamide)[24], (bottom) IP reaction between TMC and PIP resulting in polyamide. [19]

An example of another monomeric and aromatic amine is m-phenylenediamine (MPD), which is frequently used. The reaction scheme between MPD and TMC is given in Figure 9 (bottom). It should be remarked that, when using MPD, a fully aromatic cross-linked polyamide membrane develops, while a semi aromatic cross-linked polyamide layer results when using PIP. Smaller nodular structures will arise when using PIP instead of MPD. This is due to the smaller partition coefficient of PIP into the organic phase, resulting in a lower diffusion into this phase.[25] PIPs chair structure at its lowest energy state is more difficult to pack tightly, resulting in a membrane structure with a higher open volume, hence higher permeance.[26] Using monomeric amines, in comparison with polymeric amines (such as polyethylene imine), assures a more rapid diffusion of the amine into the condensation zone, resulting in a more dense and selective thin layer.[19]

Solvent

The choice of solvent is another important parameter influencing the resulting membrane. Viscosity, surface tension and density of the organic solvent have an impact on the diffusivity and solubility of the monomers. Hexane, heptane, isoparaffin and cyclohexane were investigated by Ghosh *et al.*.[27] Increasing diffusivity and decreasing solubility of MPD in the solvents results in a high performance membrane (high rejection and high flux).[27]

Additives

Addition of additives to the organic as well as to the aqueous solution is a common approach to alter the reaction conditions and to obtain different membranes. They can influence monomer solubility, diffusivity, hydrolysis and protonation.[27] For example, sodium dodecyl sulphate (SDS), a well-known anionic surfactant, improves the compatibility with the support membrane by promoting its amine absorption. Other molecules, such as phosphate based complexing agents (e.g. dibutyl phosphite) enhance the permeability and rejection, both wanted features, by controlling the reaction rate. Adding a base, such as TEA, neutralizes the solution, acts as an acid acceptor and as a catalyst. Kong *et al.* were able to control the active layer thickness by adding a co-solvent, more specifically acetone, to the organic phase in the IP process.[28] Thanks to the addition of acetone, a narrower miscibility zone in the hexane/water/acetone system was formed. This method is called 'co-solvent assisted interfacial polymerization' (CAIP). Layer thicknesses of smaller than 8 nm were obtained, resulting in an increase in permeance and no considerable solute rejection loss.

Solomon *et al.* used a mixture polyethylene glycol (PEG) and isopropanol (3:2 ratio) as conditioning agent before IP.[25] The porous support was immersed in this solution overnight and was subsequently dried. This step made the UF support more hydrophilic, enhancing the wetting of the aqueous amine solution. MPD may bind to the support through hydrogen bonding, decreasing its diffusivity to the organic phase, altering reaction conditions at the interface. Furthermore, PEG acts as pore protector, avoiding pore collapse as well as PA formation in the pores. At twice as high methanol flux was observed when using the conditioning agent compared to pristine TFC membranes. No decrease in styrene rejection was observed.[25]

Post-treatment

Membranes made via IP are often subjected to different post-treatment steps, from which curing is one. Curing temperatures from 40 to 120°C are used.[27] This treatment step is performed to stabilize the PA film by removing residual organic solvent and by crosslinking through dehydration of amine and carboxylic acid residues.[27] The porosity of the PA film is reduced by

crosslinking, resulting in a lower flow but a higher rejection. Even though, when too high curing temperatures are used, pore collapse of the support membrane can occur.[29]

Solvent activation is another recent and simple post-treatment step which results in an enhanced membrane flux without compromising rejection.[25] The membranes are contacted with the activating solvents, N,N'-dimethylformamide (DMF) or dimethyl sulfoxide (DMSO), for 10 minutes. Both solvents have similar Hildebrand solubility parameters as the polyamide toplayer, making it possible to dissolve loosely bound PA.[25] The core PA layer is not affected by this impregnation step as high rejections are maintained. An increase in methanol/polystyrene flux from 7 (±2) L/m².s to 23.9 (±2) L/m².s is observed when performing the solvent activation step with DMF. The highest flux is obtained when combining this approach with impregnation of the support with PEG i.e. a ± 6.5 fold increase in methanol/polystyrene flux.[25]

2.1.5. Disadvantages of TFC PA membranes

A key limitation to commercial PA is its low chlorine resistance. Chlorine is a commonly used disinfectant in water and in wastewater treatment plants. The conversion of the amine group to a N-Cl group upon contact with chlorine makes the toplayer more hydrophobic, resulting in a lowered water flux.[14] This hydrophobic character, even present without contact with chlorine, results in another major drawback, which is the occurrence of organic fouling.[30] Many natural organic compounds and microorganisms easily adsorb, eventually resulting in deterioration of the membrane performance.[5,18] Periodical cleaning may help to reduce fouling but it cannot prevent it from occurring.[18] The ridge and valley morphology also contributes to the low chlorine resistance and the increased likelihood to fouling.[19] Temperature sensitivity is another possible big disadvantage of TFC PA films. Pore collapse and compaction can appear when the membranes are exposed to high temperatures.[29]

2.1.6. Other preparation techniques

Several other techniques, such as dip[14] and spin coating[31], in-situ and plasma polymerization[32], photo grafting[14] and lamination[33] can also establish the selective toplayer of TFC membranes. To create a toplayer with dip coating, the substrate needs to be partially or fully immersed in the dip solution and subsequently withdrawn, resulting in a wet film on the substrate. For spin coating, an amount of coating material is applied to the centre of the substrate, which rotates at high speed. Centrifugal forces spread out the coating material on the substrate, leading to a thin film. Plasma polymerization relies on the use of a gas plasma that, by its high energy, fragments a monomer vapour. These fragments will condensate on the cooler substrate, resulting in a polymer film.[11] In photo grafting, an initiator is converted into a radical by UV adsorption. This

radical can abstract a hydrogen atom from the polymer surface, serving as substrate. The resulting radical on the surface can add reactive monomers, generating a controlled radical-chain polymerization reaction. Thin grafted films of smaller than 10 nm result from this technique.[34] Lamination is one of the oldest techniques to create a thin toplayer on a substrate. A polymer solution is float-cast on a water surface. Evaporation of the polymer solvent as well as its extraction to the water phase, generates a solid polymer layer. This layer is then laminated on a porous support [11], resulting in a thin film composite membrane.

2.1.7. Applications of TFC PA membranes

Since 1985, when Cadotte reported in-situ interfacial polymerization resulting in a PA toplayer, a new age of RO and NF membranes for aqueous applications emerged.[9] TFC membranes consisting of a PA toplayer were commercialized by Dow Filmtec[35] and are recently also patented by several others.[9,36–38] Applications of these membranes lie in diverse areas such as in water and wastewater treatment, food engineering, pharmaceutical and biotechnology.[35] Especially RO membranes are used for desalination, as they are able reject monovalent salts with high efficiency (>98% rejection). The remarkable chemical stability of PA should logically enable SRNF applications. Still, conventional TFC PA membranes are not suitable for SRNF due to limited stability of the PSf support membranes, which could dissolve or swell in harsh solvents.[25] Therefore other supports, such as PAN[39], PP[40], and cross-linked PI[25] were investigated, with good results. Only cross-linked PI was reported as a suitable support membrane in DMF.[25] A big step forward in TFC-SRNF membranes was made by Solomon *et al.*, who reported an enormous increase in permeance for several polar solvents without observing a decrease in rejection.[25] These results were obtained by subjecting the membrane to a pre-treatment step with PEG and post-treatment step with DMF or DMSO (see 2.1.4 e)). The low permeability for non-polar solvents of these modified TFC membranes is due to the hydrophilic character of the PA toplayer. To make the toplayer more hydrophobic, two strategies were used. The first one consists of grafting hydrophobic species on the membrane surface. The second method uses monomers with hydrophobic groups during the IP reaction. Both methods greatly enhance flux for non-polar solvents.[41] Summarized, TFC PA membranes can be used for aqueous applications as well as for SRNF, provided that a suitable porous support is chosen and that modifications to the toplayer are made, if necessary.

3. Mixed Matrix Membranes

3.1. Introduction

The increasing research done in the field of nanomaterials has led to a new class of membranes, where a connection between the inorganic and the organic world is established. Inorganic or hybrid nanoparticles are incorporated into a bulk phase, the polymer matrix (Figure 10). These membranes attempt to overcome the limitations of both polymeric and inorganic membranes. Inorganic membranes have a high fabrication cost, are difficult for up scaling and are brittle but often have superior separating performance along with a superior chemical, biological and thermal stability.[32] By using a flexible polymer as the continuous phase, the fragility of the inorganic membrane is less pronounced but a trade-off between permeability and selectivity should be taken into account. Other drawbacks of polymeric membranes are their poor resistance to contaminants and their low chemical and thermal stability.[42]

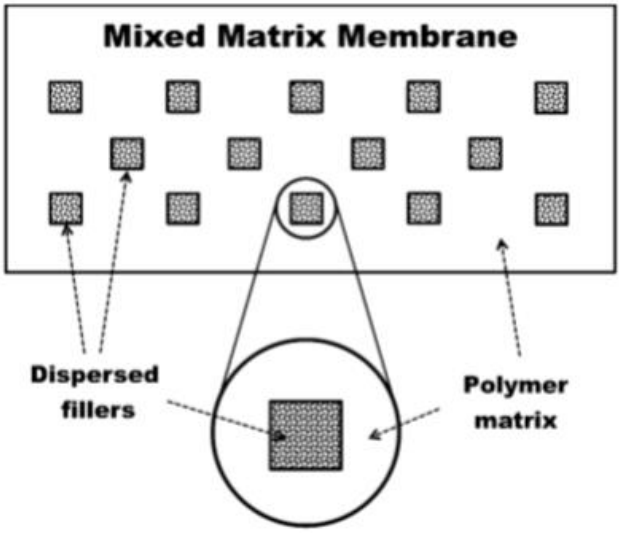

Figure 10: Structure of a Mixed Matrix Membrane.[42]

These hybrid organic/inorganic membranes are called mixed matrix membranes (MMMs) and will be further discussed in this section.

3.1.1. Models describing MMMs performance

To understand and predict the permeability and selectivity of MMMs, different analytical models were developed. Maxwell, Lewis-Nielsen, Pal and Bruggeman models all describe transport behaviour in MMMs, but are unable to describe the process accurately, according to Singh *et al.*.[43] None of them takes into account the influence of the adsorption equilibrium at the polymer/filler interface on the effective permeability. Furthermore, non-idealities, such as

polymer rigidification and interfacial voids, are not taken into consideration in these simple models, leading to possible erroneous interpretations.[43] Still, a brief description of the famous Maxwell model, based on permeability values, is provided to gain basic insight into MMM modelling.

a) Maxwell model

As predicted by the Maxwell model, the insertion of a small volume of inorganic filler can result in an overall increase in separation efficiency.[44] This model, initially based on the estimation of dielectric properties of composite materials, is now widely used for estimating the properties of MMMs. The relative permeability of species is given by equation (5),

$$P_r = \frac{P}{P_m} = \left[\frac{2(1-\Phi)+(1+2\Phi)\lambda_{dm}}{(2+\Phi)+(1-\Phi)\lambda_{dm}}\right] \quad (5)$$

where P_r is the relative permeability of species, P is the effective permeability of species in MMM, P_m is the permeability of species in the continues matrix, Φ is the volume fraction of filler particles, λ_{dm} is the permeability ratio P_d/P_m, where P_d is the permeability of species in the dispersed phase.[45]

Generally, MMMs are aimed at achieving higher permeability and selectivity compared to the pristine polymer membrane.[44] Especially the increment in permeability is confirmed by experimental results. The increase in selectivity is often the result of the molecular sieving properties of the incorporated porous particles [44] or of a strong interaction between filler and adsorbate. An illustration of this principle is the increase of CO_2/CH_4 selectivity in PSf-based MMMs up to 5 wt% Cu-benzene tricarboxylate (Cu-BTC) loading, compared to pristine PSf membranes, which is said to be the consequence of an increased diffusivity, generated by the filler.[46] Cu-BTC actually contains unsaturated Cu-sites to which CO_2 shows a high affinity.[47] The increase in flux of MMMs is depending on the porosity of the filler, providing preferential flow paths for the solvent.[48] It should be noted that the function of non-porous fillers differ from the function of porous ones. Non-porous, dense nanoparticles are incorporated into a glassy polymer to systematically manipulate the packing of the polymer chains, hence enhancing the separation properties of glassy polymeric membranes.[44]

3.1.2. Fillers

Typical solid fillers can be both porous and non-porous, zeolitic and non-zeolitic. The zeolitic ones consist of conventional zeolites, aluminium phosphates (AlPO's) and silicoaluminophosphates (SAPO's). The non-zeolitic fillers include carbon molecular sieves,

MOFs, activated carbon, silica and metal oxide nanoparticles. The use of MOFs as fillers has more advantages compared to the incorporation of other porous nanostructures such as zeolites.[48] MOFs contain organic and modifiable linkers, resulting in an increased affinity with the polymer. This would eventually lead to a more homogeneous distribution in the membrane. In addition, zeolites are rigid compared to MOFs, which are generally spoken quite supple. This agility permits alternation of their framework in presence of guest molecules[48] and a better incorporation in the polymeric matrix.

3.1.3. Incompatibility between filler and polymer

A big issue emerging with this recent class of membranes is the incompatibility between the inorganic filler and the polymeric membrane, resulting in defaults and voids in the MMM (Case 2, Figure 11). The interfacial voids give rise to a non-selective and less resistant pathway of the solute and are thought to be the major cause of the deteriorated performance of the membrane.[44] The permeability and flux will increase, but the rejection often decreases. The selectivity can decrease or maintain the same. The cause of the formation of voids is still under discussion. Vankelecom *et al.* researched the incorporation of zeolites in stiff polyimide membranes and concluded that the close packing, which is established in the bulk of the polymer, is disrupted near the zeolite particle, resulting in voids in the final membrane.[49] Mahajan reported that the voids are the result of simple repulsive forces between the polymer and the filler.[50] Li *et al.* claimed the interfacial voids arise from different expansion coefficients from the polymers versus the filler.[51] In order to resolve this adhesion problem, a wide range of surface modifications has been introduced. These modifications consist of (i) coating of the membrane with a diluted solution of a highly permeable silicone rubber to eliminate the unselective gaps often occurring in the polymers, (ii) addition of a plasticizer to reduce the intrinsic gas separation performance of polymers, (iii) using silane and amine coupling agents to improve both interfacial adhesion and gas selectivity by changing the surface properties of zeolites from hydrophilic to hydrophobic.[42] Other problems which can arise when the polymer comes in close contact with the filler are polymer chain rigidification and pore blockage, if a porous filler is used (Figure 11).[44] Rigidification (Case 3, Figure 11) occurs due to the lowered mobility of the polymer chains near the particle, compared to the ones in the bulk. Pore blockage (Case 4, Figure 11) takes place when the polymer invades the pores of the filler, which is obviously depending on the pore size of the inorganic filler. It is difficult to distinguish both phenomena and they are thought to occur simultaneously.[44]

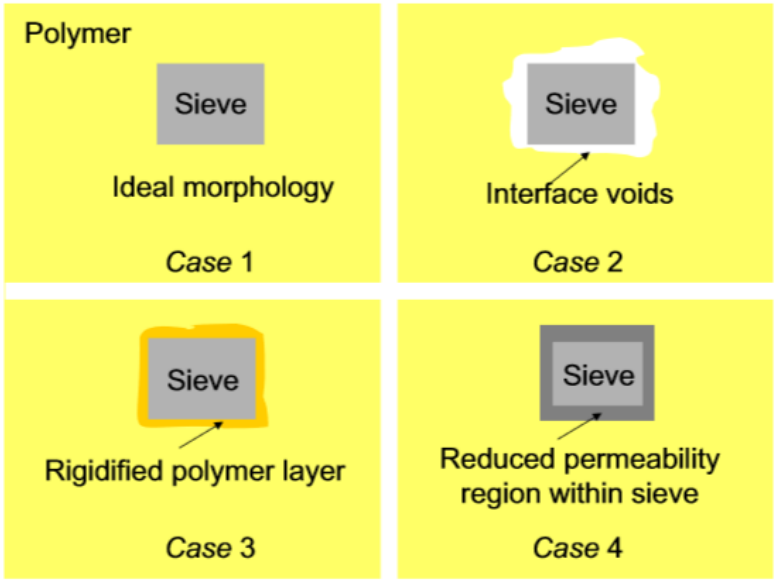

Figure 11: Schematic diagram of various morphologies at the particle/polymer interface in a MMM.[44]

3.1.4. Preparation technique

MMM can be prepared via several techniques. The most commonly used technique for making flat and dense MMM was described by Chung *et al.*.[44] A homogeneous mixture of polymer/inorganic/filler/solvent is synthesized, which is consecutively cast onto a smooth surface, often a glass plate. The solvent evaporates causing the formation of a dens film. Sometimes heat or vacuum treatments are performed to remove the residual solvent. Süer *et al.* performed three different setups for the drying stage and reported the different characteristics of the resulting MMM.[52] The first setup consists of normal drying at room temperature for one day and further annealing at 80-100 °C for 8-10 hours. In the second setup the film is placed at atmospheric pressure with nitrogen for 8-10 hours at 60-80 °C and consecutively quenched with water. For the following 16-24h, the film is dried under vacuum at 80-100 °C. The third setup is similar to the second, only the annealing step is performed in barometric conditions, while the drying step is executed under a partial pressure of N_2. The first setup gave rise to a highly permeable, non-selective membrane, letting pass all the gasses. The second and third setup gave both adequate and stable membranes. The matrix from procedure 3 is less dense, implying a higher permeation rate than the membranes made by procedure 2.[52] Vacuum degassing can aid to avoid voids between the polymer and the filler by eliminating air layer on the surface of the filler, in this case of a zeolite.[51] Li *et al.* examined the effect of the cooling procedure after the annealing step, i.e. natural cooling down or immediate quench. They conclude that a better separation performance was attained by the natural cooling down method because of the better adhesion of the polymer chains to the filler.[51]

3.1.5. Applications

The use of MMMs as gas separation devices was first discovered in the 1970s by observing the delayed diffusion time lag effect for CO_2 and CH_4 when adding zeolite particles to polydimethyl siloxane.[53] In the 1980s, UOP developed a silicalite-cellulose acetate MMM for gas separation purposes.[32] Ten years later, MMMs were developed for ethanol/ water separation via pervaporation.[54] From then on, these membranes are widely investigated for gas separations as well as for aqueous separations and SRNF. Increased performances of MMMs for gas separation, pervaporation, ion exchange and fuel cell applications are observed.[55] MMMs have at their disposal a broad panoply of other applications, e.g. sulphur removal[56], natural gas purification[57], olive oil wastewater treatment[58], bio-butanol recovery[59].

4. Thin Film Nanocomposite Membranes

4.1. Introduction

By incorporating a nano-sized filler in the toplayer of a TFC membrane, a so-called *thin film nanocomposite* (TFN) membrane is established (Figure 12). Another nomenclature used in literature for this recent class of membranes is *composite MMM*. This master thesis will especially focus on these membranes, which were first established in 2007.[60]

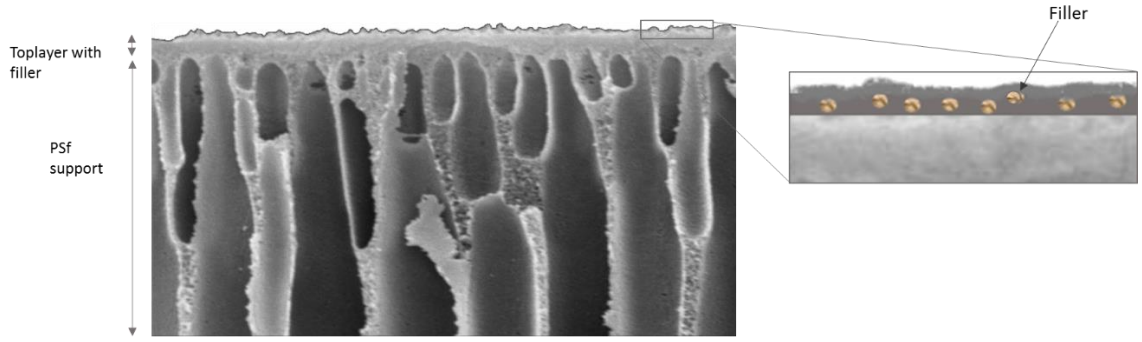

Figure 12:Illustration of a TFN membrane. The support is made via phase inversion. The filler is incorporated in the toplayer, which is synthesized via IP.

An important difference between TFN membranes and other MMMs is that the size of the nanoparticle can match the film layer thickness, providing a preferential flow path of the feed through each particle.[55] The question remains if the filler provides an increased separation efficiency or only an increased permeance. This aspect is currently highly investigated in literature. TFN membranes, compared to MMMs, benefit from the possibility of optimising each layer individually for its own function, allowing a more versatile membrane to be tailored.[22]

4.2. Preparation technique and reaction conditions

Methods of fabricating TFN membranes include IP, solution mixing and polymer melt blending techniques.[61] IP is the most commonly used method and was first reported in 2007.[60] The filler can be added to the organic as well as to the aqueous phase, depending on the filler properties. Addition of fillers to the organic phase is most commonly adopted. The filler can also be deposited on the surface by dipping a TFC membrane in the nanoparticle solution.[9] PSf, PES and PI polymer membranes are used as porous supports. In general, a certain amount of filler, ranging from 0.004 to 4 wt%, is dispersed via ultra-sonification in the phase of interest. The upper limit is set by the ability of dispersion, the lower limit by the possibility of effective incorporation. From then on, the same procedure as in the standard IP procedure is carried out.

4.3. Fillers and their influence on membrane performance

Jeong *et al.* reported the first TFN membrane via IP, which consisted of incorporated zeoliteA nanoparticles into a 50 – 200 nm thick PA toplayer.[60] This lead to a dramatically improved permeability compared to pure PA membranes, while maintaining high salt rejections. These observations are consistent with the results of Lind *et al.*.[55] Sorribas *et al.* incorporated ZIF-8, MIL-53(Al), NH_2-MIL-53(Al) and MIL-101(Cr) in the PA layer via IP on a porous PI support, made via phase inversion.[48] They confirmed the formation of the PA layer in the presence of the different fillers, without observing non-selective voids. From all tested fillers, MIL-101(Cr) provided the best results. The permeance of methanol increased by 160% when incorporating this mesoporous filler, while remaining rejections of polystyrene above 90%.[48] The high rejection of polystyrene was declared by the well-formed PA layer, surrounding the filler, as well as by the good compatibility between the organic linkers of the MOF and the PA polymer. The permeance of the TFN membranes was said to increase with increasing pore size and porosity of the added filler.[48] This observation demonstrates that the pores of the filler serve as an extra flow path for solvent molecules. Others also investigated incorporation of ZIF-8. At 0.4 wt% ZIF-8 loading, the membrane permeance increased with 162%, while maintaining NaCl rejections above 98 %, compared to pristine TFC membranes.[62] Kim and Deng introduced hydrophilized ordered mesoporous carbons (H-OMC) in the PA thin layer, made via IP.[61] An increased water permeability was observed. Another approach to enhance water permeability consisted of the incorporation of amine-functionalised multi-walled carbon nanotubes (f-MWCNT).[63] Silica nanoparticles[64,65], MCM-41[66], TiO_2 nanoparticles[67] and graphene oxide[68], and others, were likewise reported as filler. From all incorporated fillers, it can be concluded that an increase in permeance is noticed, without observing a decrease in rejection. Hypothesized mechanisms for this enhanced permeance are (i) preferential flow paths of solvent molecules through the nanoparticles embedded in the thin film; (ii) increased membrane affinity for water (when incorporating hydrophilic fillers); (iii) changes in PA structure due to heat release from the hydrated filler; (iv) high solvent fluxes through the interfacial voids present between filler and PA.[62] The first hypothesis is widely accepted in literature[19,48,60,61,66], but the exact mechanism of permeability enhancement remains unclear.

4.4. PA morphology

The morphology of the final toplayer in TFN membranes, which is an important parameter in fouling sensitivity, is highly dependent on the incorporated filler. No unanimous conclusion about the roughness of the TFN toplayer can yet be drawn. Jeong *et al.* observed an increase in

hydrophilicity, a decrease in contact angle and the appearance of a smoother surface, with increasing zeolite A particle loading.[60] However, when silver nanoparticles and f-MWCNT were employed, an increase in surface roughness was discovered.[22,69] The characteristic ridge and valley structure is not always maintained when introducing fillers to the toplayer of TFC membranes.[62]

When zeolites added to the organic phase encounter hydrated MPD molecules from the aqueous phase, they will get hydrated and release heat. At higher temperatures, the miscibility of both phases increases, producing less dense and more permeable films.[55] Nevertheless, in practice, TFN membranes do not always appear thinner than the corresponding TFC membrane.[55] This is also observed when incorporating ZIF-8 in the PA toplayer, as no big changes in selective layer thickness between the TFN and TFC membrane were visible.[62] It was demonstrated that the increase in temperature results in a lower degree of cross-linking of the PA thin film, when adding the filler to the organic phase.[51,58] No change in cross-linking degree was observed when zeolites are incorporated in the toplayer through the aqueous phase.[70]

As is the case with MMM, undesired interfacial voids between the polymer and the filler can originate, having a detrimental effect on membrane performance (see 3.1.3). The polymer chain packing is unavoidably altered near the filler.

4.5. Performance

In general, an increased permeability with no decrease in rejection is observed for TFN membranes, compared to TFC membranes. One could assume that the increased permeability is the consequence of the non-selective voids and the altered packing, as mentioned above. Jeong *et al.* could disprove this hypothesis by incorporating a porous and a pore-filled zeolite.[60] A decrease in water permeability was perceived when using pore-filled zeolites as filler, suggesting that the zeolite pores do play an active role in water permeation. However, no significant differences in salt rejection were observed for pore-filled and pore-opened zeolite TFN membranes. This was explained by increased Donnan exclusion, due to the more negative zeta potentials of the nanocomposite membranes.[60] Even though this explanation is reliable, the contribution of the non-selective voids to the increased water permeation cannot be excluded.

4.6. Position and amount of incorporated filler in the toplayer

Currently, the positioning of the filler in TFN membranes is difficult to control. Particles can be located in the cross-section of the thin film as well as at the interface with the support layer.[60] Nevertheless, it was demonstrated that when NaA zeolites were dispersed in the aqueous phase,

a two-layered PA structure arose, with a low zeolite concentration in the denser top part, and a higher concentration in the porous sublayer. Dispersion of this filler in the organic phase resulted in a homologous toplayer, where the nanoparticles where embedded throughout the whole layer and near the surface.[70] Liu *et al.* proved that when dioxane is added to the organic solution, the embedded nanoparticles (SAPO-34) were located in the top region of the PA film and some extruded out of the dense layer. Without addition of the co-solvent, the particles were completely covered within the thin film.[71] This shows that it is certainly possible to tune the location of the filler in the selective layer. However, not much evidence is found in literature on this aspect.

In literature, little evidence is found to substantiate statements over the exact filler location. Often, electron microscopy cannot provide a high enough resolution to distinct the filler from the polymer, making it difficult to exactly locate the nanoparticle in the thin layer. On the other hand, when the resolution is sufficient and particles can be clearly distinguished in the PA layer, only few can be pointed out. Therefore, the amount of truly incorporated filler relative to the amount dispersed in solution should be quantified. However, these results are generally not reported in literature.

4.7. Applications

In 2005, NanoH$_2$O Inc. introduced industry's first TFN RO membranes, by incorporating a benign nanoparticle in the toplayer of a TFC membrane, hence dramatically improving desalination efficiency. Permeability increases of 50% to 100% are observed compared to traditional RO membranes, without noticing a loss in rejection.[72] Most TFN membranes focus on liquid separations, mainly on RO and NF.[22] Recent work from Sorribas *et al.* (2013) disclose the huge potential of TFN membranes for SRNF applications. TFN membranes, with 0.2 wt% MIL-101 as filler, showed a 100 times increase in permeance of THF/PS compared to commercial integrally skinned SRNF Duramem® membranes.[48] TFN membranes for gas separation also reveal promising results. Polymethyl methacrylate-grafted MWCNTs were embedded in the PA thin film, increasing the permeance with 29% and the CO_2/N_2 selectivity with 47%, compared to pristine TFC membranes.[22]

5. Metal-Organic Frameworks

5.1. Introduction

Metal-organic frameworks (MOFs), also called porous coordination polymers (PCP), are highly porous crystalline materials consisting of transition metal nodes connected via organic linkers. Thanks to their high structural and functional tunability, the research in MOFs is a rapidly evolving branch of materials chemistry. Loads of applications were already reported because of their many promising properties. High adsorption capacities and remarkably high surface areas make gas storage, separation processes and molecular sensing a possible field of applications for MOFs. Magnetic, semi-conductor and proton-conducting MOFs also have a lot to offer in several fields of science. Easy compatibilization with organic as well as with inorganic materials opens an exciting new world, ranging from electronic devices to food packaging materials.[73] Moreover, MOFs are well and truly a phenomenon in heterogeneous catalysis.

5.2. Zeolitic Imidazolate Framework

Zeolitic Imidazolate Framework (ZIF) materials are a subclass of the group of MOFs. 'ZIFs combine the advantages of MOFs with high stability and framework diversity'.[74] In comparison with other porous materials such as zeolites, it is demonstrated in Figure 13 that ZIFs and MOFs have a higher pore volume as well as a higher surface area. Still, it should be noted that the pores volume as well as the surface area varies with the synthesis protocol. Different synthesis routes will be discussed more in detail in section 5.2.1.a).

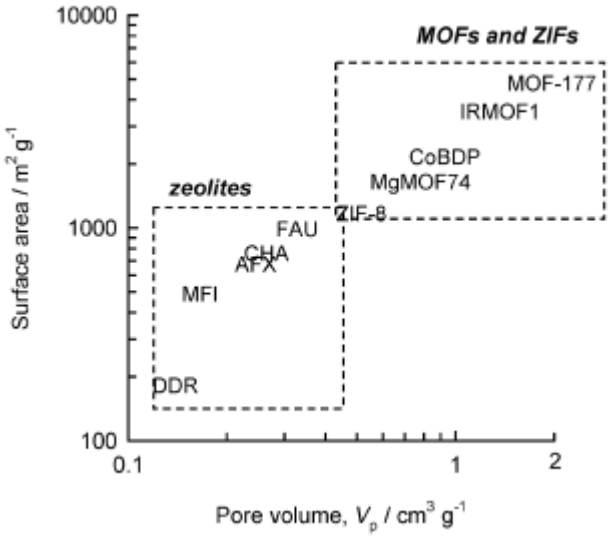

Figure 13: Data on surface area vs. pore volume for some representative zeolites, MOFs and ZIFs.[75]

ZIFs constitute of transition tetrahedral metal ions (M) (e.g. Cu, Zn, Co) which are linked by imidazolate ions (Im) and derivatives thereof. The resulting framework has topologies that are also found in zeolites, as the preferred bridging angle of 145° between Si-O-Si is also present between the M-Im-M (Figure 14).

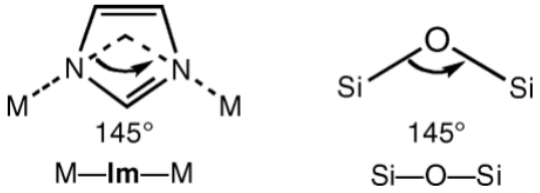

Figure 14:The structural similarity between a silicalite and a ZIF.[76]

5.2.1. ZIF-8

ZIF-8, the used porous material in this master thesis as filler in TFN membranes, was described in detail by Park *et al.*.[77] This catalytically active ZIF of sodalite topology has pore apertures consisting of 6-rings of ~3.4 Å in diameter and large cavities with a diameter of ~11.6 Å (Figure 15).[74] The transition metal is zinc (Zn) and the linker is 2-methylimidazolate. ZIF-8 exhibits excellent thermal stability up to 693 K[78] but depends on the particle size.[79] Its chemical stability in basic conditions is worth mentioning.[80,81]

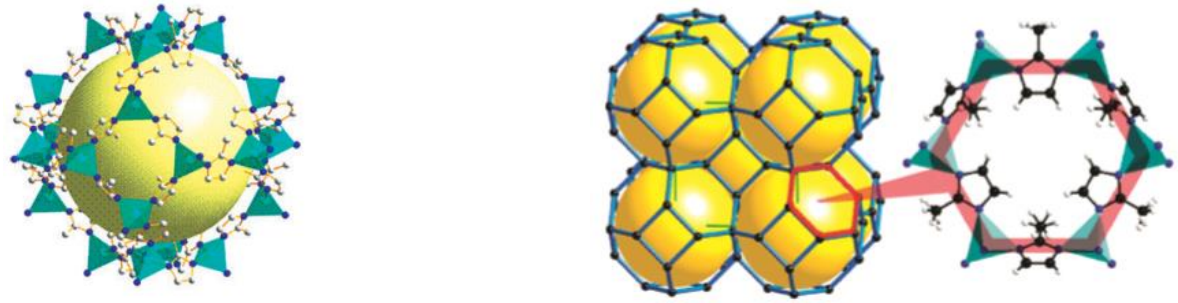

Figure 15:(left) Structure of ZIF-8[82] *, (right) Sodalite topology with 4 and 6-rings.*[83]

The small window size should make it possible to separate hydrogen (2.9 Å kinetic diameter) from other molecules such as nitrogen (3.6 Å) or methane (3.8 Å).[74] Nevertheless, experiments showed that molecules larger than the aperture where able to be adsorbed by ZIF-8, making the assumption a flexible framework plausible.[74] Fairen-Jiminez *et al.* proved that ZIF-8 is structurally modified during gas-adsorption[74], in the same way as at very high pressures (1.47 GPa), as was showed by Moggach *et al.*[84]. The structural change is caused by a reorganisation of the imidalozate bridges, resulting in an enlargement of the window size. This enlargement provokes on its turn the absorption and the elevated diffusivity of bigger molecules. Structural flexibility can also be induced be chemically tuning the linkers or by addition of other linkers.

By doing so the pore size and particle size can be varied, opening a whole new world of molecular sieving, adsorption possibilities and gas storage. Cravillon *et al.* investigated particle size tuning. Three monodentate ligands (sodium formate, 1-methylimidazole and n-butylamine) were used to tune the size of ZIF-8 crystals from 10 nm to 1µm.[79]

a) Synthesis routes

Various ZIF-8 synthesis routes were reported in literature. They consist of combining the transition metal salt (often zincnitrate hexahydrate: $Zn(NO_3)_2$ .6 H_2O) with the imidazolate units, by varying the solvent, the temperature and the drying procedure. ZIF-8 can for example be synthesized by the solvo-thermal route in DMF at 358-423 K.[83] Alternative routes are precipitation from methanol or aqueous solution at room temperature, steam-assisted synthesis, mechanochemical and ultrasound treatment.[78] Bux *et al.* reported a 4h micro-wave assisted route in pure methanol with addition of sodium formate, resulting in crystals from 300 µm.[83] Wee *et al.* prepared nanosized ZIF-8 (150 nm) from a synthesis solution which is 2.2 times more concentrated.[78] No excess solution nor chemical additives were used. The BET and Langmuir specific surface area are respectively 1388 m²/g and 2110 m²/g. The micropore volume equals 0.78 cm³/g. The activation of the ZIF was done in a vacuum oven at 423 K overnight. The yield was 53% based on zinc. Pan *et al.* reported the rapid synthesis in aqueous solution of ZIF-8 crystals, resulting in mean particle sizes of about 85 nm.[85] Venna *et al.* reported a synthesis route, at room temperature, with an excess of the 2-methylimidazolate, resulting in 50 nm crystals.[80] Cravillon *et al.* reported another route at room temperature in methanol.[79]

Venna *et al.* examined the structural evolution of ZIF-8 as function of time.[86] The entire process from gel formation to growth, passing by nucleation and crystallization, was reported. It was concluded that 100% crystallinity, proved with X-ray diffraction (XRD), was achieved after 24h in this protocol. The evolution of ZIF-8 in function of time can be divided into 3 stages. The first one consisting of the incubation stage, in which nucleation of the ZIF-8 phase occurs. The second one is the growth stage, in which the relative crystallinity increased and the third one is the stationary phase, in which the relative crystallisation rate remains constant. Cravillon *et al.* concluded that seed formation and crystal growth occur simultaneously during a few seconds.[79] As is always the case in a crystallisation process, the sZIF-8 crystallites grow at the expense of the surrounding metastable phase. The fraction of ZIF-8 phase increases until its nutrients are totally exhausted, resulting in a final ZIF-8 phase. The finalisation of this process

is a result of the Ostwald ripening mechanism. The big crystals grow at the expense of the smaller ones. The process is schematically drawn in Figure 16.

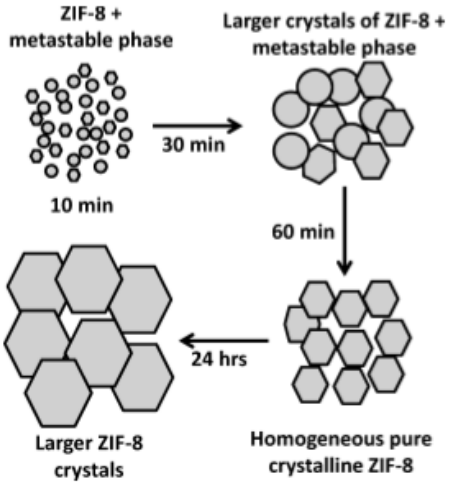

Figure 16: Proposed pathway of ZIF-8 synthesis in function of time.[80]

b) Applications

Thanks to the outstanding properties of ZIF-8, various applications are reported in literature, and many more should evolve in the near future. ZIF-8 is used as a selective sensor for chemical vapours and gases, as gas storage device, in separation processes and in catalysis.[85] Separations of ethane from ethene[87], propane from propene[88] and carbon dioxide from methane[89] were already reported. The synthesis of monoglyceride was another application of this very stable ZIF. Immobilisation of catalytically active nanoparticles in ZIF-8 is also new avenue of this new class of porous materials. The formation of membranes of ZIF-8 on an inorganic titania support was already investigated[83], as well as the formation on a polymeric support[90]. Incorporation of ZIF-8 in membranes, resulting in the formation of MMM, was also investigated by for example Dai *et al.* (2012) for the separation of CO_2 from N_2.[91]

Part II: Materials and Methods

1. Materials

1.1. ZIF-8

The chemicals used for the synthesis of ZIF-8 are:

- zincnitrate hexahydrate, Sigma Aldrich, >99%
- 2-methylimidazole, Acros Organics, 99%
- N,N'-dimethylformamide (DMF), Acros Organics, >99%
- methanol (MeOH), Fisher Chemical, 99.99%
- ethanol (EtOH), Fisher Chemical, absolute
- hexane, Chemlab, >99%

1.2. Support

The chemicals used to prepare the support are:

- non-woven polypropylene/polyethylene (PP/PE) fabric Novatex 2471, Freudenberg
- polysulfone (PSf) Udel P-1700, Solvay
- N-methyl-2-pyrrolidon (NMP), Acros, 99%
- polyimide (PI) Matrimid® 9725 US, Huntsman, Switserland

1.3. Functionalization of PI support

The chemicals used to chemically modify the PI support are:

- 4-aminobenzoic acid, Janssen Chemica, 99%
- 6-aminohexanoic acid, Sigma Aldrich, >98.5%
- triethyl amine (TEA), Sigma Aldrich, > 99%
- MeOH, Fisher Chemical, 99.99%
- milli-Q (MQ) water (18.2 MΩ.cm at 25 °C)

The chemicals used to test the binding capacity of functionalised PI are:

- zincnitrate hexahydrate, Sigma Aldrich, >99%
- ZIF-8 (self-synthesized)
- hydrochloric acid (HCl), Fisher Chemical, 37%
- milli-Q (MQ) water (18.2 MΩ.cm at 25 °C)

1.4. Toplayer

The chemicals used to prepare the toplayer are:

- trimesoyl chloride (TMC), Acros Organics, 98%
- m-phenylenediamine (MPD), Acros Organics, >99%
- hexane, Chemlab, >99%
- milli-Q (MQ) water (18.2 MΩ.cm at 25 °C)

1.5. Feed solution for filtration experiments

The chemicals used as feed solution for the filtration experiments are:

- rose Bengal sodium salt (RB), Sigma Aldrich
- sodiumchloride (NaCl), AnalaR Normapur
- milli-Q (MQ) water (18.2 MΩ.cm at 25 °C

2. Methods

2.1. ZIF-8 synthesis

Two syntheses procedures for ZIF-8 were adopted, referred to big ZIF-8 (bZIF-8) and small ZIF-8 (sZIF-8) below. To obtain bZIF-8 nanoparticles, the synthesis method reported by *Wee et al.*, was employed.[78] 2.9375g of $Zn(NO_3)_2.6H_2O$ and 6.48 g of 2-methylimidazole were separately dissolved in 50 ml DMF. The linker solution was added to the metal solution under stirring for 5 min. The solution was poured into a Duran Schott bottle and placed in an oven for 4 hours at 140 °C. The resulting solution was centrifuged for 15 min at 8000 r.p.m to separate the crystals from the supernations, and redispersed by the use of a sonification bath. Two washing steps were executed with EtOH, one with hexane. The ZIF-8 was stored in hexane until further use. All solutions were made and stored in polypropylene bottles to avoid electrostatic repulsion forces, as would be the case with glass bottles.

The second protocol used to obtain sZIF-8 was reported by Cravillon *et al.*.[83] 734.4 mg of $Zn(NO_3)_2.6H_2O$ and 810.5 mg of 2-methylimidazole are each dissolved in 50 ml of methanol. The linker solution is added to the metal solution under vigoures stirring for 10 minutes. The MOF solution is allowed to stand for 24h at room temperature, after which the solid is separated from the colloidal dispersion via centrifugation. From here on, the same protocol as for the bZIF-8 is followed.

2.1.1. Stability of ZIF-8 in MPD

0.05 g of big and small ZIF-8 were added each to 10 ml of a 2 wt% MPD/MQ solution. After sonification and thoroughly mixing for 2 hours, the solutions were centrifuged for 30 min at 2500 r.p.m. The remaining powder was dried at room temperature and analyzed via XRD.

2.1.2. Stability of ZIF-8 during IP conditions

In order to determine if the conditions of IP affect the morphology and/ or stability of the MOF, the process of IP was simulated in a syringe. The experimental set-up is shown in Figure 17**.** First, 5 ml of 0.1wt% TMC/ 0.1 wt% ZIF-8/hexane was sucked up, followed by the addition of 5 ml of 2 wt% MPD/MQ. On the interface of both solutions, the interfacial polymerization reaction took place and the film became visible to the naked eye. After 1 minute, the MPD and the TMC solutions were replaced by pure water and pure hexane, respectively, in order to remove any unreacted monomers present in the film and solution. This was done twice with the use of two small syringes, which were horizontally perforated through the big syringe: one in the organic phase, one in the aqueous phase. Subsequently, the solutions were removed by

sucking them away via the small syringes. The remaining film was dried at room temperature and analyzed via XRD.

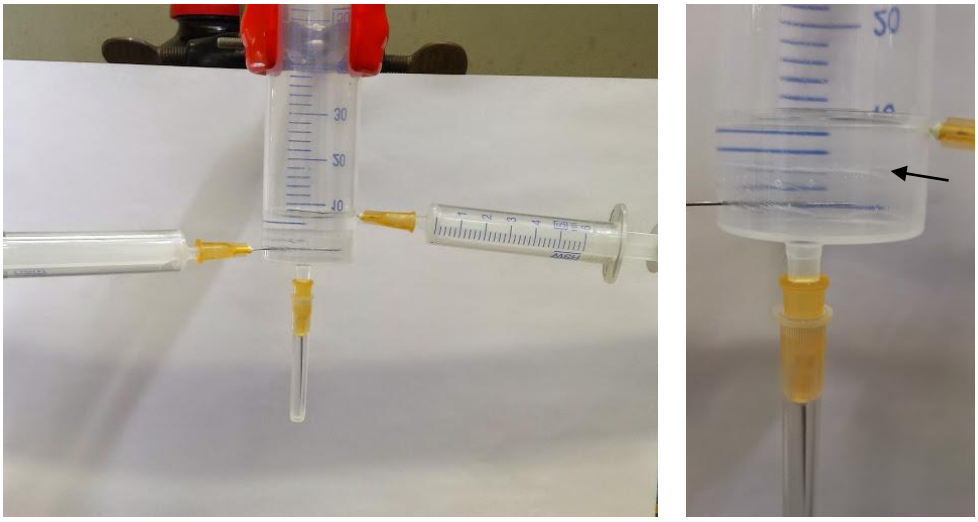

Figure 17: (left) The experimental set-up to test the stability of ZIF-8 during the conditions of IP. The two vertical syringes are used to replace the monomer solutions and to suck away the remaining liquid. (right) At the interface of both solutions (marked with the arrow), the IP reaction takes place.

2.1.3. MPD diffusion test

The diffusivity of MPD from the aqueous phase into the organic phase was tested with and without addition of ZIF-8 to the organic phase. As reference, 100 ml of pure hexane was added to 50 ml of 2 wt% MPD in water. With a small syringe, 1.4 ml was sucked up half way through the aqueous phase. The syringe was fixed on a metal stand so that the samples were always taken at exactly the same spot. This was done at different contact times (0, 1, 2, 4, 6, 8, 10, 15, 20, 30 min). To see if ZIF-8 had an influence on the diffusivity of MPD, a solution containing 0.1 wt% sZIF-8 in hexane was used instead of pure hexane. To simulate the TRAD method of making TFN membranes, the MOF solution was gently poured on the aqueous phase and samples were taken as described earlier. To simulate the ECFP method, the MOF solution was also poured on the aqueous phase, but the hexane was allowed to evaporate, resulting in deposition of the MOF on the water surface. 100 ml of hexane was subsequently added and samples were taken as described above. The general experimental set-up is shown in Figure 18.

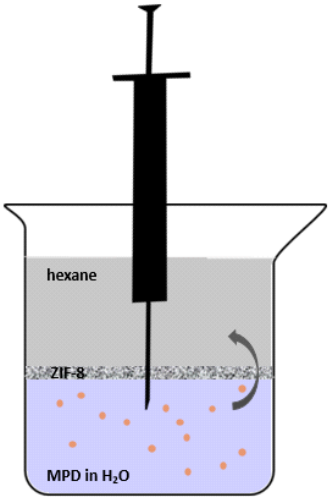

Figure 18: The experimental set-up to analyse the diffusion of MPD from the aqueous phase to the organic phase, in which ZIF-8 is dispersed. The MOF naturally accumulates at the interface. The sample is taken from the aqueous phase with a syringe.

2.2. Membrane synthesis

2.2.1. Preparation of PSf supports via phase inversion

The ultrafiltration PSf supports were fabricated by an 18% (w/v) casting solution of PSf in NMP. The PSf was first dried overnight at 110°C and added to pure NMP. The resulting viscous solution was stirred overnight to obtain a good dissolution and allowed to stand until all air bubbles disappeared. Casting was executed by an automatic casting knife (Braive Instruments, Belgium) onto a non-woven polyethylene/polypropylene support, which was attached to a metal plate and impregnated with pure NMP before casting. The casting machine was located in a room at 21°C. The casting knife was set at a thickness of 0.2 mm, moving at a constant speed of 77 mm/s. Directly after casting, the membrane was transferred into a water bath at room temperature and allowed to stand there for 10 min to complete the phase inversion process. The membranes were stored in distilled water until further use.

2.2.2. Preparation of PI supports via phase inversion

Ultrafiltration PI supports were fabricated by an 18% (w/v) casting solution of PI in NMP. The exact same protocol as for PSf supports, described in 2.2.1, was used.

2.2.3. Functionalization of PI supports

Six different solutions of 6-aminohexanoic acid (6-AHA) (1.25 wt%, 2.5 wt% and 5 wt%) in distilled water and in methanol were prepared. The same concentrations of 4-aminobenzoic acid (4-ABA) were made in MeOH, in addition to a 0.5 wt% concentration in water. Two other solutions were prepared by adding 10 ml of 2.5 wt% 4ABA to 0.625 g or 1.25 g TEA. Four small pieces (0.5 x 0.5 cm^2) of PI were placed in these 12 solutions for 1 h, after which they were stored in vials containing distilled water for minimum 5h.

a) Bonding capacity

The PI pieces placed in the solution, were taken out of the water, dabbed with a tissue and subsequently immersed in 10 ml of 0.1 % (w/v) $Zn(NO_3)_2$ in MQ-water or in 10 ml of 0.1 % (w/v) sZIF-8 in hexane . After 12h, the membrane pieces were removed from these solutions. For the Zn-containing membranes, the excess Zn solution on the surface was very gently removed with a tissue. For the MOF-containing membranes, the surface was rinsed gently with 5 ml MQ-water to remove any unbound MOF. Subsequently, an acid solution of pH 1.75 (HCl) was prepared and 10 ml of this solution was gently dropped on the surface of the membrane pieces. The Zn concentration in the resulting solution was analyzed via ICP.

2.2.4. Evaporation Controlled Filler Positioning (ECFP) method

The PSf support was placed in the amine solution (2 % (w/v) MPD in MQ-water) under stirring for at least 10 min. Different solutions of big and small ZIF-8 in hexane (0.0025, 0.005, 0.0075 0.01, 0.0125, 0.025, 0.1, 0.2, 0.4 % (w/v)) were made. As reference, no ZIF-8 was added. Only when using the bZIF, the solutions were sonicated with a finger sonicator for at least 1 min prior to the IP reaction. The membranes were removed from the amine solution and the excess solution was wiped off by the use of a rubbery wiper. A frame of 47 x 65 x 15 mm was placed upon the membrane and 12.5 ml of the ZIF-8 solution was poured in the frame and allowed to stand until all hexane evaporated (±18 min). Then, the solution of TMC in hexane (0.1 % (w/v)) was poured on the dry membrane surface. This was done very gently, to avoid redispersion and agitation of the ZIF-8 in this solution. After 1 min, the solution was removed and the membrane was washed with 30 ml of pure hexane to remove any unreacted TMC. The membrane was allowed to dry for 1 min before it was immersed in a water bath (10 min), to remove any unreacted MPD via diffusion. The membranes were stored in distilled water until further use. This synthesis protocol is schematically shown in Figure 19.

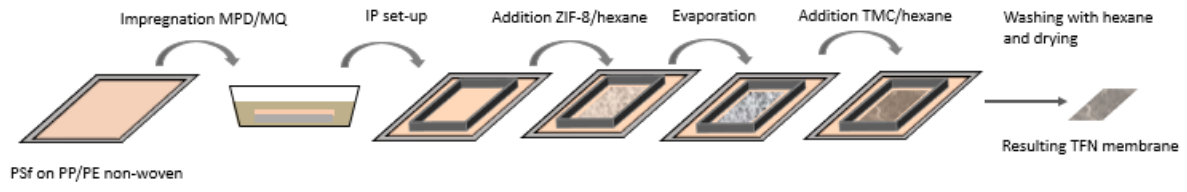

Figure 19: The synthesis procedure of TFN membranes made via the ECFP method.

2.2.5. Traditional TFN method

The PSf support was placed in the amine solution (2 % (w/v) MPD in MQ-water) under stirring for at least 10 min. The excess solution was removed by the use of a rubbery wiper. Different

ZIF-8/TMC in hexane solutions were prepared: 0.0025, 0.005, 0.0075, 0.01, 0.0125, 0.025, 0.1, 0.2 and 0.4 % (w/v). A frame of 47 x 65 x 15 mm was placed upon the membrane and 12.5 ml of this solution was poured in the frame and allowed to stand for 1 min. From here on, the procedure is in accordance with the ECFP method. The synthesis protocol of the TRAD method is schematically shown in Figure 20.

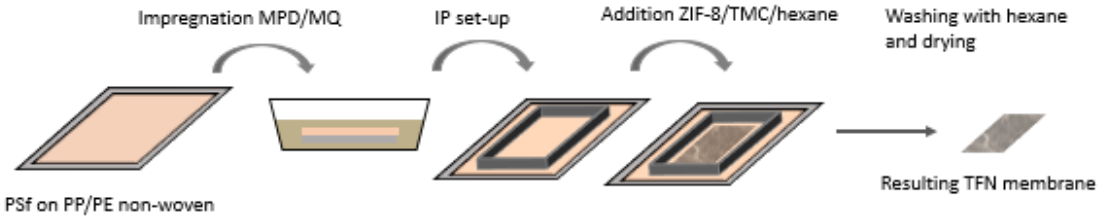

Figure 20: The synthesis protocol of TFN membranes via the TRAD method.

2.2.6. Traditional TFC method

The traditional method of making TFC membranes was executed on PSf supports. This was done in exactly the same manner as the traditional TFN membranes, except that no ZIF particles were added to the organic solution. TFC membranes operate as reference.

2.2.7. CMPI method

15.625 g TEA was added to 250 ml of a 2.5 wt% 4-ABA solution and vigorously stirred for one hour. PI sheets were put in this solution for 1 hour, after which they were displaced to a beaker containing distilled water. After 5 hours, the functionalized PI membranes were taken out of the water and used as substrate for interfacial polymerization, giving rise to a TFN membrane. Both the ECFP and TRAD method were used establish the thin toplayer. Their protocols can be found in sections 2.2.4 and 2.2.5.

2.3. Methods of characterization

2.3.1. Filtration experiments

The filtration experiments were carried out with a high throughput filtration module (invented at Centre for Surface Analysis and Catalysis, KU Leuven), in which 16 simultaneous dead-end filtrations can be executed under the exact same operating conditions. The active area of each membrane is $1{,}77*10^{-4}$ m². The pressure (N_2) was set at 10 or 20 bar and the feed was stirred at 400 rpm, to avoid concentration polarisation. The membrane performance was tested with a 35 µM solution of RB in IPA or with 1000 ppm NaCl in Milli-Q water. Steady state condition was reached before collection of the permeate of each membrane. By weighing the glass vials before and after the filtration and by measuring the filtration time, equation (4) can be used for

calculating the permeance. To convert the permeate mass to the permeate volume, the density of the used solvent is integrated in the formula. The rejection was obtained via equation (3), where C_f and C_p are the concentrations of, respectively, the final retentate and the permeate of the sample. These concentrations, for RB, were obtained via UV-VIS absorption measurements (UV-VIS Spectrophotometer, Schimadzu 1650) at 559 nm. The Lambert-Beer law is used to relate the absorption of light to the concentration of RB in the samples. To obtain rejections from the salt feed, conductivity measurements were performed (Consort multiparameter analyser C3010, Belgium). The Pt-electrode measures the conductivity of the feed, the permeate and the retentate, which is caused by the presence of Na^+ and the Cl^- ions. A linear relation between conductivity and concentration is observed, thus equation (3) is used to obtain the rejection of each membrane.

2.3.2. Attenuated total reflectance infra-red spectroscopy

Attenuated total reflectance infrared spectroscopy (ATR-IR) was performed on dried membrane surfaces as well as on MOF powders to analyse their chemical composition. The sample was placed upon a crystal, through which an IR-ray is send. The IR-ray was reflected several times on the interface with the membrane. By doing so, chemical bonds present in the toplayer and in the MOF can be characterized. A Bruker ALPHA-P FT-IR spectrometer with a diamond crystal was used with a resolution of 4 cm^{-1}. 64 scans were collected and every membrane surface was scanned at different spots.

2.3.3. X-ray photoelectron spectroscopy

To quantify the elemental composition of the membrane surface, X-ray photoelectron spectroscopy (XPS) measurements were performed with an ESCALAB 250 (Thermo Fisher Scientific), using an Al Kα X-ray source and fitted with a FEG1000 electron gun and an EX05 inert ion gas gun.

2.3.4. Dynamic light scattering

Dynamic light scattering (DLS) is used to determine the size distribution of small particles in suspension. A 90 Plus Particle Size Analyser of Brookhaven Instruments Coorporation is used for this purpose. The nanoparticles of interest are suspended in ethanol and three runs per sample are executed at 20 °C.

2.3.5. Electron microscopy

To characterize the cross-section and toplayer morphology as well as the pore structure, scanning electron microscopy (SEM) and transmission electron microscopy (TEM) are performed. In SEM, scanning of the sample with a focussed beam of electrons results in the

emittance of backscattered and secondary electrons. A detector detects these electrons in order to obtain an image of the sample. As sample preparation, the samples were first broken in liquid nitrogen and then coated with a thin layer of Au/Pd via a sputter coater (Jeol JFC-1300 Auto Fine Coater), with a coating time of 15 s. This is done to avoid charge accumulation on the membrane. TEM was performed to obtain information about the nanocomposite toplayer at higher resolution than SEM. The membrane samples are first embedded in an araldite resin (Polyscience). This resin is cut into ultrathin (70 nm) cross-section slices with the use of a Reichert Ultracut E microtome. The images were taken with a Zeiss EM900 microscope. Both SEM and TEM were also employed to characterize the ZIF-8 powders, in order to retrieves information on the particle size (distribution) and on the crystal morphology.

2.3.6. Inductively coupled plasma – optical emission spectroscopy

Inductively coupled plasma – optical emission spectroscopy (ICP-OES) is a chemical elemental analysis tool, used here to quantify the amount of trace metals in a sample. The plasma induces the excitation of atoms and ions, resulting in the emission of electromagnetic radiation at their proper characteristic wavelength. The intensity of the emitted light can be related to the amount of metal. Two spectrometers were used: the Perkin Elmer Optima 3300DV and the Jobin–Yvon Ultima. The measurement was performed at a wavelength of 213.856 nm.

2.3.7. X-ray diffraction

To determine the crystallinity of the synthesized ZIF-8, powder X-ray diffraction (PXRD) is performed with a STOE STADI MP apparatus in Bragg-Brentano mode (2θ-θ geometry; $CuK\alpha_1$), generating X-rays with a wavelength of 1.54060 Å. To attenuate the CuK_β radiation, a Ni filter is used. The diffracted X-rays are detected from -15° to 62°, via a linear position sensitive detector. The samples are placed upon a Kapton film in a sample holder, consisting of 16 positions. The obtained powder patterns are analyzed with WinXPOW software.

PART III: Results and discussion

1. ZIF-8 nanoparticles

1.1. Introduction

ZIF-8 was used as filler in the synthesized TFN membranes. Two different synthesis protocols were adopted in order to obtain nanoparticles of different sizes, referred to as big ZIF-8 (bZIF-8) and small ZIF-8 (sZIF-8). Both MOFs were characterized using different methods, including ATR-IR, XRD, SEM and DLS. The influence of the MOF on the resulting TFN membranes and its stability during the IP reaction will be discussed in the following sections.

1.2. Characterisation

1.2.1. XRD

The XRD patterns of the small and the bZIF-8 are shown in Figure 21, together with the simulated pattern from the crystallographic data of ZIF-8. The peak positions in the diffractograms of the self-synthesized ZIF powders were very similar to the theoretical ones[77], confirming ZIF-8 formation with SOD topology in both cases. From the diffractograms, it can be derived that the self-synthesized particles are highly crystalline.

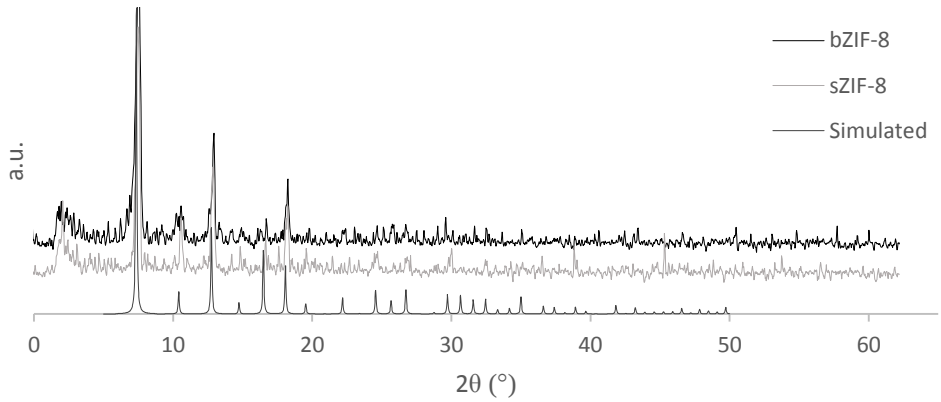

Figure 21: XRD patterns of sZIF-8 and bZIF-8. The simulated pattern, based on the crystallographic data[77], is shown for comparison.

1.2.2. SEM & DLS

SEM pictures of the big and small ZIF-8, respectively, are shown in Figure 22. Due to the resolution of the used electron microscope, blurry pictures were obtained from the powder sample of the sZIF, which made it difficult to observe the typical rhombic dodecahedron shape of the crystals. A particle size distribution (PSD) was calculated, respectively based on 98 and

124 experimental values for the bZIF-8 and sZIF-8, as obtained from the corresponding SEM pictures. It can be derived from Figure 23 (left) that 19% of the bZIF-8 nanoparticles had a size ranging from 150 to 155 nm, which is in accordance with the synthesis protocol.[78] As can be seen in Figure 24 (left), the PSD of the sZIF-8 was relatively symmetric. 43% of the sZIF particles had a size ranging from 75 to 80 nm, being roughly half of the size of the bZIF-8. The observed size was comparable to the size described in literature.[79] From the SEM images, it can be concluded that the sZIF crystals were certainly smaller than the bZIF crystals.

These PSDs were complemented with DLS measurements, which are based on the intensity of the scattered light. Intensity based distributions are more reliable than number based distributions, as less mathematical calculations and less assumptions need to be made. The PSD of bZIF-8 (Figure 23, right) showed that particle sizes of around 825 nm account for the highest intensity of scattered light. The median and mean diameters were 825.7 nm and 935 nm, respectively. For sZIF-8, the distribution maximum was situated around 240 nm (Figure 24, right). The median and mean diameters of the sZIF-8 nanoparticles were 240.4 nm and 245.9 nm, respectively.

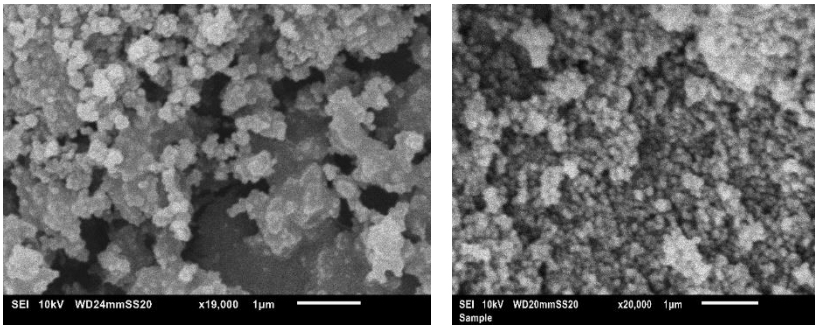

Figure 22: SEM images of bZIF-8 at a magnification of 19 000x (left) and of sZIF-8 at a magnification of 20 000x (right).

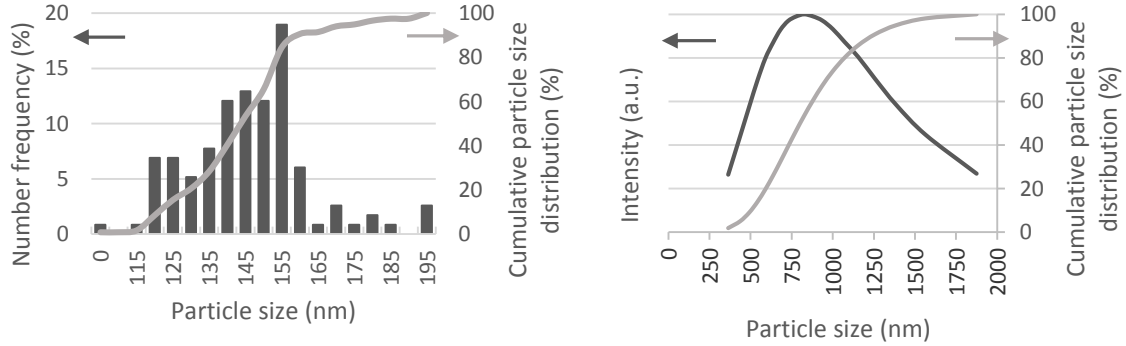

Figure 23: PSD of bZIF-8, based on SEM images (left) and via DLS (right).

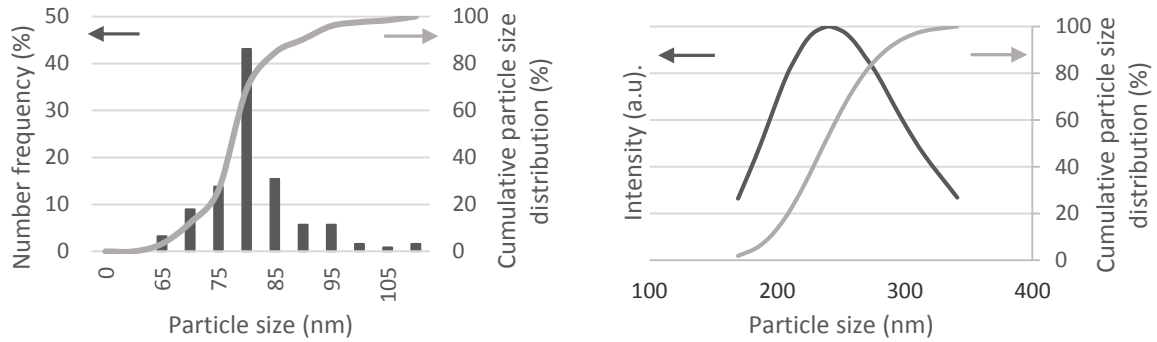

Figure 24: PSD of sZIF-8, based on SEM images (left) and via DLS (right).

The most abundant particle size of bZIF-8 nanoparticles obtained via SEM differed substantially from that obtained via DLS. This could be caused by several factors. Assumptions must be made for the calculation of the mean particle diameter based on DLS. The validity of the assumptions and of the instrument error are the parameters determining the quality of the calculated value. These large deviations between both characterization methods can most probably be ascribed to nanoparticle aggregation in solution, occurring for small as well as for big MOF nanoparticles. DLS does not take this into consideration, as it ideally presumes a monodisperse, non-aggregated system to derive the mean diameter. Therefore, the most abundant particle sizes that result from the PSD obtained via SEM images, were accepted as the true particle sizes.

1.2.3. ATR-IR

The ATR-IR spectra of the big and small ZIF-8 are shown in Figure 25. The typical bands assigned to this MOF were present in the spectra, confirming that ZIF-8 was well synthesized in both cases. The low intensity bands at 3135 and 2960 cm^{-1} were assigned to the aromatic C-H and aliphatic C-H stretches, respectively. The C-N absorption bands were found between 1100 and 1400 cm^{-1}. The peaks between 900 and 1350 cm^{-1} represented the in-plane bending of the ring, while the peaks at lower wavenumbers than 800 cm^{-1} were assigned to the out-of-plane bending. The bond between the metal atom and the organic linker, the Zn-N stretch, was observed at 425 cm^{-1}. These findings are in agreement with Vasconcelos *et al.*.[92]

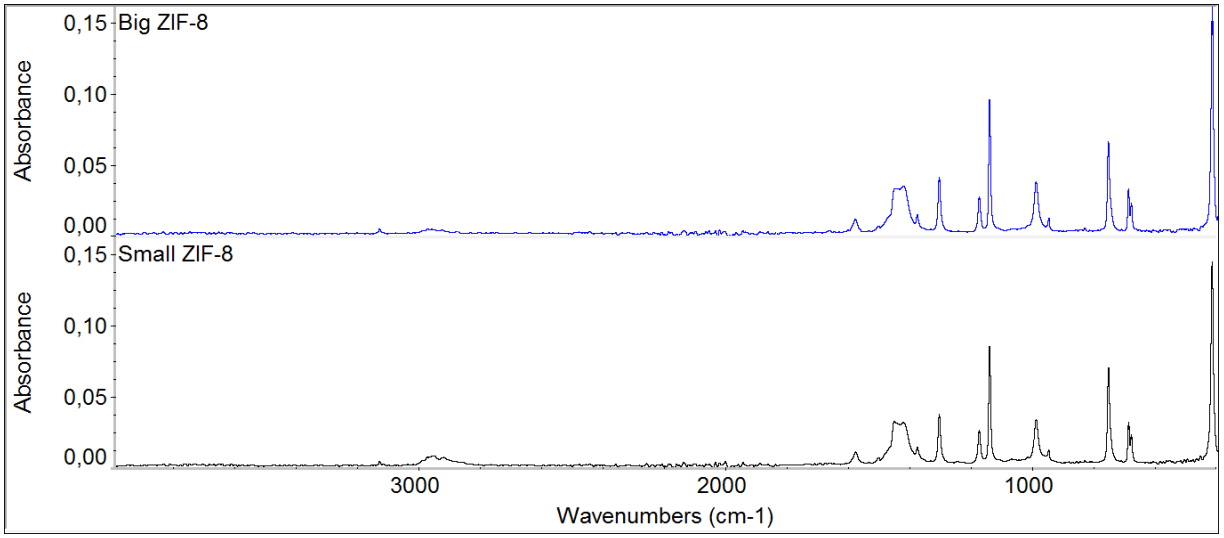

Figure 25: ATR-IR spectra of bZIF-8 (top) and sZIF-8 (bottom).

1.3. Conclusion

ZIF-8 nanoparticles were successfully synthesized and characterized. The average size of the particles was approximately 75-80 nm and 150-55 nm, for sZIF and bZIF, respectively.

2. TFN membranes

2.1. Introduction

The main purpose of TFN membranes is to obtain higher solvent fluxes than TFC membranes, without compromising solute rejection. Hypothesized mechanisms for this enhanced permeance are (i) preferential flow paths of solvent molecules through the nanoparticles embedded in the thin film; (ii) increased membrane affinity for water (when incorporating hydrophilic fillers); (iii) changes in PA structure due to heat release from the hydrated filler; (iv) high solvent fluxes through the interfacial voids present between filler and PA.[62] The first hypothesis is widely accepted in literature[19,48,60,61,66] but the exact mechanism of permeability enhancement remains unclear. Little evidence is found on the alternation of the PA toplayer when incorporating nanoparticles. These secondary effects of the filler are presumed to contribute likewise to the enhanced permeances. The changes in the structure of the selective layer (e.g. thickness, cross-linking degree, homogeneity, morphology surface hydrophilicity/hydrophobicity) as function of the size and amount of the incorporated filler were therefore investigated in this section. As it is believed that the location of the filler also plays a role in the membrane performance, TFN membranes were synthesized in an attempt to control the position of the incorporated filler in the PA toplayer via two new methods. Changes in morphology by varying the location of the filler were also investigated.

A first method, the so-called *evaporation controlled filler positioning* (ECFP) method, was developed to exactly control the position of the filler by allowing the organic solvent to evaporate. This results in the deposition of the filler on the PSf support as a dried uniform layer. By thus pre-positioning the MOF on the support, it is hypothesized that a higher filler loading can be achieved along with an exact positioning of the filler at the support/skin layer interface (Figure 26, middle). Secondly, the traditional (TRAD) method to make TFN membranes, as described in literature, was applied and used as the reference protocol.[60] The filler is dispersed in the organic phase and is caught at random in the thin film during the polymerization reaction. Therefore, no real control over the location and the amount of filler is possible (Figure 26, left). The third method, called the *chemically modified PI* (CMPI) method, consists of chemically modifying the porous support, in order to establish a coordinative bond between the support and the filler. Hereby, the filler is positioned at the top of the support layer, assumed to result in an improved incorporation in the toplayer while still providing an exact filler location (Figure 26, right).

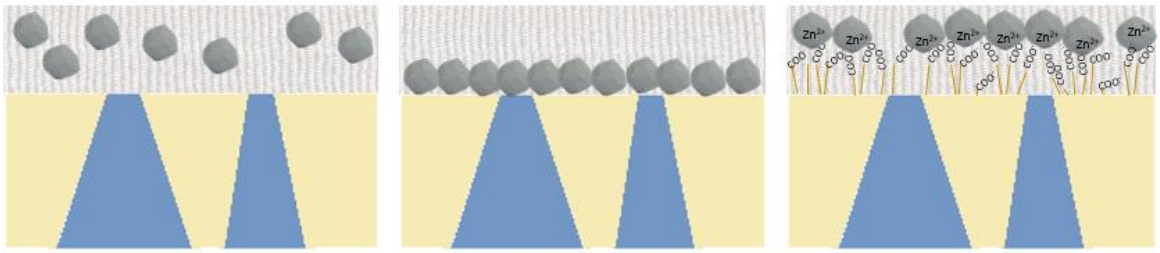

Figure 26: Illustration of the three methods used to synthesize TFN membranes. (left) TRAD method, where no control over the filler is possible; (middle) ECFP method, where the filler is located in the bottom part of the toplayer via deposition of the filler on the substrate; (right) CMPI method, where the filler is affixed to the porous support via the carboxyl groups present on the surface. ZIF-8 is represented as a grey particle. The porous PI Structure is showed in grey, while the toplayer is represented by the light brown striped rectangle

These three methods of making TFN membranes were analyzed separately in detail first, after which they were compared to examine which method produces the best performing membranes. In addition, the influence of the amount, size and position of the incorporated filler on the toplayer morphology and separation performance was investigated and compared to pristine TFC membranes, without filler. Special attention was paid to the stability of the MOF during interfacial polymerization. Different stability tests were executed to determine whether the ZIF crystals were able to maintain their properties and morphology during the conditions related to the polymerization reaction. Ultimately, the aim was to determine whether the primary or secondary effects of the filler contribute most to the enhanced performance.

A plethora of parameters influencing the morphology and performance of TFC membranes has already been well described in literature.[29,55,93] Therefore, as the main goal is to investigate the influence of the (amount of) filler and its way of being incorporated on the membrane performance, standard conditions for the synthesis of support and toplayer were employed, without detailed IP synthesis parameter optimisation.

2.2. Maxwell model for TFN membranes

The Maxwell model, primarily used to determine the selectivity and permeability of MMMs[42], was here adapted for TFN membranes. Equation (5) was employed to determine the increase in permeability when incorporating nanoparticles in the thick film. The possible contribution of the altered membrane morphology to the enhanced water flux is neglected in this model.

The Maxwell equation was applied on a TFN membrane with zeolite A as filler, described in the first paper that appeared on TFN membranes.[60] The relative permeability is equal to the ratio of permeabilities of the TFN and TFC membrane. The thickness was assumed equal for both membranes and the volume fraction of the filler was estimated via the obtained TEM image (Supplementary Figure 1), being 1.2%. The relative permeability P_r was plotted as function of

the permeability ratio (Figure 27). At very large values of , P_r asymptotically attained 1.0364. This means that, according to the Maxwell model, a maximal increase in permeance of 3.64% can be attributed to the incorporated nanoparticles. On the contrary, an increase of 200% was reported by *Jeong et al.*.[60] This suggests that other factors contribute in larger extent to the enhanced permeance. It is presumed that the secondary effects of the filler play a key role in the membrane performance.

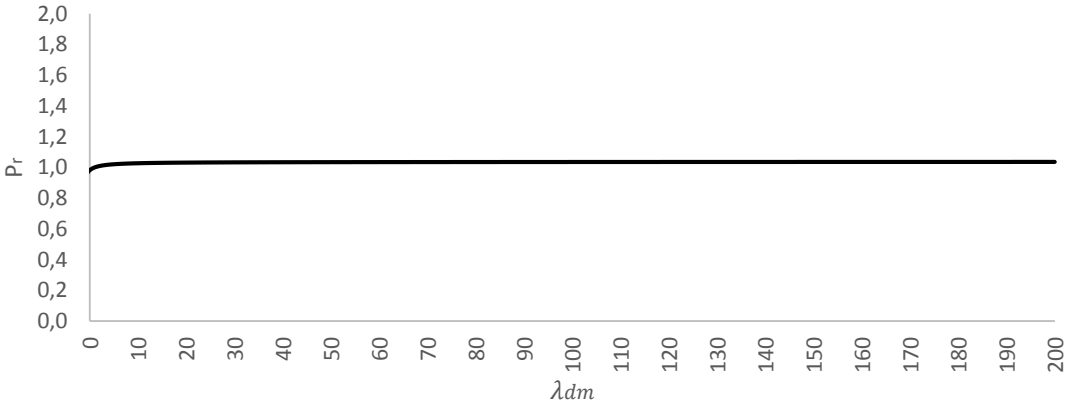

Figure 27: Maxwell model prediction for a TFN membrane.

2.3. ECFP synthesis method

2.3.1. Formation of PA

In order to investigate whether the PA toplayer was truly formed on the PSf support when nanoparticles were added to the organic solution, ATR-IR analysis of the membrane toplayer was executed. The ATR-IR spectra (Figure 28) of the prepared ECFP TFN membranes with bZIF-8 as filler showed the two typical bands assigned to the amide groups, present in PA. The amide I band (C=O stretch at 1610 cm^{-1})[94] and the amide II band (the N-H bend coupled to the C-N bend at 1540 cm^{-1})[94] were clearly visible, confirming the formation of a PA toplayer at all filler loadings, except for the 0.4 wt% loading. The toplayers of the membranes formed with this high filler concentration naturally peeled off from the support as a result of low adherence of the PA toplayer to the PSf support. This is thought to be caused by the lower contact area between the PA and the support as the MOF sits in between them. Adhesion forces that are normally responsible for the firm attachment of the toplayer to the support are consequently obstructed, resulting in places on the surface where no or loosely bound PA is formed. Therefore, only the membranes with filler loadings up to 0.2 wt% were further analyzed. The same explanation of PA formation was applicable for sZIF-8 as incorporated filler (Supplementary Figure 2).

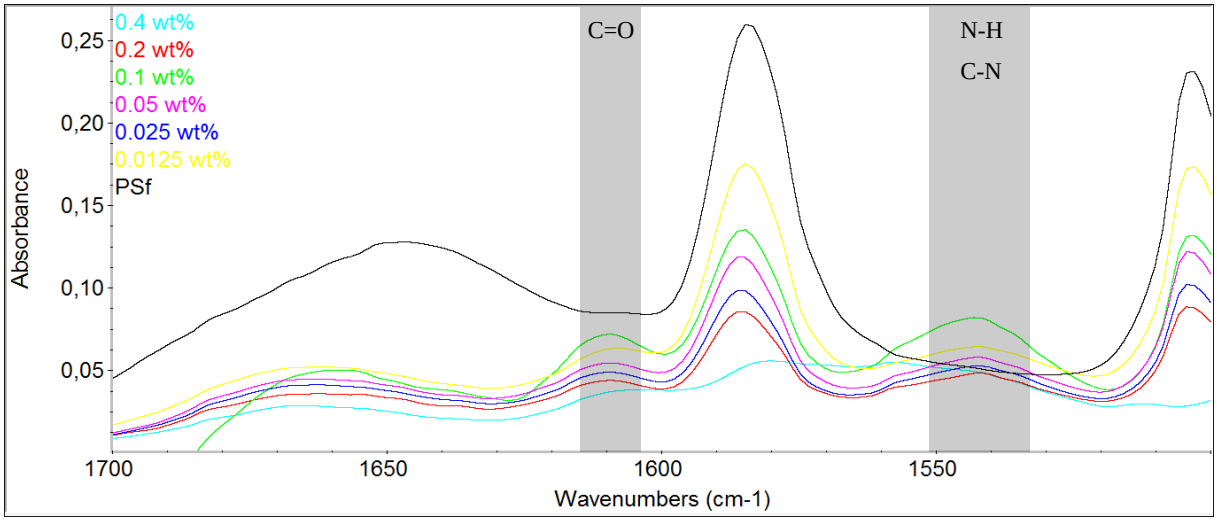

Figure 28: ATR-IR spectra of ECFP membranes, with bZIF-8 as filler. The typical C=O stretch is visible at around 1610 cm^{-1} and the N-H bend at 1540 cm^{-1} for all filler loadings, except for 0.4 wt%.

2.3.2. Incorporation of filler

IR analysis was also used to verify the presence of the filler in the toplayer. ZIF-8 strongly absorbs IR light at wavenumbers of 420 cm^{-1} and very little interference with the spectrum of PSf is present in this region. Therefore, this peak, attributed to the coordinative bond between the Zn^{2+} ion and the imidazolate linker, was used to verify the presence of the filler in the toplayer. As can be seen from Figure 29, the 420 cm^{-1} peak was present in the spectrum of 0.4 and 0.2 wt% bZIF-8 loading, confirming that the MOF is truly incorporated in the toplayer.

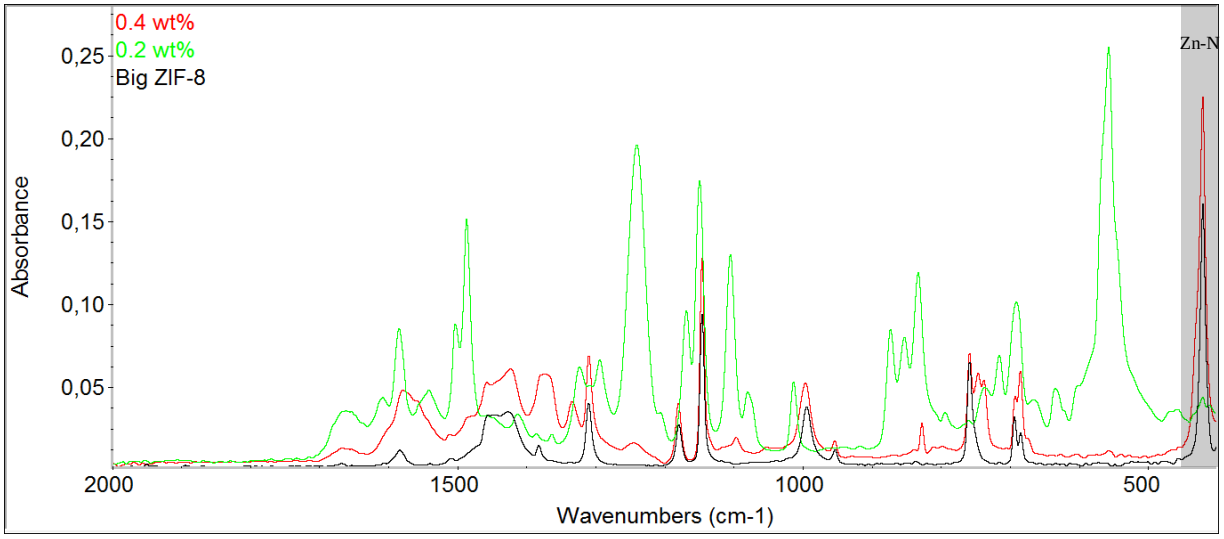

Figure 29: ATR-IR spectra to prove the incorporation of bZIF-8 via the ECFP method. The characteristic peak of the Zn-N bond around 420 cm^{-1} is visible in the spectra of high filler loadings.

At lower loadings, the characteristic peak disappeared. This can be due to the sensitivity limits of the ATR-IR technique. It was thus necessary to further seek confirmation of the presence of

the filler at low loadings with other techniques. For this purpose, SEM, TEM and ICP analysis were executed.

2.3.3. Quantification of filler

a) XPS

To quantify the amount of incorporated filler, XPS experiments were performed. As can be seen from the results shown in Table 2, the Zn^{2+} concentration in the TFN toplayer was relatively low. Nevertheless, these values are in agreement with or even higher than the values reported in literature.[62] According to XPS, there was no correlation between the amount of added sZIF to the organic phase and the amount of incorporated sZIF. Adding 0.01 wt% or 0.2 wt% resulted in the same amount of incorporated Zn, namely 0.1 atomic%. In contrast, a small difference in incorporated nanoparticles relative to the added amount was observed for bZIF-8 as filler. Addition of higher amounts of bZIF to the hexane phase resulted in slightly more incorporated nanoparticles: 0.13 atomic% for 0.005 wt% and 0.15 atomic% for 0.2 wt%. It should be underlined that the detected amounts were on the verge of the detection limit of the used XPS machine. Therefore, the observed difference may be insignificant.

Table 2: Elemental composition (in atomic percent) obtained by XPS.

Sample	Zn
ECFP SZIF 0.01 wt%	0.10
ECFP SZIF 0.2 wt%	0.10
ECFP BZIF 0.005 wt%	0.13
ECFP BZIF 0.2 wt%	0.15
Fully cross-linked PA	-
Reference PA[95]	-
ZIF-8	7.6923

2.3.4. Filtration results

a) bZIF-8

In order to test to which separation range the ECFP membranes belong, a filtration was carried out with RB in water as feed. The results are shown in Supplementary Figure 3. For all loadings, more than 90 % of the molecules were retained. Membranes accurately retaining RB are classified as UF/NF membranes as RB weighs 1017 Da, being right on the transition between UF and NF. In order to test whether the ECFP membranes had a RO separation capacity, the following filtrations were carried out with NaCl in MQ-water.

The performance of TFN membranes synthesized via the ECFP method using bZIF-8 as filler is presented in Figure 30. Before analysing the results, a note should be made on the standard deviations, as these were remarkably high. The reason for this is believed to lie in the non-

homogeneous presence of the filler on the membrane surface. ZIF-8 has electrostatic properties, causing it to be attracted and repulsed by the glass frame, used in the IP set-up. This process was visible to the naked eye. As a consequence, the different coupons cut from one membrane are believed to differ in amount of incorporated ZIF, hence influencing the filtration results. In addition, IP is a very sensitive technique, easily affected by several parameters.[27,29,93] It is therefore not uncommon to encounter high standard deviations on membranes synthesized via this technique.[96]

The average permeance of the pristine PA membrane was 0.95 L/m².h.bar with an average rejection of 85.99 %. Compared to the TFC membrane, addition of 0.0025 wt% bZIF-8 resulted in a comparable rejection, with a slightly increased permeance. The permeance further increased up to 2.75 L/m².h.bar when 0.005 wt% MOF was added, which is almost three times the value of the pure PA membrane (0.95 L/m².h.bar). As the rejection also remained high at this filler loading (82%), a TFN membrane with excellent properties was established at this low loading. At loadings up to 0.05 wt%, the standard deviations of the permeances partially overlapped with those of the permeance of the 0.005 wt% membrane, indicating that the difference between them was not statistically significant. The permeances of the 0.1 and 0.2 wt% membranes were significantly lower than that of the 0.005 wt% membrane, but still significantly higher than the pristine TFC membrane. This means that adding more nanoparticles to the organic solution not necessarily increased the permeance, suggesting that the primary effect of the filler was not dominating. This is in accordance with the prediction of the Maxwell model. Rejection is another important parameter determining membrane performance. The average rejection of the membranes from 0.0125 wt% to 0.2 wt% were significantly lower compared to the pristine TFC membrane, meaning that more salt molecules passed through when high ZIF loadings were introduced. As the 3.4 Å ZIF-8 pores can exclude 100% of the hydrated Na^+ and Cl^- ions[97], low rejections are presumed to be caused by the occurrence of unselective voids between the polymer and the filler or by aggregation of the nanoparticles.

Based on the permeance and rejection values, an optimal TFN membrane was found at 0.005 wt% bZIF-8 loading. Adding more filler to the membrane did not significantly improve its performance. From 0.05 wt% onward, the performance even deteriorated.

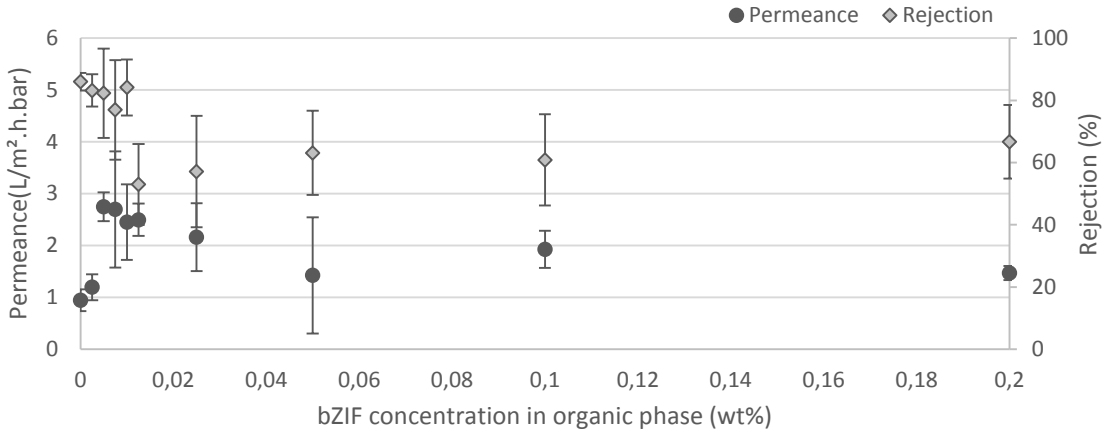

Figure 30: NaCl permeance and rejection of ECFP membranes with bZIF-8 as filler. Filtration conditions: 1000 ppm NaCl in MQ-water, 10 bar.

b) sZIF-8

The filtration results of the TFN membranes containing sZIF-8 as filler are presented in Figure 31. Compared to the pure PA toplayer, adding 0.0025 wt% had no significant influence on the membrane's permeance nor on its rejection. The average permeances of the TFC membrane and the 0.0025 wt% membrane were 0.82 L/m².h.bar and 1.04 L/m².h.bar, respectively. The average rejection of both membranes was around 65%. As the standard deviations partially overlap, the performance of the 0.0025 wt% and the 0 wt% were not statistically different. On the contrary, when adding 0.005 wt%, a significant increase in permeance was observed, without compromising rejection. The average permeance of this membrane was 3.15 times higher, compared to the pristine TFC membrane. The standard deviations on the rejections partially overlap, indicating that both membranes had rejections that do not statistically differ from each other. Therefore, incorporating 0.005 wt% sZIF clearly demonstrated the advantages that a TFN membrane possesses. Addition of 0.0075 wt% resulted in an increase in average permeance from 2.59 to 6.32 L/m².h.bar, compared to the 0.005 wt%. As these values statistically differ from each other, it can be concluded that incorporating 0.0075 wt% sZIF dramatically enhances the membrane's permeance. On the contrary, a significant drop in rejection was observed compared to lower loadings, which is undesirable. When incorporating 0.01 wt%, the permeance remained higher than the one of the 0 wt% membrane, but the average rejection dropped significantly to 44.8%. No significant increase in permeance was observed at loadings higher than 0.01 wt%, compared to the pristine TFC membrane, as high standard deviations on the permeances of 0.0125 and 0.025 wt% were present (0.87 ± 0.23 L/m².h.bar and 0.67 ± 0.36 L/m².h.bar, respectively). A decreasing trend in permeance was observed at higher loadings: from 0.05 wt% to 0.2 wt%, the average permeance decreased from 0.62 to 0.17

L/m².h.bar. The latter value is almost a factor 4 lower than the pure PA membrane, resulting in the loss of the main advantage of TFN membranes. This result was highly surprising and not observed in literature. The lowered permeance could be caused by the formation of a thicker or denser membrane when a big amount of filler is added. This suggests again that secondary effects play a more important role on the membrane permeance than the primary ones. TEM analysis was performed to test whether this hypothesis was true. As can be seen in Figure 31, the MOF loading only had a minor effect on the salt rejections, indicating that the typical trade-off between permeance and rejection was not present. This was also observed for the incorporation of NaA zeolites in the toplayer.[70]The average rejection of most of the TFN membranes varied from 50 to 70%, with often overlapping standard deviations. The 0.1 wt% membrane was an exception as it retained only 35% of the salt molecules. The 0.005 wt% membrane was another outlier, as it achieved an average rejection of 72.1 %.

The standard deviations on the rejection and permeance were still reasonably high, but remarkably lower than those of the ECFP membranes made with bZIF-8 as filler. This could indicate that a more homogeneous toplayer was formed when incorporating smaller nanoparticles. TEM and SEM analysis were used to provide information about the toplayer morphology.

Based on the permeance and rejection values, an optimum TFN membrane was found at 0.005 wt% sZIF-8 loading. Adding more filler to the membrane deteriorated the membrane performance by lowering its permeance or its rejection.

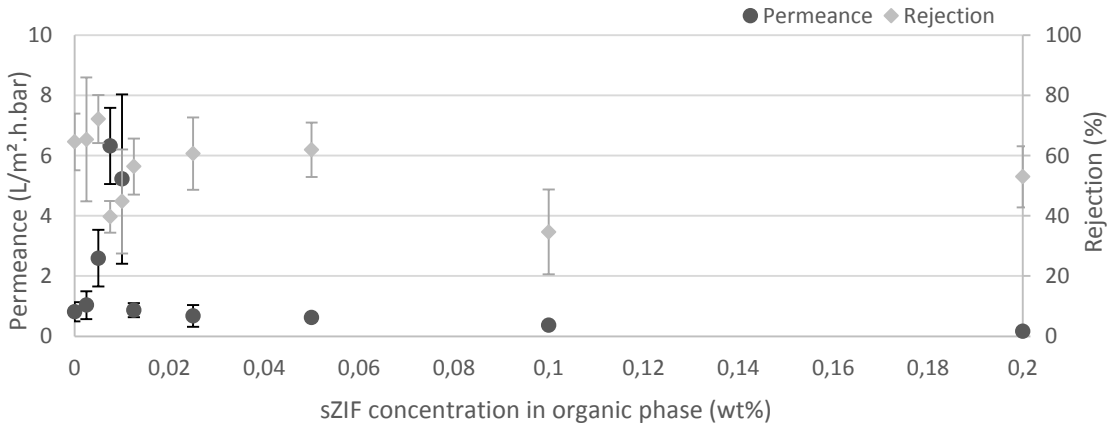

Figure 31: NaCl permeance and rejection of ECFP membranes with sZIF-8 as filler. Filtration conditions: 1000 ppm NaCl in MQ-water, 10 bar.

c) Comparison between small and bZIF-8 membranes

The influence of the particle size on the membrane performance is difficult to predict. On one hand, it is assumed that the membranes made with bZIF-8 are less performant than the membranes made with sZIF-8. The reason for this assumption is that the size of the bZIF lies in the same range as the thickness of the toplayer. The toplayer is about 150 nm thick and the bZIF particles have a diameter of around 150 nm. Therefore, it is possible that the particles are sticking out of the toplayer surface, and thus not completely surrounded by polymer. This is thought to create extra unselective voids and surface defects, and, as a consequence, deteriorates the membrane performance.[71] As the sZIF-8 nanoparticles only have a diameter of 80 nm, it is presumed that they are completely embedded in the PA layer, eliminating the occurrence of non-selective flow paths. Nevertheless, when the filler exactly matches the PA toplayer, the mist permeability increase is observed.[55] On the other hand, smaller particles are said to produce larger characteristic pores in the membrane toplayer, enhancing permeance more strongly compared to bigger particles.[55] Bigger particles can also template film growth, resulting in the growth of a thicker film than normal.[55] It is thus difficult to accurately predict whether the incorporation of big or sZIF-8 nanoparticles will result in a TFN membrane with the best properties.

When comparing bZIF-8 membranes with sZIF-8 membranes, one should take into consideration the performance of the pure PA membrane. The rejection of the pristine TFC membrane made during the same batch as the sZIF – TFN membranes, was 65 %, being 20 % lower than the TFC membrane made during the batch of the bZIF. The same trend was observed regarding the permeances, though it was less outspoken: 0.82 L/m².h.bar for the sZIF batch compared to 0.95 L/m².h.bar for the bZIF batch. These differences could be the consequence of several factors, e.g. room temperature[19], air humidity or contaminants. When comparing the performance of the bZIF membranes with the sZIF membranes, this aspect should be kept in mind.

In order to easily demonstrate the influence of the size of the filler, the permeances and the rejections of the TFN membranes made with both fillers were plotted together in Figure 32 and Figure 33, respectively. The rejections of the membranes made with big or sZIF at filler loadings above 0.01 wt% did not significantly differ from each other, as their standard deviations overlapped. This was also true for loadings of 0.0025 wt% and 0.005 wt%. The observed rejection when incorporating 0.0075 wt% and 0.01 wt% sZIF was significantly smaller compared to the same amount of bZIF. Regarding permeances, it can be concluded that

from 0.0125 wt% onward, incorporating bZIF nanoparticles resulted in significant higher permeances than incorporating sZIF nanoparticles. This is assumed to be caused by the formation a less dense or less thick film. In order to validate this assumption, TEM analysis was performed. At lower loadings, the standard deviations overlapped, indicating that the permeances of the big and small ZIF membranes did not differ statistically from each other. Only at a loading of 0.0025 wt%, sZIF incorporation resulted in significantly higher permeances compared to the addition of bZIF particles.

As the standard deviations often overlap, it was difficult to derive a trend regarding the influence of the particle size on the membrane performance. Nevertheless, it can be concluded that, at high filler loadings, incorporation of bZIF resulted in a significantly higher increase in permeance and a similar rejection, compared to the incorporation of sZIF. At low filler loadings, no real trend could be derived. However, the optimum TFN membrane was observed at 0.005 wt% for both sizes of incorporated filler. The rejection was similar to that of the TFC membrane, while the permeance increased with ± a factor 3. The rejection nor the permeance differed statistically between both fillers, proving that the diameter of the embedded nanoparticle had no influence on the membrane performance at the most favorable filler loading.

To relate the obtained filtration results to the membrane morphology, the obtained electron microscopy images are analyzed in the next section.

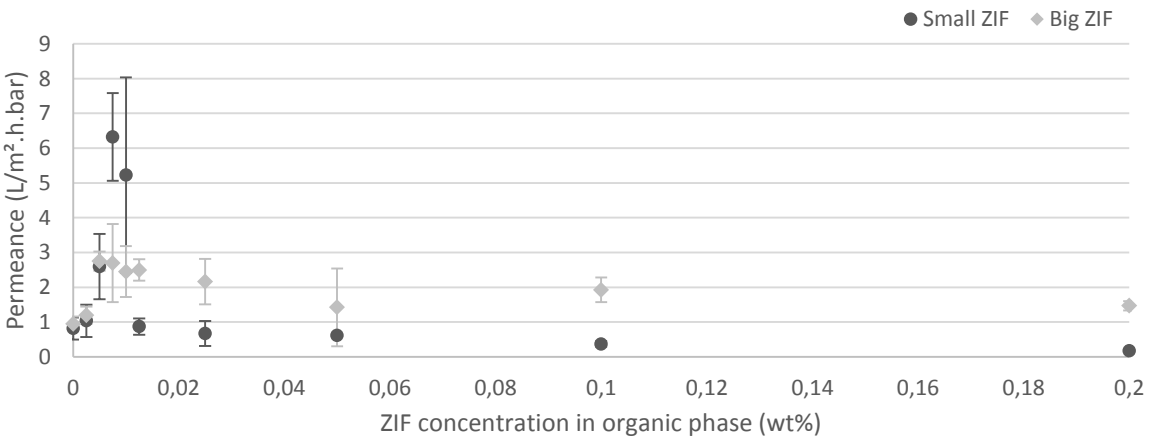

Figure 32: Comparison of the permeance between TFN membranes with sZIF and bZIF..

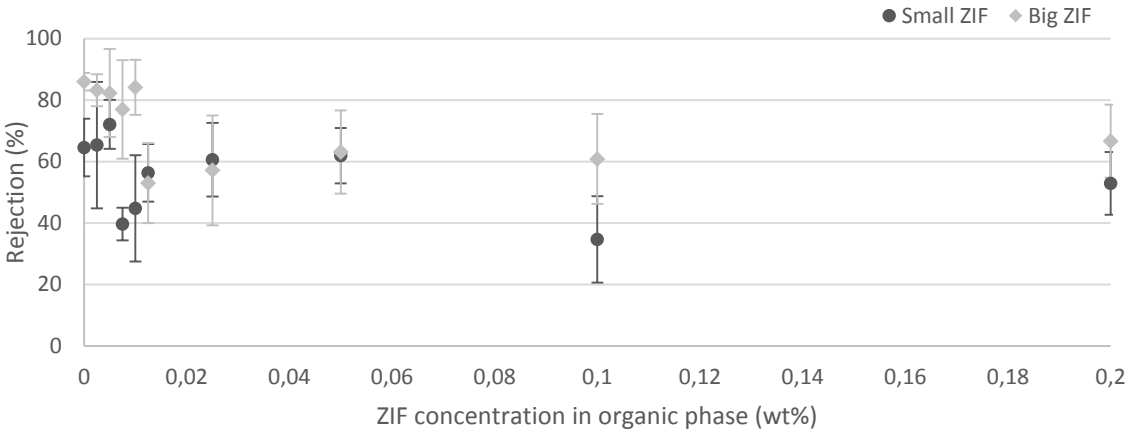

Figure 33: Comparison of the rejection between TFN membranes with sZIF and bZIF.

2.3.5. Toplayer characterisation

To study changes in active layer morphology as function of the amount of incorporated filler, SEM and TEM analysis were performed. SEM cross-sections as well as top view images were recorded, but, due to the resolution of the used electron microscope and the rugose structure of the toplayer, the incorporated nanoparticles were not visible. Not much information on the toplayer morphology nor on the toplayer thickness could be retrieved from cross-sectional images. Therefore, only toplayer SEM images are analyzed in this section. In addition, TEM was used to determine the thickness of the toplayer and to locate the incorporated filler.

a) SEM

bZIF

As can be seen from the images in Figure 34, different toplayers morphologies originated when incorporating different amounts of bZIF-8 via the ECFP method. The 0 wt% membrane showed the typical ridge and valley morphology, together with larger PA strings. These strings are not observed in PA RO membranes, synthesized via the traditional method.[23] This indicates that contacting the PSf support with hexane prior to the IP reaction had an influence on the toplayer structure. Adding 0.0025 wt%, 0.005 wt%, 0.01 wt% and 0.1 wt% bZIF-8 nanoparticles resulted in a more net-like structure, together with denser and flatter zones. These zones were visible by their darker colour. This net-like morphology is analogous to the TFC PA membranes formed with diethyl ether, ethyl acetate or acetone as co-solvent.[98] The SEM images of these TFC membranes are shown in Figure 35. Some SEM images of the self-synthesized membranes are shown in Figure 34, the others can be found in Supplementary Figure 4. Adding these co-solvents to the organic solution increases the miscibility between the organic and aqueous phase, hence enhancing the diffusivity of the amine. Toplayers with a loose PA structure over a dense PA structure emerge, resulting in membranes with higher fluxes compared to

membranes synthesized without added co-solvent. As the same fibre-like structure is observed when embedding certain concentrations of filler in the toplayer, it is presumed that the filler influences the amine diffusivity. In order to investigate this, a diffusion experiment was carried out. The results of this experiment are discussed in section 2.3.6 (Part III). The morphology of the membranes with 0.0075 wt%, 0.0125 wt% and 0.2 wt% was similar to the ridge and valley structure, but less pronounced. The 0.025 wt% membrane had characteristics from both types of morphologies. The top view of the 0.05 wt% membrane showed spots where no PA was formed on the PSf support. The inhomogeneity of the toplayer could account for the high standard deviations on the permeance. Nevertheless, it is improbable that coupons of membranes without PA toplayer are tested, as rejection would be extremely low and the permeance extremely high.

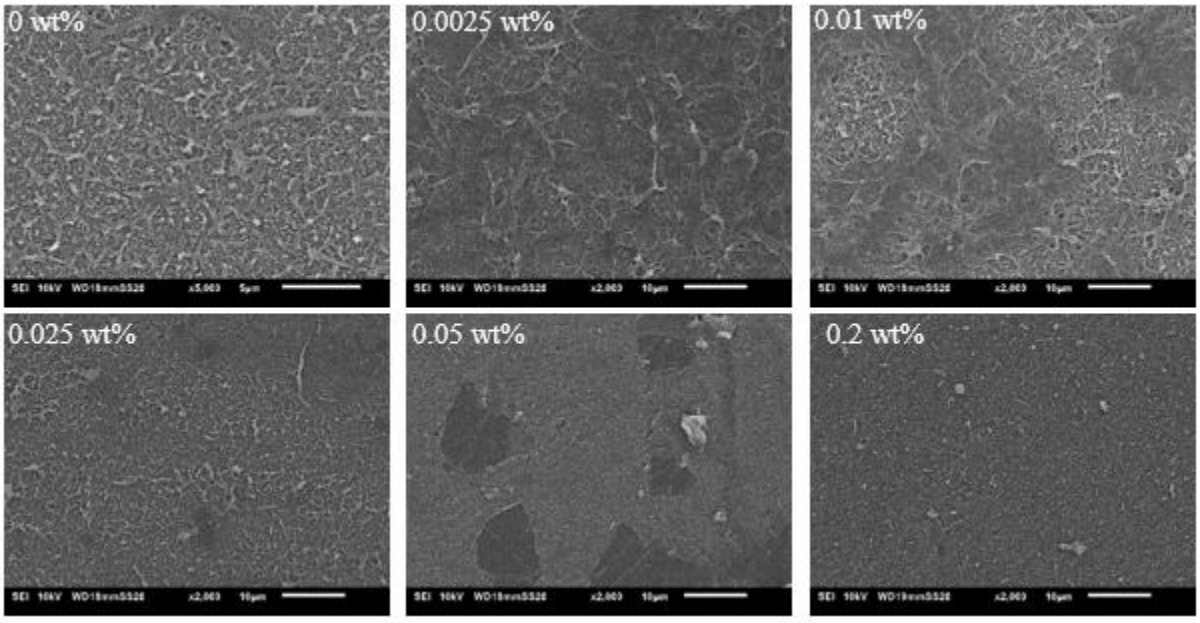

Figure 34: SEM images of the ECFP membranes made with bZIF as filler, at a magnification of 2000x. The filler loading is shown on the image.

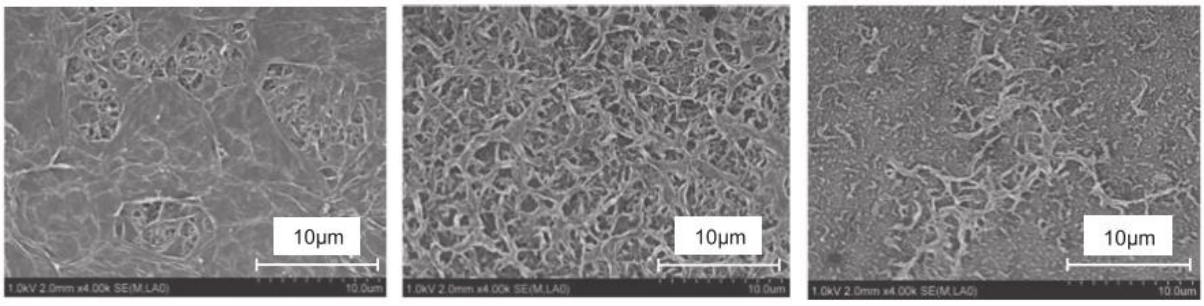

Figure 35: SEM images of the TFC membranes with added co-solvents. From left to right: acetone, ethyl acetate, di ethyl ether.

sZIF

A selection of the obtained SEM images is shown in Figure 36. The whole series is presented in Supplementary Figure 5. The toplayer of the unfilled membrane possessed the typical ridge and valley structure, together with larger PA strings. This is in accordance with the 0 wt% membrane, made during the bZIF batch. The toplayers of the 0.0125 wt% and 0.025 wt% membranes also showed a ridge and valley structure, but the presence of PA strings could not be confirmed on these images. Nevertheless, these strings are presumed to be present on other spots. All other self-synthesized membranes had properties of the net-like morphology as well as of the ridge and valley structure. A gradation was visible on the images, as can clearly be seen on the toplayer of the 0.005 wt% membrane. The ridge and valley structure is visible at the right side, while the net-like structure is present at the left side. In the centre, a denser zone is observed, analogous to the toplayer of the TFC membrane synthesized with acetone as co-solvent (Figure 35). The 0.2 wt% membrane had an outspoken net-like structure, with only small zones possessing the ridge and valley structure. From the SEM images, it can be concluded that the toplayer morphology greatly varied, not only from membrane to membrane, but also throughout one membrane surface. In addition, the morphologies of the TFN toplayers differed from their TFC analogue, suggesting that the introduction of the filler influences the toplayer formation.

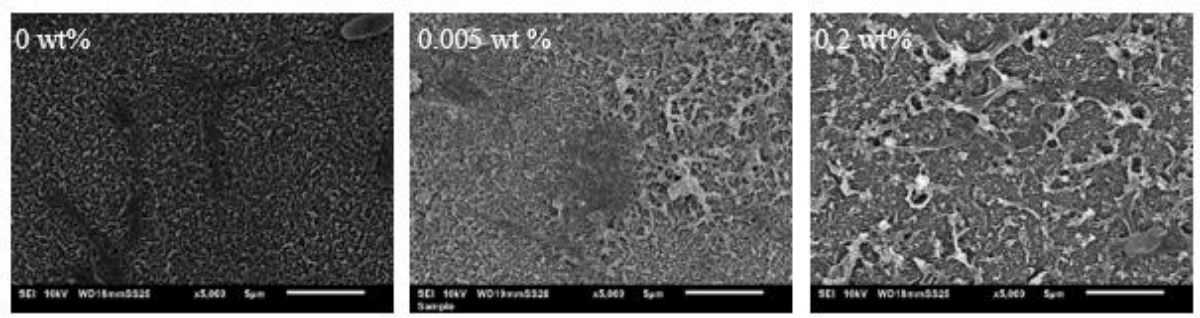

Figure 36: SEM images of the ECFP membranes made with sZIF as filler, at a magnification of 2000x. The filler loading is shown on the image

b) TEM

bZIF

TEM analysis was used to determine the thickness of the selective layer and to locate the embedded filler. The thickness of the dense nodular base of the PA toplayer of the TFN membranes was in the same order of magnitude as that of the TFC analogue, namely between 100 and 200 nm. Nevertheless, it was difficult to precisely determine the toplayer thickness, because of the resolution of the microscope and the rugose morphology of the thin film. Loosely

bound PA strings, present upon the dense toplayer were sometimes encountered, as can be seen in Figure 37 (0.0125 wt%). No relation could be derived between the obtained TEM image and the membrane performance, determined via the filtration experiments. In addition, the difference between the net-like and the ridge and valley morphology, as observed with SEM, was not easy to observe via TEM.

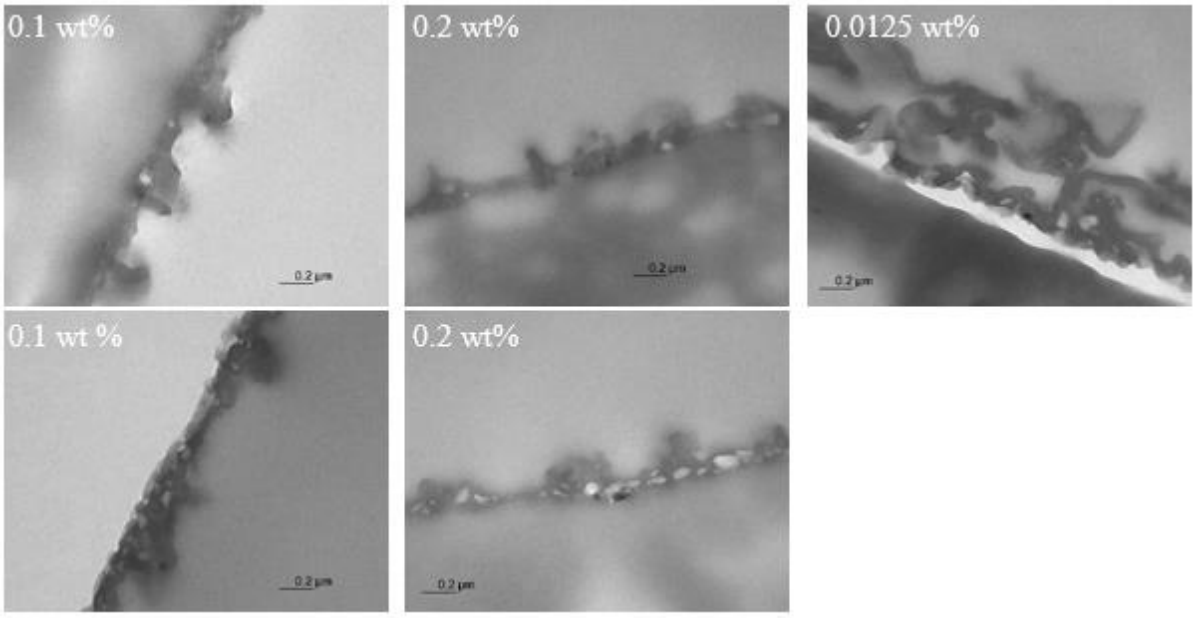

Figure 37: TEM images of ECFP TFN membranes with bZIF as filler. The different filler loadings are shown on the image.

Black spots, visible on some of the obtained images, are presumed to be MOF nanoparticles (Figure 37 and Figure 38). The black colour of the spot indicates that more electrons are absorbed by the heavier elements present in the crystal structure. The edges of the spots were not rounded, but sharp, which suggests the crystalline nature of the nanoparticles.

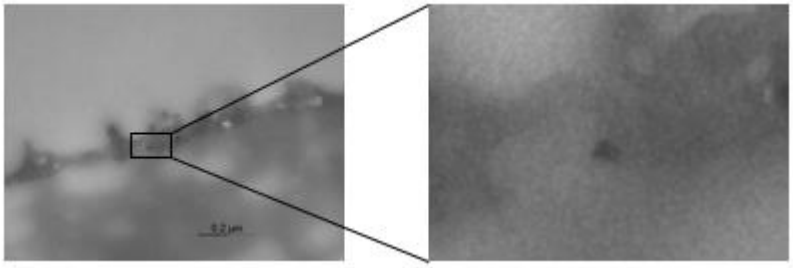

Figure 38: TEM image of an ECFP membrane, made with 0.2 wt% bZIF as filler. The inset shows that the particles are not round, but sharp.

However, the number of black spots was low, indicating that 100 % incorporation was not achieved. For the given example, only one nanoparticle can be pointed out on a cross-section of about 0.80 μm. Theoretically, assuming 100 % incorporation and a spherical shape of the filler, almost 8 multilayers of particles should be present. Nevertheless, this low degree of

incorporation is also observed by Jeong *et al.*, where only 2 nanoparticles are visible on a cross-section of 1 µm.[60] It is possible that the used microscope was not able to adequately distinguish the MOF from the PA strings, meaning that the particles were incorporated but not visible on the images. This inability to visualize the embedded filler is also encountered in literature, even with filler sizes up to 300 nm.[55] Another explanation for this substantial difference between the number of added and incorporated particles can be the (partial) degradation of the MOF during the IP reaction. A third possible reason for the low degree of incorporation is that the MOF diffuses from the organic phase to the water phase. This results in the loss of incorporated nanoparticles, as the IP reaction does not occur in the aqueous phase.[11,18,19]Another reason could be that the particles remain in the organic solution, which is disposed of after the IP reaction. In order to investigate which process takes place, stability and diffusion tests of the MOF were executed. Their results are found in section 2.5 (Part III).

When analyzing the cross-sections (Figure 37) in more detail, it can be observed that the filler was most of the time present near the porous support. This is assumed to be caused be the deposition of the filler as the hexane is allowed to evaporate during the ECFP protocol. Generally, fillers introduced in the organic solution, are mostly incorporated in situ during the interfacial reaction. Therefore, they reside mostly in the middle and top region of the selective layer.[61,67,70] This position differs from the one of the incorporated filler via the ECFP method. Therefore, the hexane evaporation step certainly had an influence on the position and visibility of the filler in the toplayer. ZIF-8 was more easily visualized on the TEM images compared to those presented in literature.[62]

sZIF

The 0.2 wt% membrane showed a much lower permeance, compared to the 0 wt% membrane. The reason for this is expected to be caused by a thicker or denser toplayer. This hypothesis is confirmed in Figure 39, showing a toplayer of ± 100 nm for the 0 wt% membrane and one of ± 500 nm for the 0.2 wt% membrane. Different parameters affect the thickness of the toplayer, e.g. temperature, reaction time, monomer concentration, miscibility enhancers, filler loading and filler size.[19,27,93] When ZIF nanoparticles come in contact with the aqueous MPD solution, they will hydrate and consequently release heat. This causes a less dense membrane, with a more permeable toplayer.[55] The opposite effect was observed here. Nevertheless, at lower loadings than 0.2 wt%, more or less the same thickness was observed as that of the 0 wt% membrane. This is in accordance with findings in literature[56,63], suggesting that the 0.2 wt% membrane was an exception. However, the toplayer thickness and morphology are not constant

throughout the cross-sections, proving that incorporation of nanoparticles altered the PA structure. This is illustrated in Figure 39 for the 0.1 wt% membrane, but was also observed at other loadings.

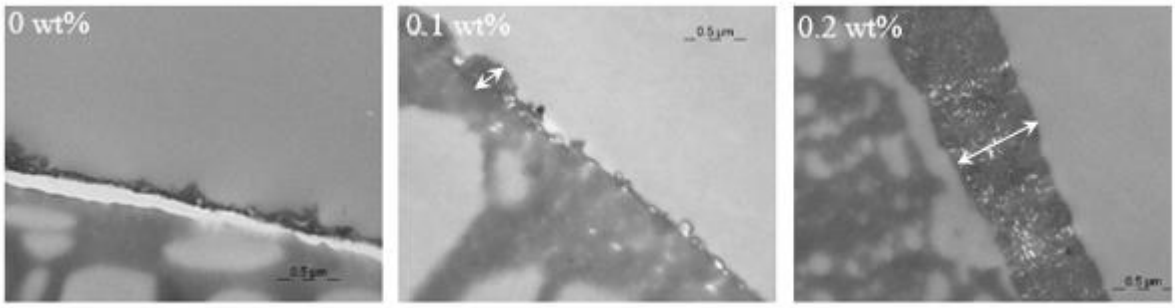

Figure 39: TEM images of the ECFP membranes, made with sZIF as filler. The thickness is indicated with an arrow, where possible.

The location of the incorporated sZIF nanoparticles in the toplayer differed from that of the incorporated bZIF particles. This can be seen in Figure 40, for several loadings. The small filler was more present in the middle and at the top region of the selective layer, than at the bottom. This is presumed to be caused by redispersion of the sZIF in the TMC/hexane solution, which is poured over the support, covered by nanoparticles. This redispersion is believed to occur to a lesser extent with the bZIF particles, as they weigh almost a factor two more than the small ones. Derivation of a direct relation between the position of the filler and the membrane performance should be done with caution, as many parameters can influence both properties. However, at high filler loadings, a higher permeance was observed when the nanoparticles were located in the bottom region of the PA layer.

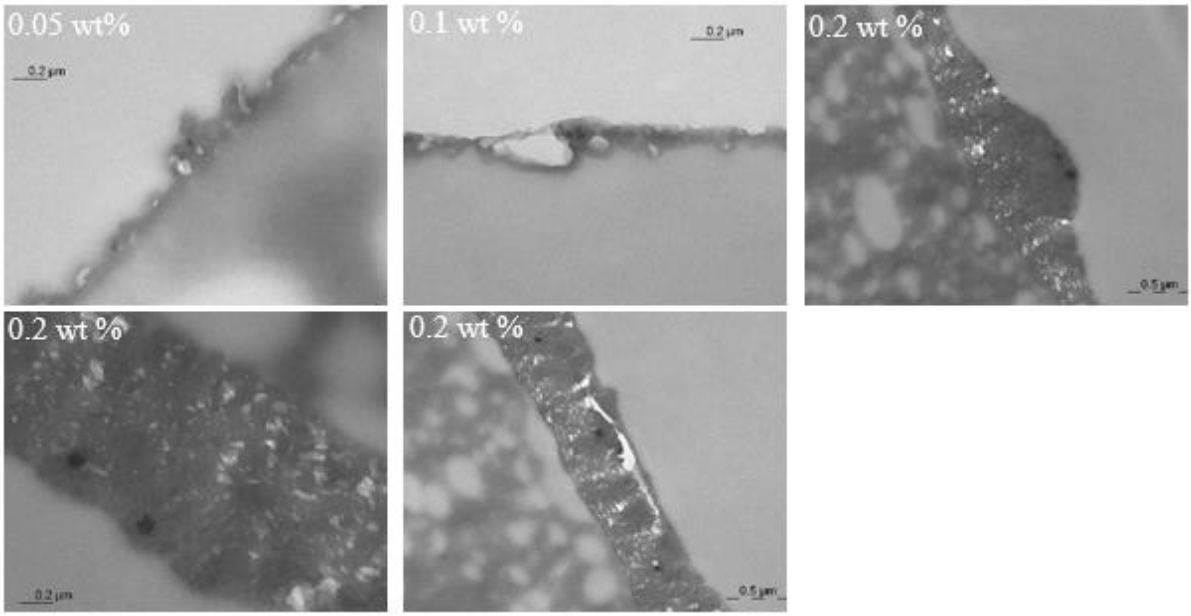

Figure 40: TEM images of ECFP membranes made with sZIF as filler.

c) XPS

XPS was used to study the chemical composition of the active layer. The results are shown in Table 3. Theoretically, a fully aromatic cross-linked PA layer consists of a C:N:O composition of 75:12.5:12.5. In practice, the ratio can vary during the polymerization reaction.[94] Higher C/N and O/N ratios can be assigned to higher concentrations of carboxylic acid groups in the thin toplayer, indicating that the toplayer is less cross-linked.[99] All TFN membranes had higher C/N and O/N ratios compared to the reference membrane, indicating that a less cross-linked toplayer is formed. This finding is confirmed by Duan *et al.*.[62] Incorporating sZIF-8 nanoparticles resulted in a higher degree of cross-linking than incorporating bZIF-8 nanoparticles, suggesting that the size of the filler plays a role in the cross-linking mechanism. The results suggested that the amount of added ZIF-8 to the organic phase was not a dominant factor on the degree of cross-linking. In general, it is accepted that a high crosslinking extent of MPD/TMC is needed to reduce permeance and achieve high rejection.[62] This was confirmed by the obtained filtration results for the 0.2 wt% membranes. On the contrary, the same trend could not be ratified for the 0.01 wt% and 0.2 wt% sZIF membranes.

Table 3: Elemental composition (in atomic percent) and ratios obtained by XPS.

Sample	C	N	O	C/N	C/O	O/N
ECFP SZIF 0.01 wt%	71.34	9.85	18.81	7.24	3.79	1.91
ECFP SZIF 0.2 wt%	73.00	10.05	16.84	7.26	4.33	1.68
ECFP BZIF 0.005 wt%	0.76	9.41	14.77	0.08	0.05	1.57
ECFP BZIF 0.2 wt%	72.88	8.58	18.38	8.49	3.97	2.14
Fully cross-linked PA	75.00	12.50	12.50	6.00	6.00	1.00
Reference PA [95]	72.60	10.90	16.50	6.66	4.40	1.51

2.3.6. Diffusion experiment

As mentioned before, it is presumed that the presence of ZIF-8 during the IP influences the diffusivity of MPD from the aqueous phase to the hexane phase. The experimental set-up is shown in Figure 18. Samples were taken from the aqueous phase at different contact times and analyzed via UV-Vis, to determine the amine concentration. The result from this experiment is shown in Figure 41, in which the aqueous MPD concentration, relative to the reference concentration at time 0, was plotted against the contact time. No real trend could be determined and high standard deviations were present. However, the hypothesis that ZIF-8 increases the diffusivity of the amine to the organic phase is countered by these results.

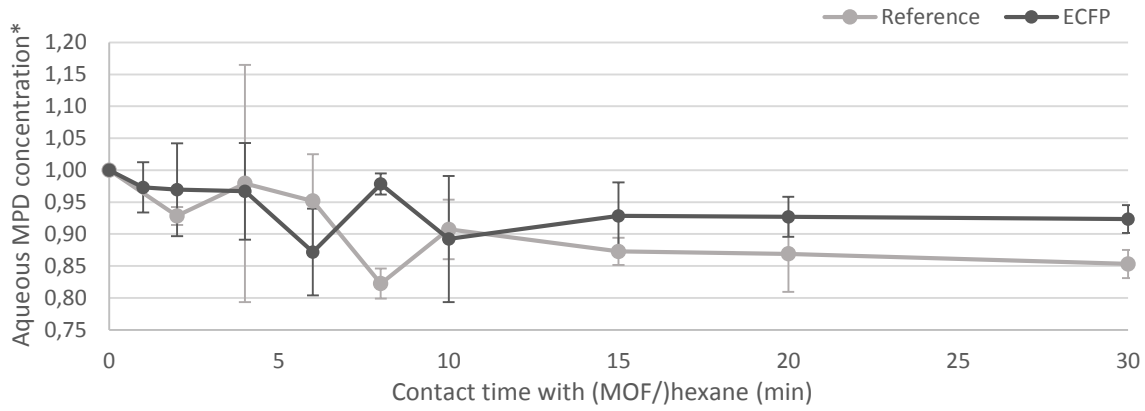

*Figure 41: Effect of added ZIF on the time course of MPD concentration in water, simulated on the ECFP method. The samples are taken right under the interface, in the aqueous solution. * relative to the MPD concentration at 0 min.*

As a consequence, the hypothesis that the net-like morphology of the toplayers (Figure 34 and Figure 36) is caused by an increased amine diffusivity is also countered by the above results. As the net-like structure arises from an increased concentration of amine in the organic phase, another theory is presented to substantiate the observed toplayer morphology. During the ECFP method, a solution of MOF in hexane is poured over the surface. As no TMC is present in this phase, the interfacial polymerization reaction is not initiated. Nevertheless, diffusion of MPD towards the organic place will take place, as it is fairly soluble in organic solvents.[100] As the

hexane is allowed to evaporate, the ZIF nanoparticles remain on the surface of the porous support. It is believed that the amine present in the organic phase is also deposited on the interface, possibly at the outer-surface of the MOF. In addition, capillary forces can suck the aqueous solution into the inter-crystalline voids, causing an increased MPD concentration at the interface. This is schematically drawn in Figure 42. When the TMC/hexane solution is then poured over the surface, the polymerization reaction takes place. The increased amount of MPD molecules alters the interfacial reaction and causes a net-like morphology to originate. Kamada *et al.* showed that a net-like structure occurs when more amine is present in the organic phase, caused by co-solvent addition.[98] Here, it is demonstrated that ZIF nanoparticles do not increase the diffusivity of the amine. Nevertheless, the increased MPD concentration at the organic side of the interface was caused by the hexane evaporation step during the ECFP protocol.

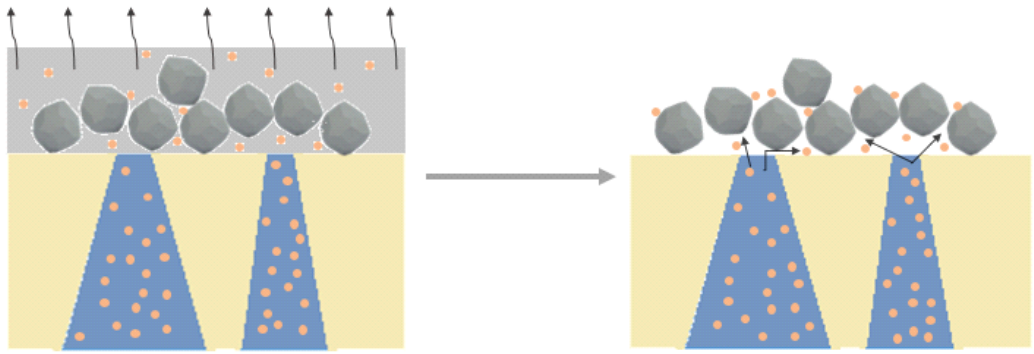

Figure 42: Schematic drawing of the increased MPD concentration at the interface, before (left) and after (right) hexane evaporation. Orange circles = MPD molecules, grey dodecahedrons = ZIF-8 nanocrystals, blue = aqueous solution present inside the pores of the PSf support (beige). The arrows indicate the capillary forces.

2.3.7. Conclusion

From the results shown above, it can be concluded that the optimum filler concentration lies at 0.005 wt% for both fillers, suggesting that it is mainly the weight/volume ratio and not the size of the filler that determines the membrane performance. At this loading, an increase of almost 220 %, compared to the TFC analogue, was achieved when incorporating sZIF nanoparticles. For bZIF, this increase was almost 200%. These results are promising as they greatly exceed those found in literature.[48,60,61,64,66,70,101,102] Only incorporating CNTs and silicalite-1 showed a greater enhancement of permeance, namely 233%.[103,104] The filtration results of the ECFP membranes showed that a further increase in permeance was not consistently present when increasing the nanoparticle concentration in the organic solution. This suggests that the primary effect of the filler is not dominating and that secondary effects play a key role in the enhanced membrane performance. This is in accordance with the Maxwell model (Part III, section 2.2). It was possible to locate the embedded nanoparticles in the selective layer via TEM. Although

only few particles were visible, their location seemed to be depending on their size. The bZIF particles were present in the bottom part of the selective layer, while the small ones were located in the middle and top regions. This is supposed to be caused by the redispersion of the sZIF particles in the TMC/hexane solution. The toplayers of the ECFP membranes often possessed a net-like morphology. However, some regions also contained ridge and valley structures. The net-like morphology was not caused by an increased MPD diffusion, but rather by deposition of the amine on the outer surface of the ZIF crystals when all hexane had evaporated. The toplayer thickness seemed not to be strongly dependent on the filler loading, neither on its size. Thicknesses varying between 100 and 200 nm were observed. Introducing nanoparticles in the toplayer lowered the cross-linking degree of the selective layer. This effect was more pronounced when big ZIF-8 crystals were introduced in the thin film.

2.4. TRAD synthesis method

2.4.1. Formation of PA

ATR-IR analysis confirmed the presence of a polyamide toplayer, formed via the TRAD method with bZIF-8 as filler. The spectra of these membranes are shown in Figure 43. The characteristic peaks for PA were present in the spectra of all filler loadings, except for the 0.4 wt% loading. Here, MOF aggregates lying on the surface were visible with the naked eye. In addition, the toplayer peeled off the PSf support, resulting in spots without a PA toplayer. These results were in agreement with the ECFP method.

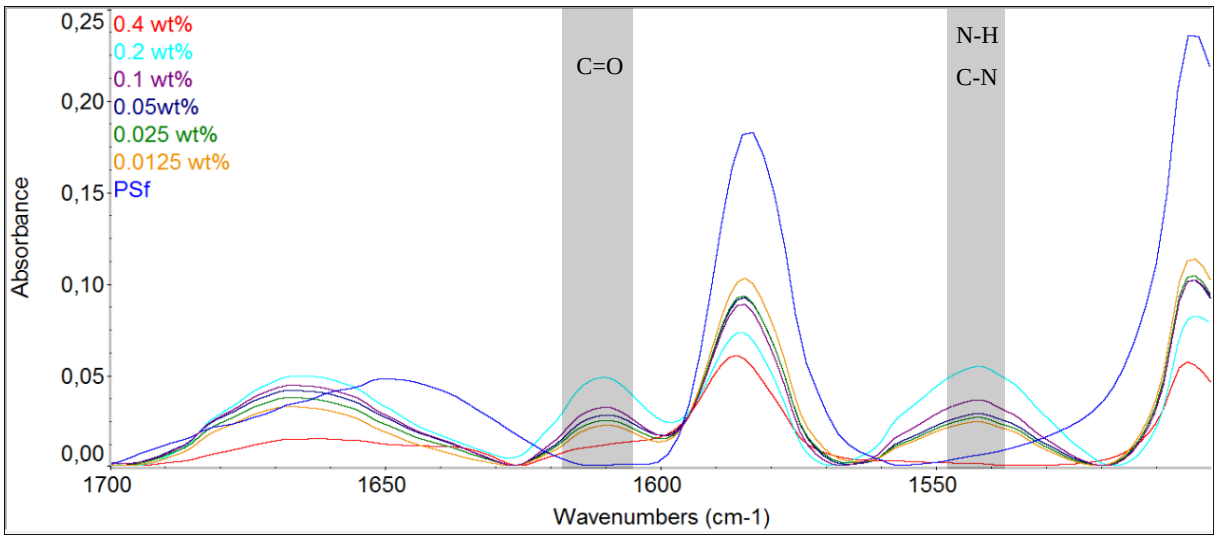

Figure 43: ATR-IR spectra of all TRAD membranes, with bZIF-8 as filler. The typical C=O stretch is visible at around 1610 cm^{-1} and the N-H bend at 1540 cm^{-1} for all filler loadings, except for 0.4 wt%.

2.4.2. Incorporation of filler

ATR-IR analysis was used to investigate the presence of the filler in the toplayer. The presence of ZIF-8 was not confirmed via this method as the characteristic ZIF-8 IR-peaks were not visible in any of the spectra of the TRAD membranes, not even at the highest filler loading (0.4 wt%). Other techniques to investigate whether the filler was truly incorporated in the toplayer were thus needed. Therefore, XPS and TEM analyses were performed. The hypotheses to clarify the low amount of incorporated filler and the results of the different stability tests of the filler, mentioned in section 2.4.2 (a), (b) and (c) of Part III, are likewise valid for this method.

2.4.3. Quantification of filler

a) XPS

The amount of incorporated filler was measured via XPS (Table 4). No difference was observed between a bZIF loading of 0.0125 wt% and 0.1 wt%. The results showed an atomic percent of 0.07 for both loadings. This puts the results too close to the detection threshold of this analytical technique, making them unreliable.

Table 4: Elemental composition (in atomic percent) obtained by XPS.

Sample	Zn
TRAD BZIF 0,0125 wt%	0,07
TRAD BZIF 0,1 wt%	0,07
Fully cross-linked PA	-
Reference PA [95]	-
ZIF-8	7,6923

2.4.4. Filtration results

a) bZIF-8

The performance of the TRAD TFN membranes synthesized using various amounts of bZIF-8 is presented in Figure 44. The average permeance of the pristine PA membrane was 1.03 L/m².h.bar with an average rejection of 81.5%. At every loading, except for the 0.01 wt%, TFN membrane permeability was higher than that of the TFC membrane. Nevertheless, adding more nanoparticles to the organic solution not necessarily resulted in a higher permeance, indicating that secondary effects also contributed to the enhanced permeance. The average rejection of the TFN membranes always laid underneath that of the TFC membrane, but standard deviations often overlapped.

When adding 0.0025 wt% MOF, the average permeance increased up to 8.46 L/m².h.bar, while the rejection dropped to an average value of 12.4%. Addition of 0.005 wt% further increased the permeance up to 13.7 L/m².h.bar but lowered the rejection to only 7.36 %, indicating that

the thin PA wasn't formed correctly. Membranes with particle loadings of 0.0075 wt% had a permeance of 2.91 L/m².h.bars, being significantly lower compared to the low loadings, but still significantly higher than the permeance of the pristine membrane. The rejection of these TFN membranes was 49.65%, being significantly lower than the 0 wt% membrane. As the permeance and rejection were not extreme outliers, it is thought that the PA toplayer formation took place, but not in a homogeneous way. The standard deviations on the permeance of the 0.01 wt% and 0 wt% overlapped, indicating that their permeance do not differ statistically from each other. The advantageous effect of a TFN membrane was thus not present here. Even though the permeance of the 0.025 wt% membrane was statistically higher than the one of the 0 wt% membrane, the rejection was worse. At loadings of 0.01, 0.0125 and 0.05 wt% the standard deviations on the rejections partially overlapped with the ones of the 0 wt% membrane, indicating that no loss in rejection was observed. On the contrary, the permeance of the 0.0125 (1.56 ± 0.08 L/m².h.bar) and the 0.05 wt% (1.47 ± 0.21 L/m².h.bar) membrane was statistically higher compared to the 0 wt% membrane (1.03 ± 0.22 L/m².h.bar). An increase in permeance, compared to the pristine PA membrane, without observing a loss in rejection was observed. For that reason, these membranes had the best performance in this concentration series. Their standard deviations on the rejection and permeance overlapped and therefore, their performance should be seen as equivalent. Keeping in mind that it is desirable for the production process to use the lowest amount of materials, the membrane with a loading of 0.0125 wt% bZIF was chosen as the optimal TFN membrane synthesized via the TRAD method. For the 0.2 wt% membrane, the average permeance was 16 L/m².h.bar, with high standard deviations (±9.09) and a rejection of only 34 %. These membranes are presumed to contain defects in their toplayers.

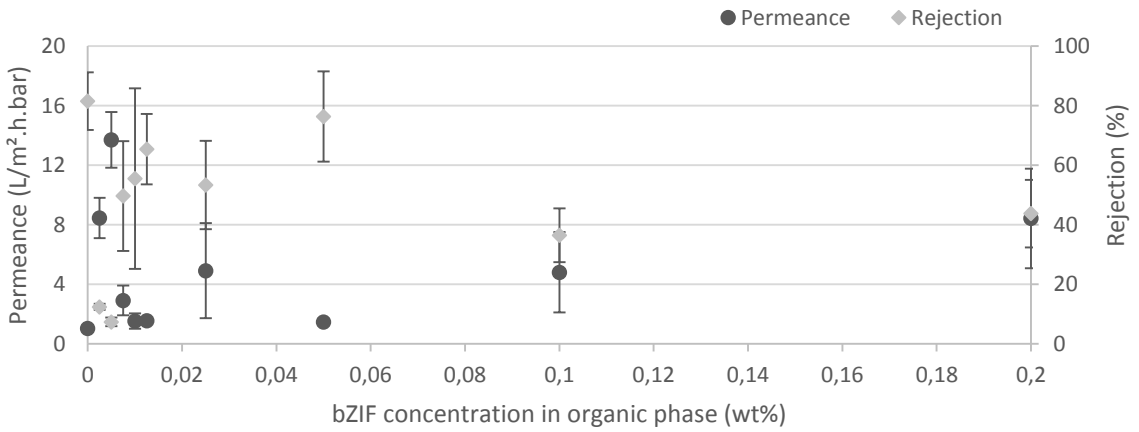

Figure 44: NaCl permeance and rejection of TRAD membranes with bZIF-8 as filler. Filtration conditions: 1000 ppm NaCl in MQ-water, 10 bar.

The incorporation of ZIF-8 in a PA toplayer on a porous PSf support was recently described in literature.[62] The size of the nanoparticles lies in the range of 100-200 nm, being of the same magnitude as the self-synthesized ZIF nanoparticles. In addition, the employed synthesis method is exactly the same as the TRAD method. It is therefore useful to compare the results from the experiments with the results described in literature. The concentration of the embedded particles was varied between 0.05 and 0.4 (w/v)%. At a loading of 0.05 (w/v)%, an increase in in permeance of 88% was observed, compared to the 0 wt% membrane,. At a loading of 0.4 (w/v)%, the permeance increased up to 162%, while maintaining high NaCl rejections.[62]These results are far more promising than the obtained results from the TRAD method. Nevertheless, the best performing membrane obtained via the TRAD method in this research project contains only 0.0125 wt% bZIF, being a factor 4 lower than the lowest loading used in the article. An increase in average permeance of 52% was observed at 0.0125wt%, without observing a decrease in NaCl rejection compared to the 0 wt% membrane. It can be concluded that a trade-off between the amount of filler and the desirable membrane performance was present.

b) sZIF-8

The filtration results of the sZIF – TRAD membranes are presented in Figure 45. The average permeance of the pristine PA membrane was 1.97 L/m².h.bar and its average rejection 68.62 %. Addition of 0.0025 and 0.005 wt% sZIF resulted in the complete loss of the separation power of the membrane as rejections lower than 10 % were obtained. The toplayer was most probably of bad quality, containing surface defects and nanogaps.[71] This also caused permeances over 7 L/m².h.bar. SEM was used to draw decisive conclusions on the thin film morphology. The performance of the 0.01 and 0.0125 wt% membrane was not statistically different from the 0 wt% membrane as the standard deviations on both the permeance and rejection overlapped. At higher filler loadings, the rejection dropped under 50%, being significantly lower than the pristine membrane. This resulted in TFN membranes with a lower overall performance than the TFC membrane.

From the results, it can be concluded that it is not advantageous to incorporate sZIF nanoparticles via the TRAD method, as no improvement in performance was observed at any loading. This observation was unexpected and was not in accordance with the bZIF TRAD membranes nor with the ECFP membranes. It was difficult to predict what caused these bad results, as many parameters can affect the toplayer formation. SEM and TEM images were used to get more insight on the toplayer morphology and thickness. In any case, it would be interesting to replicate the sZIF TRAD batch in order to verify the obtained results.

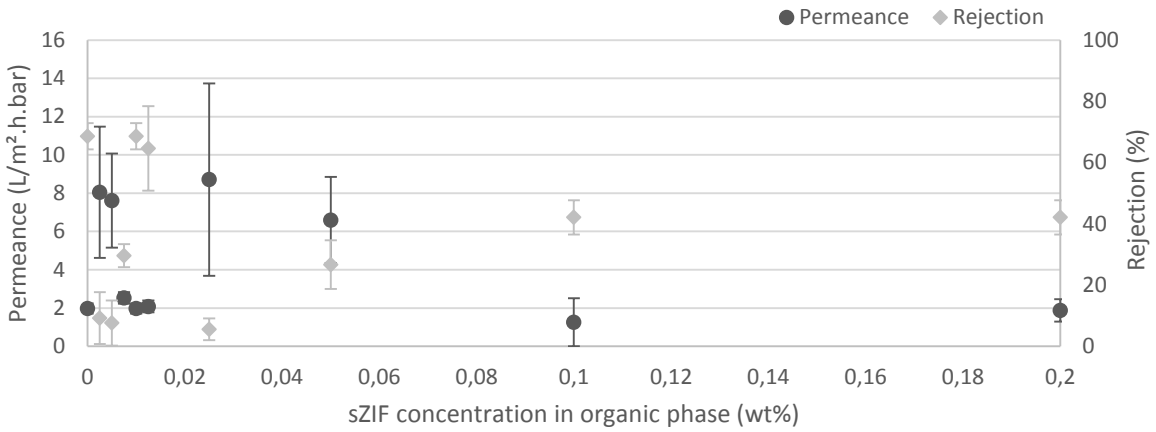

Figure 45: NaCl permeance and rejection of TRAD membranes with sZIF-8 as filler. Filtration conditions: 1000 ppm NaCl in MQ-water, 10 bar.

c) Comparison between small and bZIF-8 membranes

No significant improvement in membrane performance, compared to the TFC membrane, was observed when incorporating sZIF-8 nanoparticles. When incorporating 0.0125 wt% bZIF, the permeance increased with 52% and the rejection of the pristine membrane was maintained. From the obtained results, it can be concluded that it is more advantageous to incorporate particles of 155 nm rather than nanoparticles of 80 nm in the PA toplayer via the TRAD method.

2.4.5. Toplayer characterization

a) SEM

bZIF

From the obtained SEM images, it can be seen that toplayers with low amounts of incorporated fillers possessed a ridge and valley like morphology, analogous to the unfilled toplayer (Figure 46 and Supplementary Figure 6), At higher filler loadings, the ridge and valley structure became more pronounced and large PA strings were visible on the toplayer. The net-like PA structure was slightly visible on different spots of toplayers with different filler concentrations, but less pronounced compared to the ECFP membranes. In general, the toplayers originating via the TRAD method possessed a more ridge and valley-like structure, rather than a net net-like one. This suggests that that the synthesis protocol influences the morphology of the selective layer.

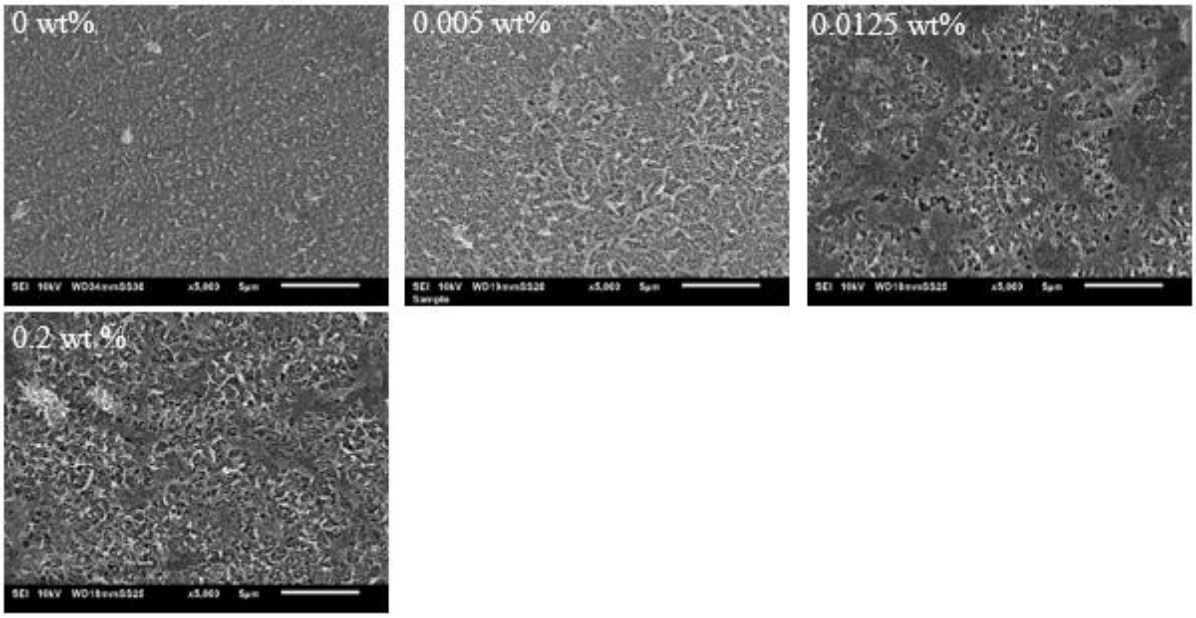

Figure 46: SEM images of the TRAD membranes made with bZIF as filler, at a magnification of 2000x. The filler loading is shown on the image.

sZIF

When looking at the membranes at a low magnification (50x - 85x), spots without toplayer were present at the centre of the sample (Figure 47 and Supplementary Figure 7). Naked pieces of PSf, recognizable by their darker colour, were also visible at the outer surface of the sample, but these were the result of the sample preparation. The spots where no selective layer was formed, occured at all filler loadings and not at the 0 wt% loading. Therefore, it is believed that these spots were caused by ZIF-aggregates, present in the organic solution. These aggregates are assumed to induce defects in the toplayer [105] as well as bad adhesion of the toplayer to the porous support. Nevertheless, when looking at the toplayers at a higher magnification, the typical ridge and valley structure was observed at all loadings (Figure 47 and Supplementary Figure 8). This indicates that the polymerization reaction occurred. The sZIF –TRAD membranes did not possess a net-like structure, not even at small regions, as was the case with the bZIF TRAD membranes. It should be kept in mind that the performance of these membranes was very poor. This can be the result of a large number of parameters, acting at the nanoscale as well as at the macroscale. Hence, it is not appropriate to relate the membrane performance to its morphology.

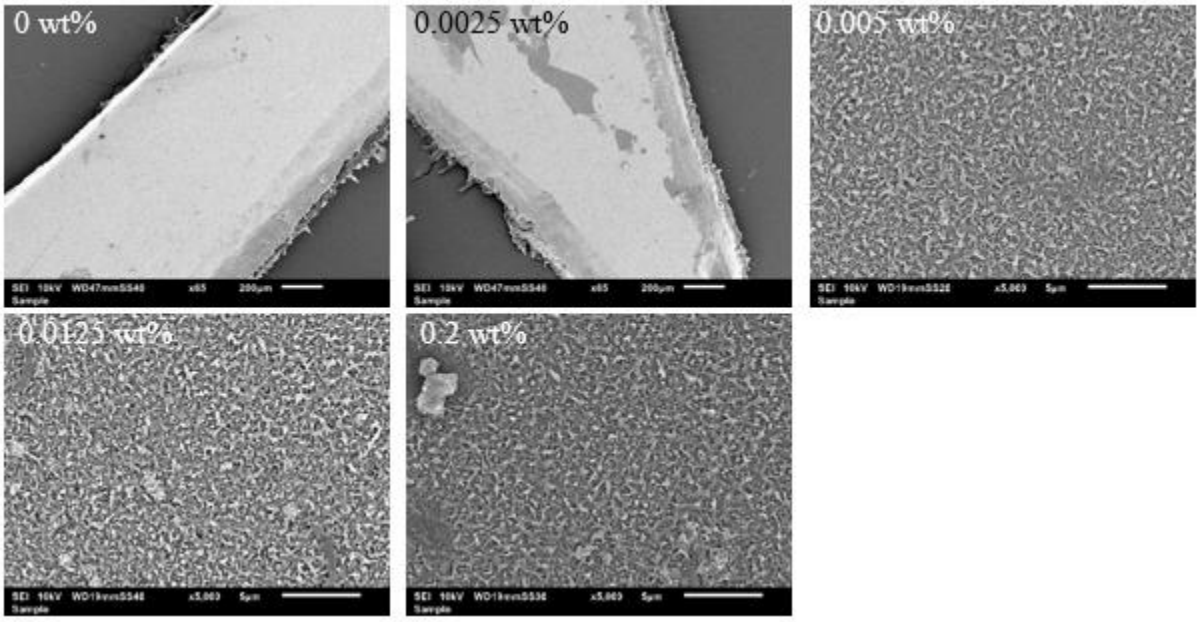

Figure 47: SEM images of the TRAD membranes made with sZIF as filler, at a magnification of 65x (0 wt% and 0.0025 wt%) or 2000x (0.005 wt%, 0.0125 wt%, 0.2 wt%).

b) TEM

bZIF

The toplayer of the 0 wt% membrane had a ridge and valley morphology with a thickness of ± 150 nm (Figure 48). The thickness of the toplayers of the TRAD membranes with different loadings of bZIF varied between 100 and 200 nm, analogous to the ECFP membranes. The 0.2 wt% membrane was an exception, as its selective layer was more than 400 nm thick. However, these values not representative for the whole toplayer, as the toplayer thickness and morphology were not continuous throughout the complete cross-section. This was clearly visible on the TEM image of the membrane containing 0.005 wt% bZIF. The vast majority of the analyzed toplayers contained the ridge and valley structure. Large PA strings, observed on the SEM images of the 0.0125 wt% membrane, were likewise visible on the TEM image.

Nanoparticles could not be pointed out on the obtained images. Only on the 0.2 wt% membrane, the filler was visible in the top region of the PA layer. As one observation is not representative for the whole concentration series, no conclusions can be drawn about the exact position of the incorporated nanoparticles.

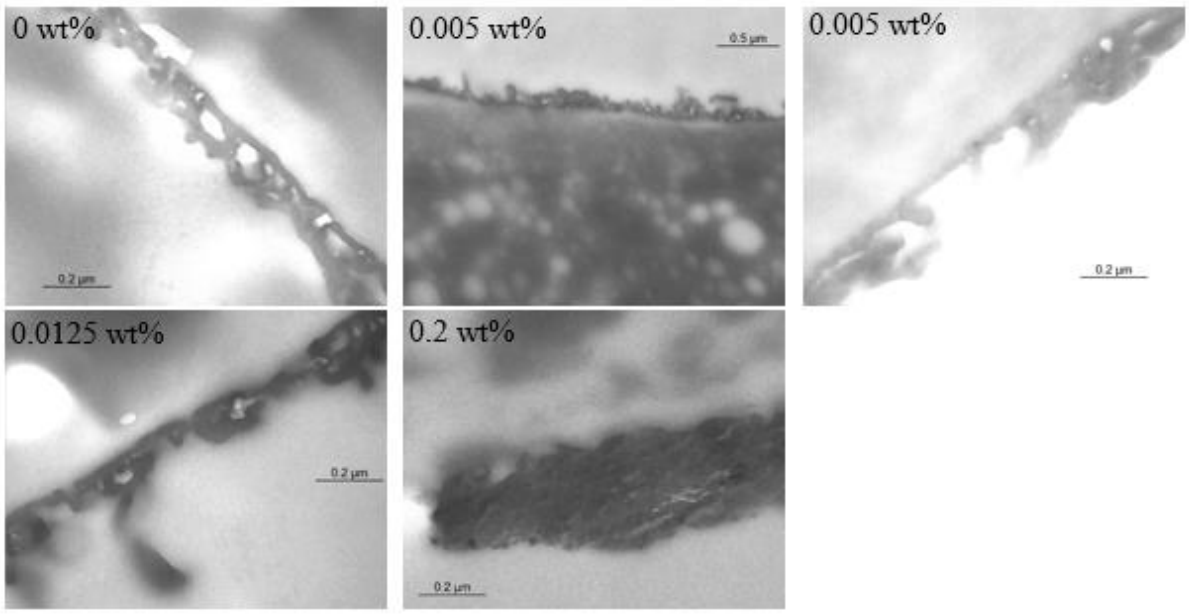

Figure 48: TEM images of the TRAD membranes, made with bZIF as filler.

sZIF

The same observations, as described above, are applicable for the TRAD membranes made with sZIF as filler. The ridge and valley structure was present and the toplayer's thickness varied between 100 and 200 nm for all analyzed membranes (Figure 49). Nevertheless, more loosely bound PA strings were visible upon the dense PA layer at different filler loadings. The incorporated filler was clearly visible at a loading of 0.0125 wt% and less pronounced in the 0.2 wt% membrane. The detectable nanoparticles were located in the top part of the selective layer, in accordance with the bZIF – TRAD membranes. The defects causing the bad performance of these membranes were not visible at the nanoscale.

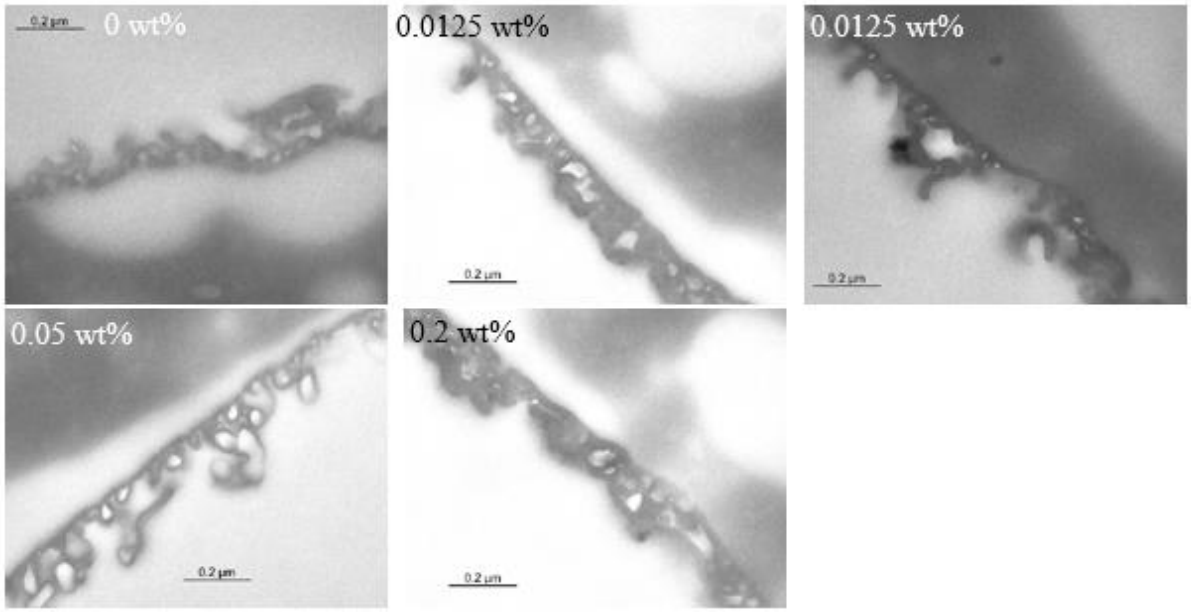

Figure 49: TEM images of TRAD membranes made with sZIF-8 as filler.

c) XPS

The XPS results of the membranes synthesized via the TRAD method are shown in Table 5. The TFN membrane with a bZIF loading of 0.0125 wt% had higher C/N and O/N ratios, indicating that the toplayer was less cross-linked, compared to the 0.1wt% membrane. This finding was not supported by the filtration results, as there, the 0.0125 wt% had a significantly lower permeance. This confirms the observation that the toplayers were not homogeneously formed upon the porous support. As can be seen from the table, both TFN membranes had higher C/N and O/N ratios compared to the reference TFC membrane, confirming that the PA structure altered because of the incorporation of nanoparticles. This is consistent with the findings of Jeong *et al.*.[60]

Table 5: Elemental composition (in atomic percent) and ratios obtained by XPS.

Sample	C	N	O	C/N	C/O	O/N
TRAD bZIF 0.0125 wt%	73.23	7.01	19.76	10.45	3.71	2.82
TRAD bZIF 0.1 wt%	71.29	9.08	19.62	7.85	3.63	2.16
Fully cross-linked PA	75.00	12.50	12.50	6.00	6.00	1.00
Reference PA [95]	0.73	0.11	0.17	6.66	4.40	1.51

2.4.6. Diffusion experiment

In order to investigate whether ZIF-8 influences the diffusivity of MPD from the aqueous to the organic phase, a diffusion experiment was carried out. Its specifications are given in section 2.3.6. of Part II. As can be seen from Figure 50, the reference line laid consistently under the TRAD line, sometimes with overlapping standard deviations. Adding ZIF nanoparticles to the

organic solution thus caused less diffusion of MPD from the aqueous to the organic phase. This is in agreement with the observed SEM images. Most of the TRAD membranes did not possess the net-like morphology, which was assumed to be caused by a higher concentration of MPD in the organic phase.

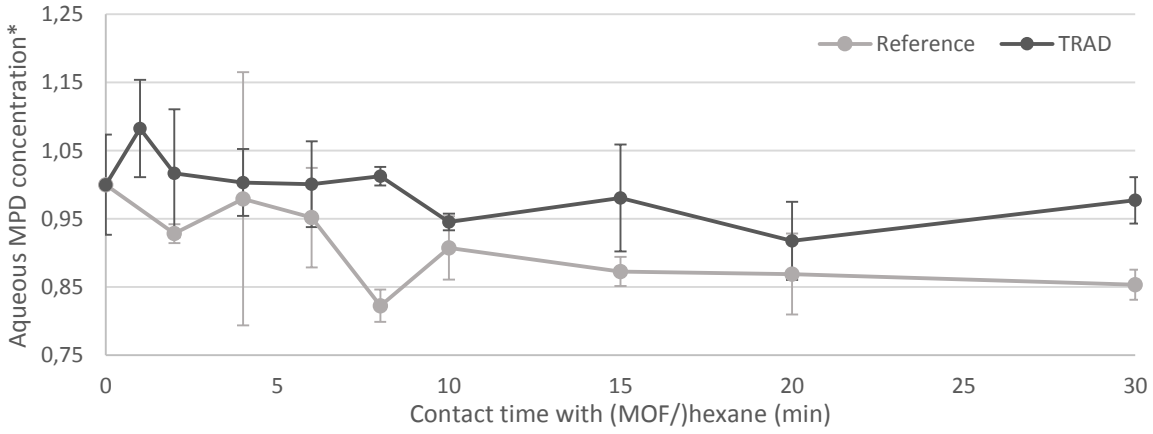

*Figure 50: Effect of added ZIF on the time course of MPD concentration in water, simulated for the TRAD method. * relative to the MPD concentration at 0 min.*

2.4.7. Conclusion

From the above results, it can be concluded that the optimum concentration for big ZIF as filler was 0.0125 wt%, resulting in an increase in permeance of around 50%, compared to the membrane with no filler. The TFN membranes made with sZIF as filler did not show an increase in performance compared to their TFC analogue. It was thus more beneficial to incorporate bZIF nanoparticles via the TRAD method. It can be stated that adding more nanoparticles to the organic solution not necessarily resulted in an increased permeance. This suggests that secondary effects also contribute to the enhanced water flux. Most of the synthesized toplayers possessed a ridge and valley morphology, with a thickness varying between 100 and 200 nm. No significant differences in toplayer thickness were observed at different filler loadings. Nevertheless, the degree of cross-linking of the selective layer was lower when nanoparticles were embedded in it. Furthermore, it was demonstrated that the presence of ZIF nanoparticles in the organic solution did not enhance MPD diffusion. On the contrary, the results suggest that less MPD molecules diffused toward the organic phase, or that their migration was slowed down.

2.5. Stability tests of ZIF-8

As could be seen from the TEM images and ICP analysis, only a small amount of ZIF-8 was truly incorporated in the toplayer. As mentioned before, different phenomena can be responsible

for this low degree of incorporation. It is possible that the aromatic amine, present in the aqueous phase, influences the morphology and/or stability of the filler. As ZIF-8 is an acid-sensitive MOF, it could (partially) degrade during the IP reaction. The nanoparticles could also diffuse from the organic phase to the water phase, resulting in the loss of incorporated nanoparticles, as the IP reaction does not occur in the aqueous phase.[11,19,100] In order to investigate which process takes place, stability and diffusion tests of the MOF are executed.

2.5.1. Stability of ZIF-8 contacted with MPD

The first step of the IP protocol consists of impregnating the PSf support with an amine solution. Subsequently, the organic solution, containing the acyl chloride, is poured over the support and the IP reaction takes place (Figure 7). As the MOF is dispersed in this organic solution, it encounters the amine present in the aqueous phase. Especially for the ECFP method, the contact time between the two phases is quite long as it takes about 18 minutes for the hexane to evaporate completely. The metal ion in ZIF-8 has a high affinity for the N-atoms of 2-methyl imidazole, being the organic linker. It is thus probable that the Zn^{2+} ion also shows affinity for the N-atoms present in MPD. If this is the case, different phenomena can possibly occur. Firstly, a post-synthetic ligand exchange reaction can take place. If 2-methyl imidazolate would be exchanged for MPD, a new MOF with possibly another composition will originate, influencing the MOF's sieving properties. Secondly, it is possible that MPD binds to the outer surface of the MOF by displacing the loosely bound solvent molecules. This can have an effect on the diffusion rate of the amine during the IP reaction, altering the reaction conditions of the interface and thus influencing the formation of the thin film. The result of the diffusion experiment is shown in sections 2.3.6 and 2.4.6 (Part III). MPD adsorption inside the pores of ZIF-8 is unlikely to happen, as the pore aperture sizes of the MOF are smaller than the kinetic diameter of the difunctional amine.

In order to verify these hypotheses, the stability of ZIF-8 was tested in an aqueous MPD solution. The diffractograms are shown in Figure 51. As ZIF-8 is proven to be stable in aqueous conditions [77], the XRD pattern of ZIF-8 immersed in MQ-water was used as reference. The diffractogram clearly shows that ZIF-8 remained crystalline and stable when exposed to MPD. As the peak positions did not shift, the ZIF-8 crystal preserved its SOD topology, proving that a post-synthetic exchange reaction was unlikely to occur. The fact that no MOFs with MPD as linker were found in literature, supports the obtained results. The above explanation is valid for both big and small ZIF-8.

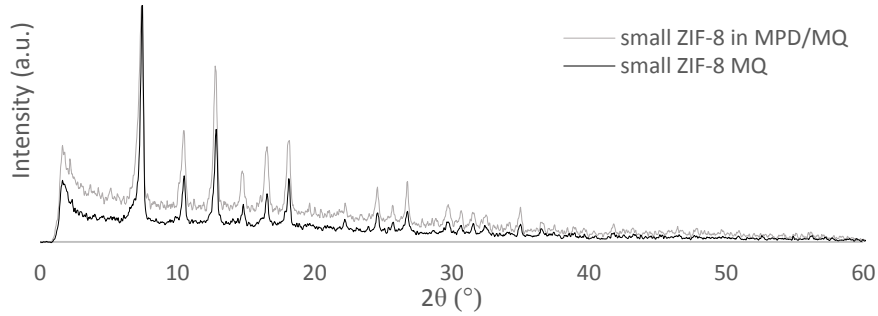

Figure 51: PXRD patterns of sZIF-8 immersed in an aqueous MPD solution and of sZIF-8 immersed in pure MQ-water.

2.5.2. Stability of ZIF-8 during the IP reaction

During the interfacial polymerization reaction, HCl is released, causing the pH to decrease, primarily at the interface. However, the exact value of the lowest pH-value reached at the interface is not exactly known. As ZIF-8 is an acid-sensitive MOF, its morphology could be damaged or altered during the reaction. In order to investigate whether the IP reaction has an influence on the stability of the MOF, the process was simulated in a syringe (Figure 17**.** The thin polymer film that resulted from this experiment was analyzed via XRD. The diffractogram is shown in Figure 52. Especially the characteristic peaks at low 2θ angles were visible in the pattern of PA with ZIF-8 and missing in that of pure PA. Even though the signal to noise ratio of these patterns was quite high, it can be excluded that the MOF completely degraded during the polymerization reaction.

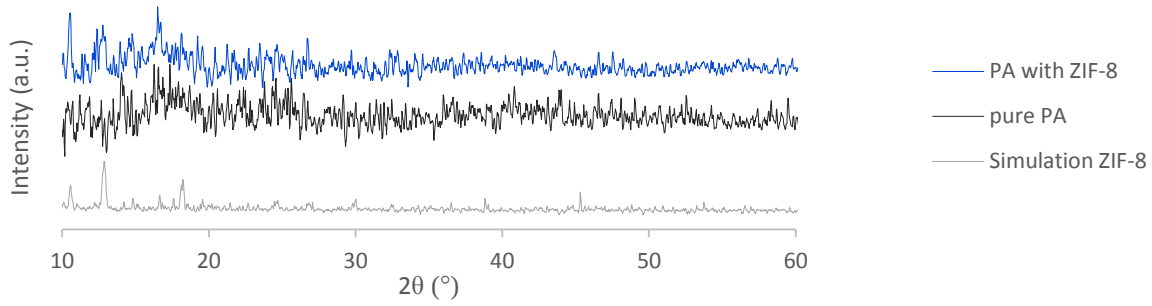

Figure 52: XRD patterns of PA with ZIF-8 (yellow) and pure PA (blue). The simulated pattern of ZIF-8 is shown in grey.

2.5.3. Phase preference hexane/water

When ZIF-8 is added to the organic solution, either to pure hexane (ECFP method) or to TMC/hexane (TRAD method), it is possible that the ZIF migrates to the aqueous solution, present inside the pores of the PSf support. This phenomenon is most likely to occur during the ECFP procedure, as PA almost instantaneously overgrows the interface. In order to investigate the behavior of ZIF when contacted with both solutions, a simulation was executed: 0.1 wt%

ZIF-8 in hexane was added to pure water and allowed to stand for 4 h. The resulting picture (Figure 53) shows that the MOF accumulated at the interface of both solutions, without diffusing into the water phase. From this simulation experiment, it can be concluded that the ZIF present in the pristine organic solution remained in this solution, and that the loss of incorporated MOF in comparison with the added MOF cannot be attributed to migration into the aqueous phase.

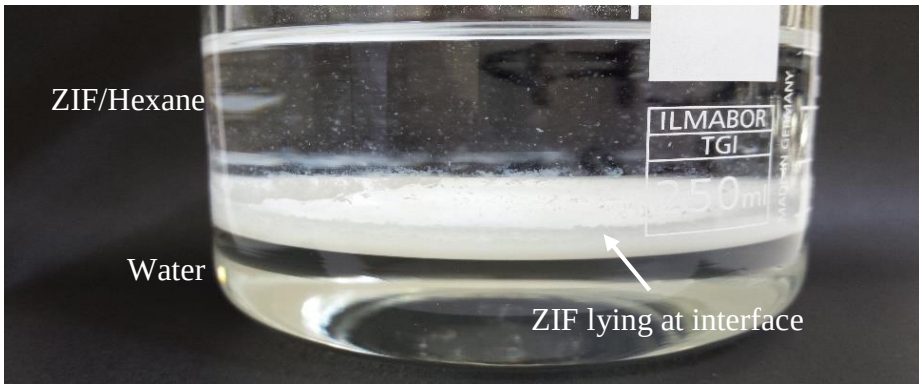

Figure 53: The MOF dispersed in the hexane phase does not diffuse into the water phase, but accumulates at the interface.

Nevertheless, this conclusion is based on mere visual observations and therefore, diffusion of a few nanoparticles into the water phase cannot be excluded. In order to investigate whether this happens at the nanoscale, TEM analysis was performed on the TFN membranes. Cross-section TEM image of TRAD TFN membranes with 0.2 wt% loading is shown in Figure 54.

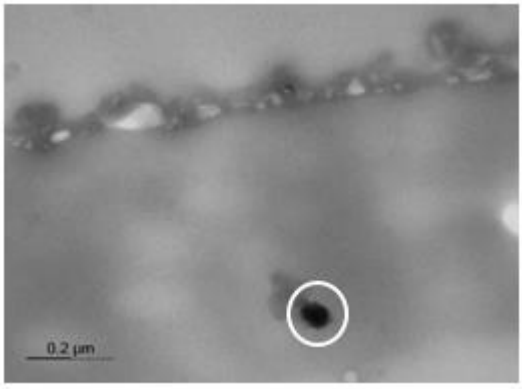

Figure 54: TEM images of a TFN membrane (0.2 wt% bZIF-8.) in which the filler diffused into the pores of the porous support (marked with the white circles).

As mentioned before, the black dots (marked with the white circle) are assumed to be MOF nanoparticles because of their darker color and crystalline structure. As visible on the image, the filler was not only lying in the PA toplayer, but also in the pores of the porous PSf support. This proves that particle diffusion from the aqueous to the organic phase occurred, at high particle loading. Nevertheless, this was very seldom observed and thus seen as an exception.

2.5.4. Conclusion

The above results show that the low degree of incorporation in the PA toplayer was not caused by the degradation of the ZIF nanoparticles, neither by their migration from the organic to the aqueous phase. Other phenomena should thus be responsible for the low concentration of embedded nanoparticles in the selective layer, compared to the added concentration in the organic phase.

2.6. Comparison between TRAD and ECFP method

The obtained results for the TRAD and ECFP method, described above, were compared to determine whether the synthesis protocol of TFN membranes had a significant influence on the membrane performance and morphology.

It was possible to detect the incorporated nanoparticles in the toplayer of ECFP membranes via ATR-IR. This was not possible for the TRAD membranes. In addition, the optimum concentration of the ECFP membranes was the same for both fillers, lying at 0.005 wt%. For the TRAD membranes, the optimum for bZIF-8 was observed at a loading of 0.0125 wt%. The ECFP method could thus offer an advantage for industrial TFN membrane production, as less nanoparticles are needed to achieve the optimum performance. In addition, at the optimum loadings, an increase in permeance of almost 200% was achieved for the ECFP method, while for the TRAD method that increase was only 50%. The ECFP performance also greatly exceeds that of ZIF-8 TFN membranes reported in literature.[62]

Furthermore, it was possible to point out ZIF nanoparticles on some of the obtained TEM images of ECFP membranes, this being difficult for the TRAD membranes. The filler was located near the porous support, in the lower region of the PA toplayer. Even though the concentration of the truly incorporated ZIF nanoparticles could not be determined accurately, the obtained results suggest that a higher degree of incorporation was achieved via deposition of the MOF prior to the interfacial polymerization reaction. It should be kept in mind that the degree of incorporation of both methods was still extremely low. The reason for this could not be identified but was certainly not the degradation of the ZIF nanoparticles nor their migration into the aqueous phase. Differences in toplayer morphology were also observed when comparing both methods, but were not caused by an increase in MPD diffusion towards the organic phase, as was hypothesized before. In general, the membranes synthesized via the ECFP method show a net-like structure, while the TRAD membranes usually possessed a ridge and valley morphology. However, the appearance of the PA layer was not homogeneous throughout

the membrane. The thickness of the toplayers of all synthesized membranes, including TFC membranes, varied between 100 and 200 nm. Differences in the cross-linking degree were also observed when comparing the size of the filler, the loading concentration and the synthesis methods, but no real trend could be uncovered. The obtained results indicate that the position, the size and the amount of incorporated filler influenced the polymerization process, and subsequently the membrane performance. As the morphology is greatly altered when varying the conditions, it is considered that not only the porosity of the filler enhances the permeance, as is often mentioned in literature.[19,48,60,61,66] Secondary effects, induced by introduction of the filler in the PA layer, are believed to contribute in a bigger extent to the permeance increase of the TFN membranes. The mathematical model, explained in section 2.1 (Part I), substantiates this theory.

2.7. CMPI synthesis method

PI membranes were chemically modified in order to establish a coordinative bond between the support and the MOF, hence fixating the nanoparticles at the PA/support interface. The chosen protocol was based on the crosslinking mechanism of PI with a diamine, converting imide groups into intermolecular amide groups. As a result, a crosslink between two polymer chains was established. For the CMPI synthesis method, not a diamine but a molecule with only one amine and a carboxyl-group was employed. The amine was presumed to react with the imide, affixing the molecule to the polymer chain. The carboxylic-group should remain unreacted, hence able to form a coordinative bond with a Zn atom present at the outer surface of ZIF-8. 4-aminobenzoic acid (4-ABA) and 6-aminohexanioc acid (6-AHA) were chosen as linkers with appropriate functional groups and different degree of structural flexibility. The reaction scheme for 4-ABA is shown in Figure 55.

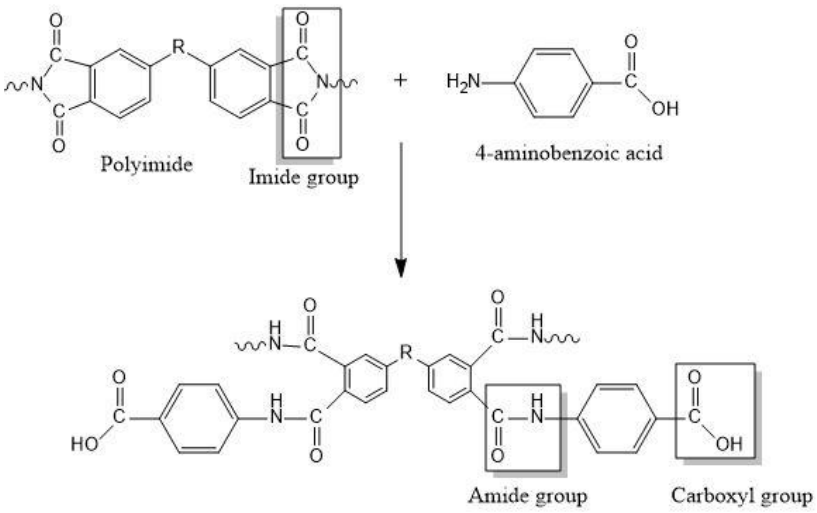

Figure 55: Reaction scheme of the reaction of PI with 4-ABA, consisting of an imide ring-opening reaction. The imide group is converted into an amide group. The carboxyl group of 4-ABA remains unreacted, hence able to bind subsequently with Zn ions of ZIF-8.

Both linkers were tested and the best functionalized support was then analyzed for its bonding capacity of the Zn^{2+} ion and of sZIF-8, to verify the validity of this approach. Subsequently, the functionalized PI supports were used as substrate for interfacial polymerization, giving rise to a TFN membrane. Both ECFP and TRAD methods were used establish the thin toplayer.

2.7.1. Amine selection

Solutions with different 4-ABA or 6-AHA concentrations in MeOH or water were tested. It was not possible to dissolve 1.25 wt% in 6-AHA in MeOH, meaning that its solubility in MeOH was already exceeded at this concentration. Therefore, the complete series (1.25, 2.5, 5 wt%) of 6-AHA were only made in MQ-water. As the solubility of 4-ABA in water is 5.88 g/L, only a 0.5 wt% solution was made. In MeOH, the same concentration series were made for 4-ABA as for 6-AHA in water. Pieces of PI membrane were thus only functionalized in the solutions with a clear background in Table 6.

Table 6: Tested linker solutions. The ones marked in grey were not used to functionalize PI.

Solvent	6-AHA (wt%)	4-ABA (wt%)
MQ-water	0.5	0.5
	1.25	1.25
	2.5	2.5
	5	5
MeOH	1.25	1.25
	2.5	2.5
	5	5

If the reaction between the linker and the support takes place as anticipated, the typical amide. at 1540 cm^{-1} (amide II band) and at 1610 cm^{-1} (amide I band) should become visible in the ATR-IR spectra (Figure 56 and Figure 57). As reference, the spectrum of cross-linked PI with hexane diamine (HDA) is used. The peak at 1610 cm^{-1} is present for all conditions. The intensities at this wavenumber for the different concentrations of 4-ABA are higher than those of 6-AHA, indicating that relatively more 4-ABA is incorporated. The opposite was in fact expected as the amine group of 6-AHA is a stronger nucleophile than the one of 4-ABA, thanks to the electron donating properties of the alkyl chain and the delocalisation of π-electrons in the phenyl ring. A possible explanation for the unexpected results may lie in the fact that 4-ABA is pre-positioned on the support via π-π stacking between the benzene groups of the support and of the linker. The amine group then comes in closer proximity of the imide, facilitating the nucleophilic attack on the imide-ring. In addition, the higher hydrophobicity of 4-ABA compared to 6-AHA may also influence the reaction.[106] Nevertheless, the peak at 1540 cm^{-1} is not only missing in the spectra of all concentrations of 6-AHA, but also in the spectra of the whole concentration series of 4-ABA. The typical vibrations of the carboxylic group are not visible either. Therefore, it can be concluded that the ring-opening reaction of the imide with the linker did not occur, or at least not sufficiently to be detected with ATR-IR analysis.

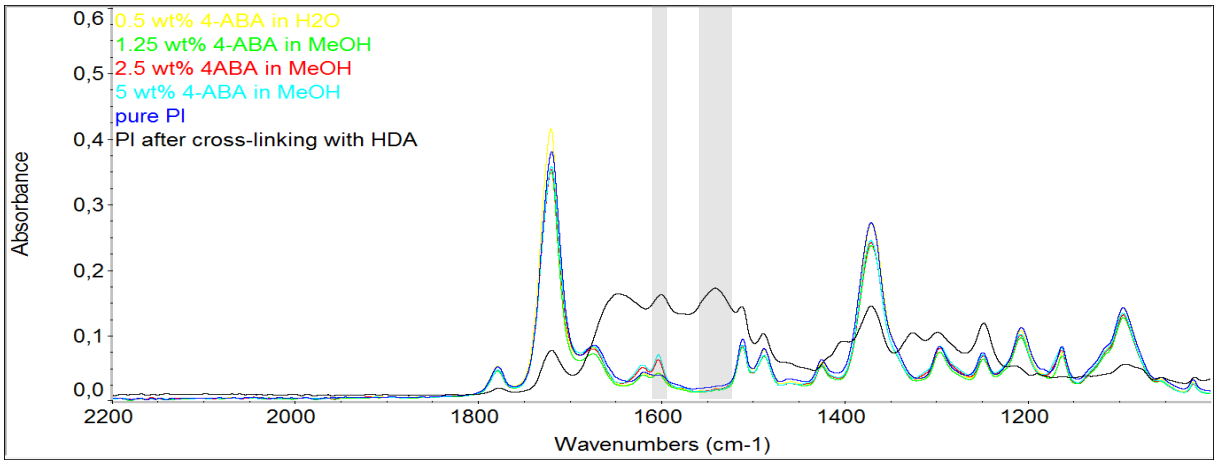

Figure 56: ATR-IR spectra of functionalized PI with 4-ABA.

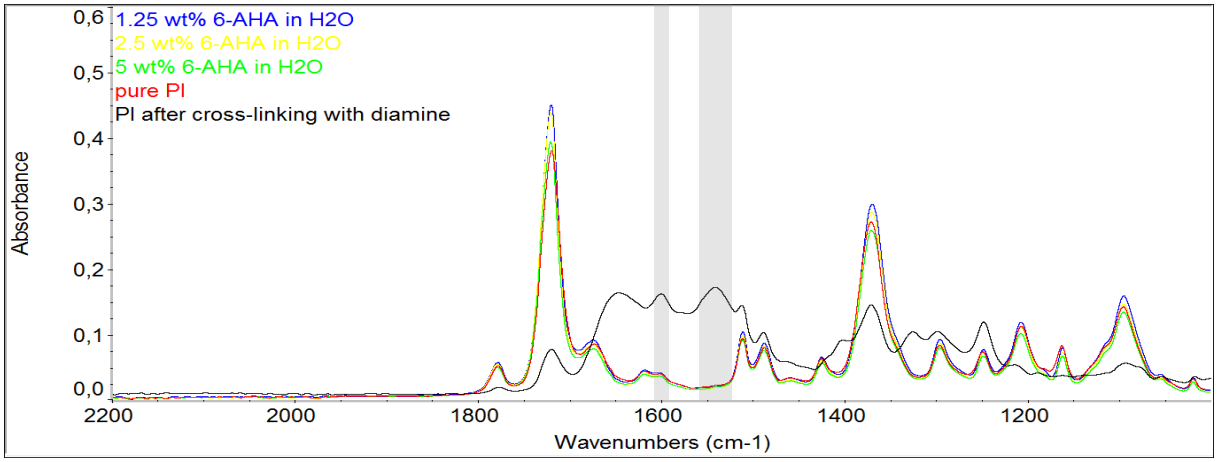

Figure 57: ATR-IR of functionalized PI with 6-AHA.

It is possible that the nucleophilic properties of the linkers are too weak to attack the partially positively charged C-atom of the imide. A strong base, tri-ethyl amine (TEA), was therefore added to the linker-solution in which the PI is immersed. TEA is presumed to deprotonate the linker, making it a stronger nucleophile, hence able to attack the imide. Covalent incorporation of TEA into the PI network is unlikely to occur as TEA it is a strong steric hindered base. TEA was added to the 2.5 wt% 4-ABA in MeOH solution, as this concentration gave the highest relative intensity for the amount of used linker. The C=O peak remains visible, and the amide II band now appears, proving that an amide is formed when 0.625 g or 1.25 g TEA is added to the solution (Figure 58). It should be noted that the typical peaks which should ideally arise because of the bonds present in 4-ABA are not visible. This is assumed to be caused by the limited incorporation of the linker, hence not reaching the ATR-IR detection limit.

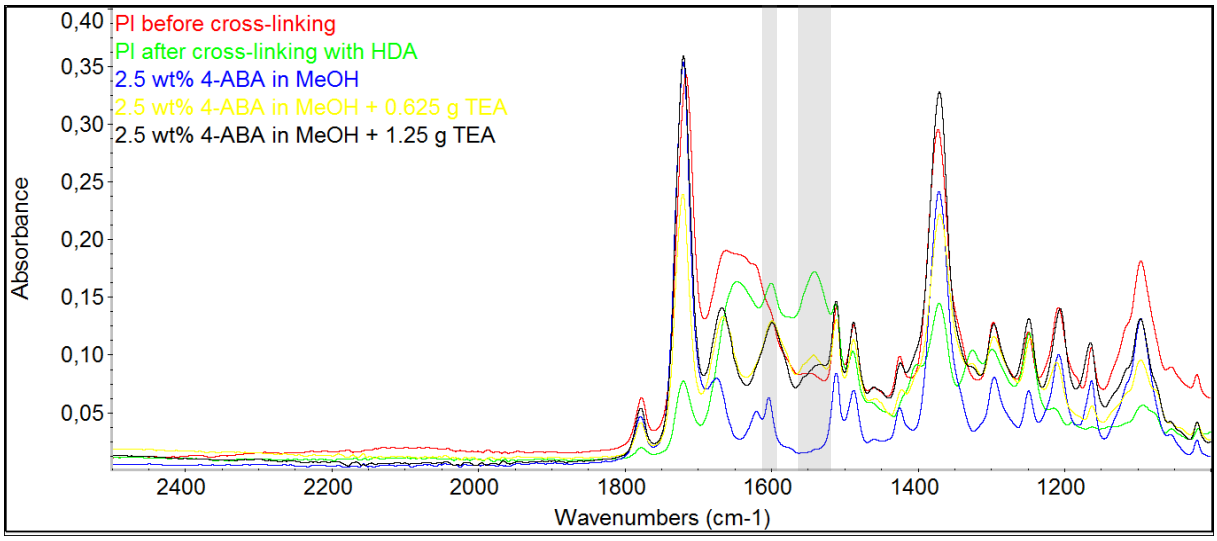

Figure 58: ATR-IR spectra of the functionalization of PI with 4-ABA, in addition of TEA.:

2.7.2. Bonding capacity of Zn^{2+}

The bonding capacity of PI membranes modified in a 2.5 wt% 4-ABA/ 0.625 g TEA in MeOH solution was then analysed for Zn^{2+} ions as well as for MOF nanoparticles as bonding agents.

The modified PI membranes were immersed in a 0.1 wt% $Zn(NO_3)_2$ aqueous solution. The free carboxyl groups on the support are presumed to coordinatively bind with the Zn^{2+} ions in the solution. In order to subsequently quantify the amount of bound Zn^{2+} ions, the membranes underwent an acid treatment with HCl to reprotonate the carboxyl groups and to release the Zn^{2+} ions. The acid solution, which now contained the metal ions, was quantified via ICP analysis (Figure 59). The membrane modified without TEA was used as reference. Significantly more Zn^{2+} ions bound to the TEA-modified PI membrane, proving that the base had a positive influence on the amount of incorporated linker, as assumed by ATR-IR analysis.

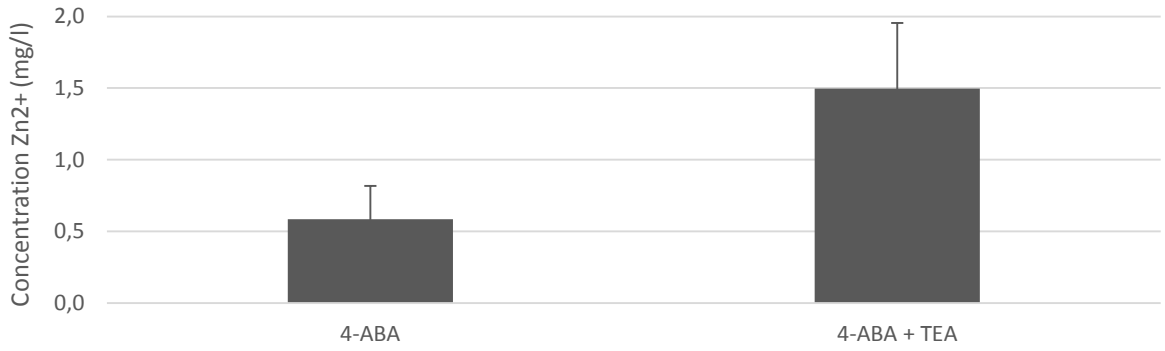

Figure 59: Zn^{2+} bonding capacity of functionalised PI membranes with 4-ABA and 4-ABA/TEA.

2.7.3. Bonding capacity of ZIF-8

As the final goal of these experiments was to obtain TFN membranes, the bonding capacity of modified PI membranes for MOF nanoparticles was also tested. Functionalized PI supports with and without TEA were immersed in a hexane solution of 0.1 wt% sZIF-8. Subsequently, a washing step with water was performed, to remove nanoparticles that were loosely attached to the PI surface, and to ensure that only the coordinatively bound ZIF remained. The same acid leaching procedure as described earlier was then performed. As ZIF-8 is an acid-sensitive MOF[81], the acidity of the leaching solution will degrade the particles, making it possible to measure the Zn concentration with ICP. It can be seen in Figure 60 that the bonding capacities of the membranes with and without addition of TEA did not significantly differ from each other. The effect of the added base thus disappeared and the amount of free carboxyl groups seemed to have no influence on the amount of adsorbed MOF. It is highly improbable that a one on one relation exists between the carboxylic acid groups and the nanoparticles. More acid groups will be needed to affix one nanoparticle. Furthermore, the size of a nanoparticle greatly exceeds the

size of a functional group. Therefore, it is possible that the additional acid groups, introduced with the help of TEA, are not available for new nanoparticles to bind. Nevertheless, the addition of TEA can only be advantageous for the number of present carboxylic groups on the surface and thus indirectly also for the overall bonding strength of a nanoparticle to the surface. Therefore, functionalized membranes with 2.3 wt% 4-ABA/ 5.76 wt% TEA were be used as support to make TFN membranes.

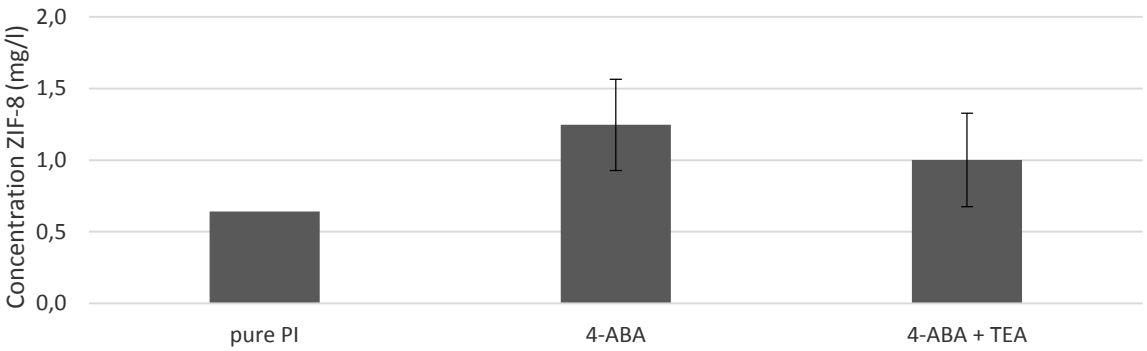

Figure 60: Bonding capacity of functionalized PI membranes for ZIF-8.

2.7.4. Filtration results

The CMPI membranes were synthesized via the ECFP method as well as via the TRAD method, with filler loadings of 0.005 wt% and 0.1 wt%. In order to see if the size of the filler has an influence on the membrane performance, small and bZIF nanoparticles were incorporated in the toplayer. As reference, no ZIF was added to the organic phase. The performance of the synthesized membranes via both methods and with both fillers sizes was very poor (Figure 61 and Supplementary Figures 9 to 11). Even the reference membranes had rejections under 10%, and permeances up to 30.55 L/m².h.bar, indicating that large defects were present in the selective layer. Hence, no decisive conclusions could be drawn on the influence of the synthesis method, nor on the influence of the filler size on the membrane performance.

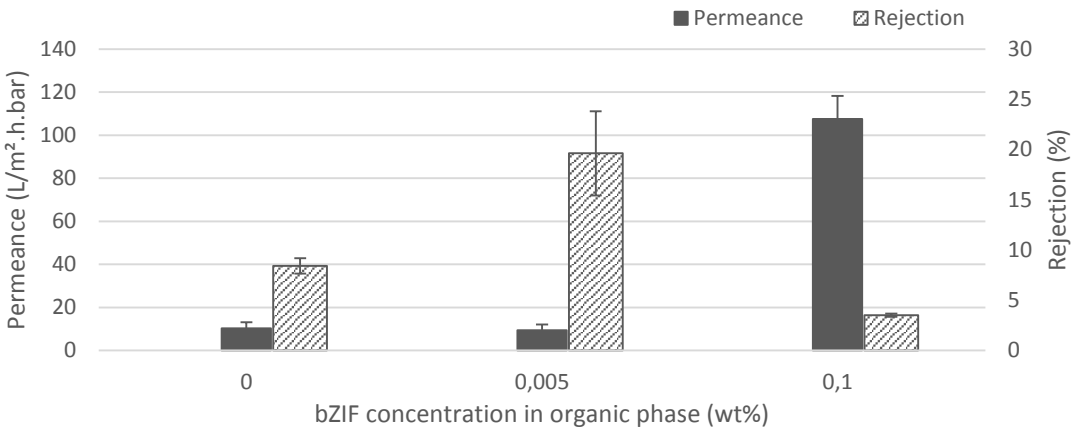

Figure 61: NaCl permeance and rejection of ECFP CMPI membranes with bZIF-8 as filler. Filtration conditions: 1000 ppm NaCl in MQ-water, 10 bar.

2.7.5. SEM

The SEM-images from the CMPI membranes at low magnification show that the porous support layer is not fully covered with PA. The PA is brighter, while the exposed PI is darker. As this is observed for every synthesized membrane, even for the reference, the reason for the bad adhesion cannot be caused by the ZIF nanoparticles. This result is in agreement with the filtration data. Therefore, it is presumed that the formed PA layer shows less affinity for the altered chemical structure of the PI. When looking at a higher magnification, the typical ridge and valley structure becomes visible. This proves that the interfacial polymerization reaction occurs and is not (strongly) altered by the chemically modified PI layer.

2.7.6. Conclusion

Relatively more 4-ABA was incorporated compared to 6-AHA. Adding TEA to the 4-ABA linker solution had an advantageous effect on the amount of incorporated linker and thus on the amount of free carboxyl groups on the PI surface, as proven by the increased Zn2+ bonding capacity. This validates the concept of the CMPI method. Nevertheless, the performance of the TFC as well as of the TFN membranes made with functionalized PI as support, was very poor. This is believed to be caused by bad adhesion of the PA to the support. Optimisation of this method is thus required

Part IV: General conclusion

A recent category of membranes, called thin film nanocomposite (TFN) membranes, received a lot of attention lately. The main purpose of these membranes is to obtain higher solvent fluxes than TFC membranes, without compromising solute rejection. This enhanced permeance is achieved by incorporating nanoparticles in the selective layer, but the exact mechanism remains unclear. The most widely accepted hypothesis is that preferential flow paths of solvent molecules through the nanoparticles emerge and thus result in an overall higher flux. It is also possible that the PA toplayer's structure changes in the presence of nanoparticles, but little evidence is found in literature to substantiate this. Nevertheless, this secondary effect of the filler is believed to also contribute to the enhanced water flux. The changes in the structure of the selective layer, (e.g. thickness, cross-linking degree, homogeneity, morphology surface hydrophilicity/hydrophobicity) as function of the size and amount of the incorporated filler, were therefore investigated in this research thesis. In addition, it is believed that the location of the filler also plays a role in the membrane performance. Therefore, TFN membranes were synthesised with the purpose in mind to control the position of the incorporated filler in the PA toplayer via two new methods. Ultimately, the aim was to determine whether the primary or secondary effect of the filler contributes most to the enhanced performance.

The first part of this thesis was devoted to the synthesis of ZIF-8. Two different synthesis protocols were adopted in order to obtain nanoparticles of different sizes, referred to as big ZIF-8 (bZIF-8) and small ZIF-8 (sZIF-8). The sZIF crystals had an average size of 80 nm, while the bZIF crystals had a size of approximately 155 nm. Both fillers were incorporated in the selective layer via three methods: the traditional (TRAD) method, the evaporation controlled filler positioning (ECFP) method, and the chemically modified polyimide (CMPI) method.

The ECFP and TRAD methods were explored in the second part of this research project, while the CMPI method was covered thereafter. For the TRAD method, the highest increase in permeance, without compromising rejection, was 50 % and was achieved at a loading of 0.0125 wt% bZIF. The performance of the sZIF – TRAD membranes was very poor, probably due to inferior adhesion of the toplayer, caused by the presence of aggregated ZIF-8 crystals. The ECFP method was invented to pre-position the filler on the support by allowing the organic solvent to evaporate. The optimum performance was achieved at a loading of 0.005 wt%, for both sZIF and bZIF as filler, resulting in a respective increase in permeance of 220% and 200%,

compared to the membrane without filler. Compared to the TRAD method, the membranes resulting from the ECFP method attained a higher performance at a lower filler concentration. From the filtration results, it can be concluded that membranes synthesized using the ECFP method, show an increased performance compared to the TRAD membranes. It must be noted that adding more nanoparticles to the organic solution does not necessarily result in a higher permeance of the membrane. This suggests that the primary effect of the filler is not dominating and that secondary effects contribute in a higher degree to the enhanced permeance. This confirms the predictions from the adapted Maxwell model for TFN membranes.

The obtained IR and TEM data confirmed that a higher amount of ZIF nanoparticles was incorporated in the selective layer when using the ECFP method. This suggests that pre-positioning the filler on the porous support has a positive influence on the degree of incorporation. The bZIF crystals were usually located at the bottom part of the PA layer, as was presumed to occur by the deposition of the crystals on the support. SZIF crystals were present more in the middle and top regions, but this is believed to be caused by their redispersion in the TMC/hexane solution. Therefore, the ECFP method succeeds in controlling the position of the filler in the thin film. Detection of the filler on the TEM images of the TRAD membranes was more difficult. It should be kept in mind that the amount of incorporated nanoparticles was very low for both methods. The reason for this low degree of incorporation could not be identified but is certainly not the degradation of the ZIF nanoparticles nor their migration into the aqueous phase. The experiments showed that ZIF-8 crystals remained stable during the conditions of interfacial polymerization and that migration from the organic towards the aqueous phase was negligible.

The morphology of the toplayers differed significantly for both methods. The toplayers of the ECFP-membranes often possessed a net-like structure, while those of the TRAD membranes generally had a ridge and valley morphology. This implies that the synthesis method, and consequently the position and amount of incorporated filler, influence the toplayer morphology. In addition, the cross-linking degree altered when adding nanoparticles to the organic solution. It was always lower for the TFN membrane compared to the TFC analogue and bigger nanoparticles seemed to deteriorate it to a bigger extent than the smaller fillers. No influence of the filler size on the toplayer thickness was observed. All toplayers had a thickness that varied between 100 and 200 nm. However, determination of the exact thickness on the obtained TEM images was difficult.

The CMPI method was explored in the third part of this research project and was invented to coordinatively affix the nanoparticles to the PA/support interface. This was achieved by a ring-opening reaction of the PI with 4-ABA. A free carboxyl group was introduced in the PI network, which can form a coordinative bond with a Zn^{2+} ion, present at the outer surface of ZIF-8. The modification of the PI was carried out in the presence of TEA, which was required to enhance the nucleophilic properties of the linker. As a proof of concept, Zn^{2+} and ZIF-8 bonding capacity tests on the modified membranes were carried out and demonstrated that the membranes were able to affix ZIF-8 crystals as well as Zn^{2+} ions to its surface. Consequently, the CMPI membranes were used as support for interfacial polymerization, giving rise to a TFN membrane. Both ECFP and TRAD methods were used to establish the thin toplayer. However, the separation power of the resulting membranes was very poor, due to bad adhesion of the PA toplayer to the modified PI. Although the interfacial polymerization took place as desired, optimisation of this method is required.

To conclude, the obtained results from this Master thesis showed that TFN membranes synthesized via the ECFP method were a huge improvement on the conventional PA TFC membranes. In addition, the results suggested that secondary effects (influence on toplayer morphology, degree of cross-linking, toplayer thickness, etc.) dominate in the enhanced permeance of a TFN membrane. The amount of truly incorporated porous filler was too low to contribute solely to the increased water flux. Therefore, the alternation of the toplayer morphology due to the presence of nanoparticles is believed to play a major role in the obtained performance of a TFN membrane

Prospectives

In order to determine whether the primary or secondary effects of the filler dominate in causing the exceptional increase in permeance of a TFN membrane, various other parameters need to be varied to get a more complete picture. The incorporated filler can be seen as an additional degree of freedom in designing TFN membranes. Examples of filler properties that can be varied include the porosity, the hydrophilicity/hydrophobicity, the size, the charge and the shape. In addition, it would be interesting to use nanoparticles that are intrinsically coloured to facilitate the visualisation of the filler in the thin toplayer. Cu-BTC could be a potential candidate. When analysing the secondary effect of these nanoparticles, additional characterization methods including AFM, zeta potential and contact angle measurements need to be used. Positron annihilation light spectroscopy (PALS) can also offer additional insight in the layered structure and free-volume properties of asymmetric membranes.[107] In addition, it would be interesting to quantify the amount of incorporated filler. SEM-EDX and XPS could not provide information regarding this aspect, as the amount of embedded nanoparticles fell under (or near) the detection limit. It is possible that the highly sensitive analytical ICP technique can offer a solution. When TFN membranes undergo an oven treatment at around 650°C, it is believed that the organic matrix is burned away and that the inorganic residue remains. This inorganic residue is an indicator of how much filler was truly incorporated in the toplayer. The residue can be dissolved in an acid solution, and consequently analyzed via ICP. This technique combines the principle of thermo-gravimetric analysis (TGA) with the sensitivity of ICP.

Other mechanisms to control the position of the filler could also be attempted. For example, a covalent bond between a modified UiO-66 and the support, rather than a coordinative one, could be established via the polymerization mechanism of caprolactam. The mechanism is shown in Supplementary Figure 12. The free amine group can then be used as nucleophile to induce the ring-opening reaction of the PI, analogous to the CMPI method. Even though this concept is purely theoretical and not yet tested in practice, it seems to offer many possibilities, also in other fields of membrane technology, e.g. MMMs. Another possible method to affix the nanoparticles at the PA/support interface is via the use of the magnetic properties, present in some MOFs.[108] The particles can be drawn towards the interface by another magnet, placed underneath the support.

Vulgarized summary

A membrane is a selective filter, through which some molecules can pass via the filter pores, while others cannot. This results in the separation of a mixture of molecules. Membrane technology is currently used in several industries (e.g. desalination, food and beverage processing), as it has a lot of advantages to offer compared to other separation techniques. These advantages include lower energy consumption and milder operating conditions. Nevertheless, membrane separation is an emerging technology that is still in its infancy compared to conventional separation techniques. Therefore, a lot of research is necessary to achieve highly stable, performing and re-usable membranes that can compete with traditional separation techniques.

Recently, a new class of membranes emerged, in which very small (porous) particles are introduced in the thin toplayer. This is done in order to achieve an even higher increase in permeance, as the solvent now can pass through the pores of the polymer as well as through the pores of the particles. These membranes, called thin film nanocomposite (TFN) membranes, are already operational in industry. Today, an increase of 50 to 100 % in permeability compared to conventional desalination membranes, containing no nanoparticles, is achieved. Nevertheless, very few research is done on the position of the particle in the toplayer and on its influence on the membrane morphology. Therefore, the aim of this thesis is to control and optimize the position of the filler. Research on changes in morphology when introducing nanoparticles is also conducted.

Two methods were used to introduce the filler in the thin toplayer and to control its position. In method 1, the filler is deposited on the substrate before the thin toplayer is synthesized. In method 2, the support is modified so that the filler can chemically bind to it. Both methods were compared to the traditional method of making TFN membranes. The performance of the membranes made with method 1 was much higher. The membranes resulting from method 2 still require further optimisation. The obtained results suggest that the size, the amount and the position of the incorporated filler influence the membrane performance in a bigger extent than the porosity of the filler does.

Bibliography

1. Pereira Nunes, S. & Peinemann, K.-V. *Membrane Technology in the Chemical Industry*. (2006).
2. Humphrey, J. L. & Keller, G. E. *Separation process technology*. (McGraw-Hill, 1997).
3. Mulder, M. Basic Principles of Membrane Technology. *Zeitschrift für Phys. Chemie* **72,** 564 (1998).
4. Baker, R. W. *Membrane Technology and Applications*. (John Wiley & Sons, Ltd, 2012).
5. Loeb, S. & Sourirajan, S. Sea water demineralization by means of an osmotic membrane. *Adv. Chem. Ser.* **38,** 117–132 (1962).
6. Duval, J. M. Adsorbent filled polymeric membranes. (1993).
7. Vankelecom, I. F. J. *Membrane Technology*. (KU Leuven, 2013).
8. Wu, P. & Imai, M. in *Adv. Desalin.* 57–81 (2012).
9. Shenvi, S. S., Isloor, A. M. & Ismail, A. F. A review on RO membrane technology: Developments and challenges. *Desalination* (2015).
10. Kwak, S.-Y. & Kim, S. S. Hybrid Organic / Inorganic Reverse Osmosis (RO) Membrane for Bactericidal Anit-Fouling. Preparation and Characterization of TiO2 Nanoparticle Self-Assembled Aromatic Polyamide Thin-Film-Composite (TFC) Membrane. *Environ. Sci. Technol.* **35,** 2388–2394 (2001).
11. Petersen, R. J. Composite reverse osmosis and nanofiltration membranes. *J. Memb. Sci.* **83,** 81–150 (1993).
12. Ghosh, A. K. & Hoek, E. M. V. Impacts of support membrane structure and chemistry on polyamide–polysulfone interfacial composite membranes. *J. Memb. Sci.* **336,** 140–148 (2009).
13. Xie, W. *et al.* Polyamide interfacial composite membranes prepared from m-phenylene diamine, trimesoyl chloride and a new disulfonated diamine. *J. Memb. Sci.* **403-404,** 152–161 (2012).
14. Lau, W. J., Ismail, A. F., Misdan, N. & Kassim, M. A. A recent progress in thin film composite membrane: A review. *Desalination* **287,** 190–199 (2012).
15. Huang, J., Virji, S., Weiller, B. H. & Kaner, R. B. Polyaniline nanofibers: facile synthesis and chemical sensors. *J. Am. Chem. Soc.* **125,** 314–5 (2003).
16. Damgé, C., Michel, C., Aprahamian, M., Couvreur, P. & Devissaguet, J. P. Nanocapsules as carriers for oral peptide delivery. *J. Control. Release* **13,** 233–239 (1990).
17. Hermans, S., Mariën, H., Dom, E., Bernstein, R. & Vankelecom, I. F. J. Simplified synthesis route for interfacially polymerized polyamide membranes. *J. Memb. Sci.* **451,** 148–156 (2014).
18. Freger, V. Kinetics of Film Formation by Interfacial Polycondensation. *Am. Chem. Soc.* **21,** 1884–1894 (2005).
19. Feinberg, B. J. & Hoek, E. M. V. in *Encycl. Membr. Sci. Technol.* 1–15 (2013).
20. Alsvik, I. & Hägg, M.-B. Pressure Retarded Osmosis and Forward Osmosis Membranes: Materials and Methods. *Polymers.* **5,** 303–327 (2013).
21. Clayden, J., Greeves, N. & Warren, S. in *Org. Chem.* 197–221 (2001).
22. Wong, K. C., Goh, P. S. & Ismail, A. F. Gas separation performance of thin film nanocomposite membranes incorporated with polymethyl methacrylate grafted multi-walled carbon nanotubes. *Int. Biodeterior. Biodegrad.* 1–7 (2015).
23. Pacheco, F. A., Pinnau, I., Reinhard, M. & Leckie, J. O. Characterization of isolated polyamide thin films of RO and NF membranes using novel TEM techniques. *J. Memb. Sci.* **358,** 51–59 (2010).
24. Mansourpanah, Y., Madaeni, S. S. & Rahimpour, A. Fabrication and development of interfacial polymerized thin-film composite nanofiltration membrane using different surfactants in organic phase; study of morphology and performance. *J. Memb. Sci.* **343,** 219–228 (2009).
25. Jimenez Solomon, M. F., Bhole, Y. & Livingston, A. G. High flux membranes for organic solvent nanofiltration (OSN)—Interfacial polymerization with solvent activation. *J. Memb. Sci.* **423-424,** 371–382 (2012).
26. Jegal, J., Min, S. G. & Lee, K.-H. Factors affecting the interfacial polymerization of polyamide active layers for the formation of polyamide composite membranes. *J. Appl. Polym. Sci.* **86,** 2781–2787 (2002).
27. Ghosh, A. K., Jeong, B.-H., Huang, X. & Hoek, E. M. V. Impacts of reaction and curing conditions on polyamide composite reverse osmosis membrane properties. *J. Memb. Sci.* **311,** 34–45 (2008).
28. Kong, C., Shintani, T., Kamada, T., Freger, V. & Tsuru, T. Co-solvent-mediated synthesis of thin polyamide membranes. *J. Memb. Sci.* **384,** 10–16 (2011).
29. Hermans, S., Bernstein, R., Volodin, A. & Vankelecom, I. F. J. Study of synthesis parameters and active layer morphology of interfacially polymerized polyamide-polysulfone membranes. *React. Funct. Polym.* **86,** 199–208 (2015).
30. Freger, V., Gilron, J. & Belfer, S. TFC polyamide membranes modified by grafting of hydrophilic polymers: an FT-IR/AFM/TEM study. *J. Memb. Sci.* **209,** 283–292 (2002).

31. Li, R. H. & Barbari, T. A. Performance of poly(vinyl alcohol) thin-gel composite ultrafiltration membranes. *J. Memb. Sci.* **105,** 71–78 (1995).
32. Lee, K. P., Arnot, T. C. & Mattia, D. A review of reverse osmosis membrane materials for desalination-Development to date and future potential. *J. Memb. Sci.* **370,** 1–22 (2011).
33. Chennamsetty, R. K. Evolution of two polymeric nanofiltration membranes following ion beam irradiation. *ProQuest* (2007).
34. Rangby, B. Surface modification and lamination of polymers by photografting. *Int. J. Adhes. Adhes.* **19,** 337–343 (1999).
35. Mohammad, A. W. *et al.* Nanofiltration membranes review: Recent advances and future prospects. *Desalination* **356,** 226–254 (2014).
36. Sasaki, T., Fujimaki, H., Uemura, T. & Kurihara, M. Interfacially synthesized reverse os- mosis membrane, U.S. Patent No 4,758,343. (1988).
37. Sasaki, T., Fujimaki, H., Uemura, T. & Kurihara, M. Process for preparation of semiper- meable composite membrane, U.S. Patent No 4,857,363. (1989).
38. Hachisuka, H. & Ikeda, K. Reverse osmosis compositemembrane and reverse osmosis treatment method for water using the same, U.S. Patent No 6,413,425. (2002).
39. Kim, I.-C., Jegal, J. & Lee, K.-H. Effect of aqueous and organic solutions on the performance of polyamide thin-film-composite nanofiltration membranes. *J. Polym. Sci. Part B Polym. Phys.* **40,** 2151–2163 (2002).
40. Korikov, A. P., Kosaraju, P. B. & Sirkar, K. K. Interfacially polymerized hydrophilic microporous thin film composite membranes on porous polypropylene hollow fibers and flat films. *J. Memb. Sci.* **279,** 588–600 (2006).
41. Jimenez Solomon, M. F., Bhole, Y. & Livingston, A. G. High flux hydrophobic membranes for organic solvent nanofiltration (OSN)—Interfacial polymerization, surface modification and solvent activation. *J. Memb. Sci.* **434,** 193–203 (2013).
42. Vinh-Thang, H. & Kaliaguine, S. Predictive models for mixed-matrix membrane performance: a review. *Chem. Rev.* **113,** 4980–5028 (2013).
43. Singh, T., Kang, D.-Y. & Nair, S. Rigorous calculations of permeation in mixed-matrix membranes: Evaluation of interfacial equilibrium effects and permeability-based models. *J. Memb. Sci.* **448,** 160–169 (2013).
44. Chung, T.-S., Jiang, L. Y., Li, Y. & Kulprathipanja, S. Mixed matrix membranes (MMMs) comprising organic polymers with dispersed inorganic fillers for gas separation. *Prog. Polym. Sci.* **32,** 483–507 (2007).
45. Pal, R. Permeation models for mixed matrix membranes. *J. Colloid Interface Sci.* **317,** 191–198 (2008).
46. Car, A., Stropnik, C. & Peinemann, K.-V. Hybrid membrane materials with different metal–organic frameworks (MOFs) for gas separation. *Desalination* **200,** 424–426 (2006).
47. Nik, O. G., Chen, X. Y. & Kaliaguine, S. Functionalized metal organic framework-polyimide mixed matrix membranes for CO2/CH4 separation. *J. Memb. Sci.* **413-414,** 48–61 (2012).
48. Sorribas, S., Gorgojo, P. & Livingston, A. G. High Flux Thin Film Nanocomposite Membranes Based on Metal − Organic Frameworks for Organic Solvent Nano filtration. *J. Am. Chem. Soc.* **135,** 15201–8 (2013).
49. Vankelecom, I. F. J. *et al.* Silylation to improve incroporation of zeolites in Polyimide Films. *J. Phys. Chem.* **100,** 3753–3758 (1996).
50. Mahajan, R. Formation, characterization and modeling of mixed matrix membrane materials. (2000).
51. Li, Y., Chung, T., Cao, C. & Kulprathipanja, S. The effects of polymer chain rigidification, zeolite pore size and pore blockage on polyethersulfone (PES)-zeolite A mixed matrix membranes. *J. Memb. Sci.* **260,** 45–55 (2005).
52. Süer, M. G., Bac, N. & Yilmaz, L. Gas permeation characteristics of polymer-zeolite membranes. *J. Memb. Sci.* **91,** 77–86 (1994).
53. Bastani, D., Esmaeili, N. & Asadollahi, M. Polymeric mixed matrix membranes containing zeolites as a filler for gas separation applications: A review. *J. Ind. Eng. Chem.* **19,** 375–393 (2013).
54. Rodríguez-Calvo, A., Silva-Castro, G. A., Osorio, F., González-López, J. & Calvo, C. Novel Membrane Materials for Reverse Osmosis Desalination. *Hydrol. Curr. Res.* **5,** 1000167 (2014).
55. Lind, M. L. *et al.* Influence of zeolite crystal size on zeolite-polyamide thin film nanocomposite membranes. *Langmuir* **25,** 10139–45 (2009).
56. Lin, L., Wang, A., Zhang, L., Dong, M. & Zhang, Y. Novel mixed matrix membranes for sulfur removal and for fuel cell applications. *J. Power Sources* **220,** 138–146 (2012).
57. Ward, J. K. & Koros, W. J. Crosslinkable mixed matrix membranes with surface modified molecular sieves for natural gas purification: II. Performance characterization under contaminated feed conditions. *J. Memb. Sci.* **377,** 82–88 (2011).

58. Zirehpour, A., Rahimpour, A., Jahanshahi, M. & Peyravi, M. Mixed matrix membrane application for olive oil wastewater treatment: Process optimization based on Taguchi design method. *J. Environ. Manage.* **132,** 113–120 (2014).
59. Liu, S., Liu, G., Shen, J. & Jin, W. Fabrication of MOFs/PEBA mixed matrix membranes and their application in bio-butanol production. *Sep. Purif. Technol.* **133,** 40–47 (2014).
60. Jeong, B.-H. *et al.* Interfacial polymerization of thin film nanocomposites: A new concept for reverse osmosis membranes. *J. Memb. Sci.* **294,** 1–7 (2007).
61. Kim, E.-S. & Deng, B. Fabrication of polyamide thin-film nano-composite (PA-TFN) membrane with hydrophilized ordered mesoporous carbon (H-OMC) for water purifications. *J. Memb. Sci.* **375,** 46–54 (2011).
62. Duan, J. *et al.* High-performance polyamide thin-film-nanocomposite reverse osmosis membranes containing hydrophobic zeolitic imidazolate framework-8. *J. Memb. Sci.* **476,** 303–310 (2014).
63. Amini, M., Jahanshahi, M. & Rahimpour, A. Synthesis of novel thin film nanocomposite (TFN) forward osmosis membranes using functionalized multi-walled carbon nanotubes. *J. Memb. Sci.* **435,** 233–241 (2013).
64. Jadav, G. L. & Singh, P. S. Synthesis of novel silica-polyamide nanocomposite membrane with enhanced properties. *J. Memb. Sci.* **328,** 257–267 (2009).
65. Wu, H., Tang, B. & Wu, P. Optimizing polyamide thin film composite membrane covalently bonded with modified mesoporous silica nanoparticles. *J. Memb. Sci.* **428,** 341–348 (2013).
66. Yin, J., Kim, E.-S., Yang, J. & Deng, B. Fabrication of a novel thin-film nanocomposite (TFN) membrane containing MCM-41 silica nanoparticles (NPs) for water purification. *J. Memb. Sci.* **423-424,** 238–246 (2012).
67. Lee, H. S. *et al.* Polyamide thin-film nanofiltration membranes containing TiO2 nanoparticles. *Desalination* **219,** 48–56 (2008).
68. Chae, H.-R., Lee, J., Lee, C.-H., Kim, I.-C. & Park, P.-K. Graphene oxide-embedded thin-film composite reverse osmosis membrane with high flux, anti-biofouling, and chlorine resistance. *J. Memb. Sci.* **483,** 128–135 (2015).
69. Lee, S. Y. *et al.* Silver nanoparticles immobilized on thin film composite polyamide membrane : characterization, nanofiltration, antifouling properties. *Polym. Adv. Technol.* **18,** 562–568 (2007).
70. Huang, H., Qu, X., Dong, H., Zhang, L. & Chen, H. Role of NaA zeolites in the interfacial polymerization process towards a polyamide nanocomposite reverse osmosis membrane. *RSC Adv.* **3,** 8203–8207 (2013).
71. Liu, T., Liu, Z., Zhang, R., Van der Bruggen, B. & Wang, X. Fabrication of a thin film nanocomposite hollow fiber nanofiltration membrane for wastewater treatment. *J. Memb. Sci.* **488,** 92–102 (2015).
72. LG NanoH2O. Frequently Asked Questions. at <http://www.lg-nanoh2o.com/technology/faqs>
73. Gascon, J., Corma, A., Kapteijn, F. & Llabre, F. X. Metal Organic Framework Catalysis : Quo vadis ? *Am. Chem. Soc.* **4,** 361–378 (2014).
74. Fairen-Jimenez, D. *et al.* Opening the gate: framework flexibility in ZIF-8 explored by experiments and simulations. *J. Am. Chem. Soc.* **133,** 8900–2 (2011).
75. Krishna, R. & van Baten, J. M. In silico screening of metal-organic frameworks in separation applications. *Phys. Chem. Chem. Phys.* **13,** 10593–616 (2011).
76. Keeffe, M. O. & Yaghi, O. M. New Microporous Crystalline Materials: MOFS, COFS and ZIFS.
77. Park, K. S. *et al.* Exceptional chemical and thermal stability of zeolitic imidazolate frameworks. *Proc. Natl. Acad. Sci.* (2006).
78. Wee, L. H. *et al.* Hierarchical Zeolitic Imidazolate Framework-8 Catalyst for Monoglyceride Synthesis. *ChemCatChem* **5,** 3562–3566 (2013).
79. Cravillon, J. *et al.* Controlling Zeolitic Imidazolate Framework Nano- and Microcrystal Formation : Insight into Crystal Growth by Time-Resolved In Situ Static Light Scattering. *Chem. Mater.* **23,** 2130–2141 (2011).
80. Venna, S. R., Jasinski, J. B. & Carreon, M. a. Structural evolution of zeolitic imidazolate framework-8. *J. Am. Chem. Soc.* **132,** 18030–3 (2010).
81. Sun, C.-Y. *et al.* Zeolitic imidazolate framework-8 as efficient pH-sensitive drug delivery vehicle. *Dalt. Trans.* **41,** 6906–6909 (2012).
82. Aguado, S. *et al.* Guest-induced gate-opening of a zeolite imidazolate framework. *New J. Chem.* **35,** 546–550 (2011).
83. Bux, H. *et al.* Zeolitic imidazolate framework membrane with molecular sieving properties by microwave-assisted solvothermal synthesis. *J. Am. Chem. Soc.* **131,** 16000–1 (2009).
84. Moggach, S. A., Bennett, T. D. & Cheetham, A. K. The Effect of Pressure on ZIF-8: Increasing Pore Size with Pressure and the Formation of a High-Pressure Phase at 1.47 GPa. *Angew. Chemie* **121,** 7221–7223 (2009).

85. Pan, Y., Liu, Y., Zeng, G., Zhao, L. & Lai, Z. Rapid synthesis of zeolitic imidazolate framework-8 (ZIF-8) nanocrystals in an aqueous system. *Chem. Commun.* **47,** 2071–2073 (2011).
86. Venna, S. R., Jasinski, J. B. & Carreon, M. A. Structural evolution of zeolitic imidazolate framework-8. *J. Am. Chem. Soc.* **132,** 18030–3 (2010).
87. Bux, H., Chmelik, C., Krishna, R. & Caro, J. Ethene/ethane separation by the MOF membrane ZIF-8: Molecular correlation of permeation, adsorption, diffusion. *J. Memb. Sci.* **369,** 284–289 (2011).
88. Li, K. *et al.* Zeolitic imidazolate frameworks for kinetic separation of propane and propene. *J. Am. Chem. Soc.* **131,** 10368–9 (2009).
89. Venna, S. R. & Carreon, M. a. Highly permeable zeolite imidazolate framework-8 membranes for CO2/CH4 separation. *J. Am. Chem. Soc.* **132,** 76–8 (2010).
90. Li, Y., Wee, L. H., Volodin, A., Martens, J. a & Vankelecom, I. F. J. Polymer supported ZIF-8 membranes prepared via an interfacial synthesis method. *Chem. Commun.*. **51,** 918–20 (2015).
91. Dai, Y., Johnson, J. R., Karvan, O., Sholl, D. S. & Koros, W. J. Ultem®/ZIF-8 mixed matrix hollow fiber membranes for CO2/N2 separations. *J. Memb. Sci.* **401-402,** 76–82 (2012).
92. Vasconcelos, I. B. *et al.* Cytotoxicity and slow release of the anti-cancer drug doxorubicin from ZIF-8. *RSC Adv.* **2,** 9437–9442 (2012).
93. Prakash Rao, A., Desai, N. V. & Rangarajan, R. Interfacially synthesized thin film composite RO membranes for seawater desalination. *J. Memb. Sci.* **124,** 263–272 (1997).
94. Tang, C. Y., Kwon, Y. N. & Leckie, J. O. Effect of membrane chemistry and coating layer on physiochemical properties of thin film composite polyamide RO and NF membranes. I. FTIR and XPS characterization of polyamide and coating layer chemistry. *Desalination* **242,** 149–167 (2009).
95. Kang, G., Liu, M., Lin, B., Cao, Y. & Yuan, Q. A novel method of surface modification on thin-film composite reverse osmosis membrane by grafting poly(ethylene glycol). *Polymer.* **48,** 1165–1170 (2007).
96. Zhang, R.-X. *et al.* Effect of the manufacturing conditions on the structure and performance of thin-film composite membranes. *J. Appl. Polym. Sci.* **125,** 3755–3769 (2012).
97. Hu, Z., Chen, Y. & Jiang, J. Zeolitic imidazolate framework-8 as a reverse osmosis membrane for water desalination: Insight from molecular simulation. *J. Chem. Phys.* **134,** 134705–1 – 134705–6 (2011).
98. Kamada, T., Ohara, T., Shintani, T. & Tsuru, T. Controlled surface morphology of polyamide membranes via the addition of co-solvent for improved permeate flux. *J. Memb. Sci.* **467,** 303–312 (2014).
99. Tang, C. Y., Kwon, Y. N. & Leckie, J. O. Probing the nano- and micro-scales of reverse osmosis membranes-A comprehensive characterization of physiochemical properties of uncoated and coated membranes by XPS, TEM, ATR-FTIR, and streaming potential measurements. *J. Memb. Sci.* **287,** 146–156 (2007).
100. Freger, V. Nanoscale Heterogeneity of Polyamide Membranes Formed by Interfacial Polymerization. *Langmuir* **37,** 4791–4797 (2003).
101. Na, Y. H., Sooriyakumaran, R., Vora, A. & Diep, J. Thin film composite membranes embedded with molecular cage compounds, U.S. Patent Application 13/175,661. (2011).
102. Zhao, H. *et al.* Improving the performance of polyamide reverse osmosis membrane by incorporation of modified multi-walled carbon nanotubes. *J. Memb. Sci.* **450,** 249–256 (2014).
103. Ratto, T. V., Holt, J. K. & Szmodis, A. W. Membranes with embedded nanotubes for selective permeability, U.S. Patent No 7,993,524. (2011).
104. Huang, H. *et al.* Acid and multivalent ion resistance of thin film nanocomposite RO membranes loaded with silicalite-1 nanozeolites. *J. Mater. Chem. A* **1,** 11343–11349 (2013).
105. Kong, C., Shintani, T. & Tsuru, T. 'Pre-seeding'-assisted synthesis of a high performance polyamide-zeolite nanocomposite membrane for water purification. *New J. Chem.* **34,** 2101–2104 (2010).
106. Vanherck, K., Cano-Odena, A., Koeckelberghs, G., Dedroog, T. & Vankelecom, I. A simplified diamine crosslinking method for PI nanofiltration membranes. *J. Memb. Sci.* **353,** 135–143 (2010).
107. Chen, H. *et al.* Free-Volume Depth Profile of Polymeric Membranes Studied by Positron Annihilation Spectroscopy: Layer Structure from Interfacial Polymerization. *Macromolecules* **40,** 7542–7557 (2007).
108. Kurmoo, M. Magnetic metal-organic frameworks. *Chem. Soc. Rev.* **38,** 1353–79 (2009).

Supplementary information

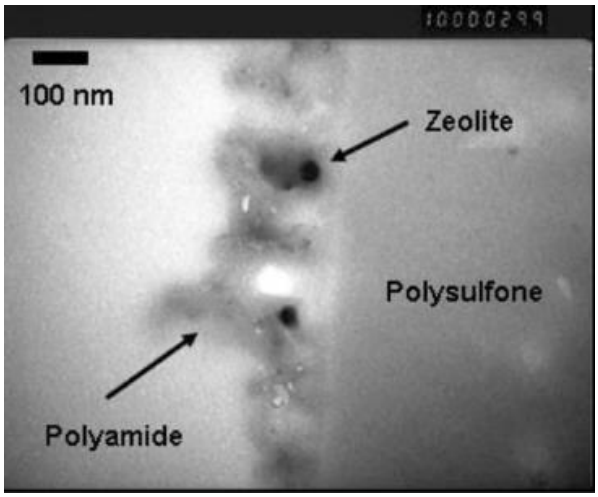

Supplementary Figure 1: TEM image on which the Maxwell model was applied.[60]

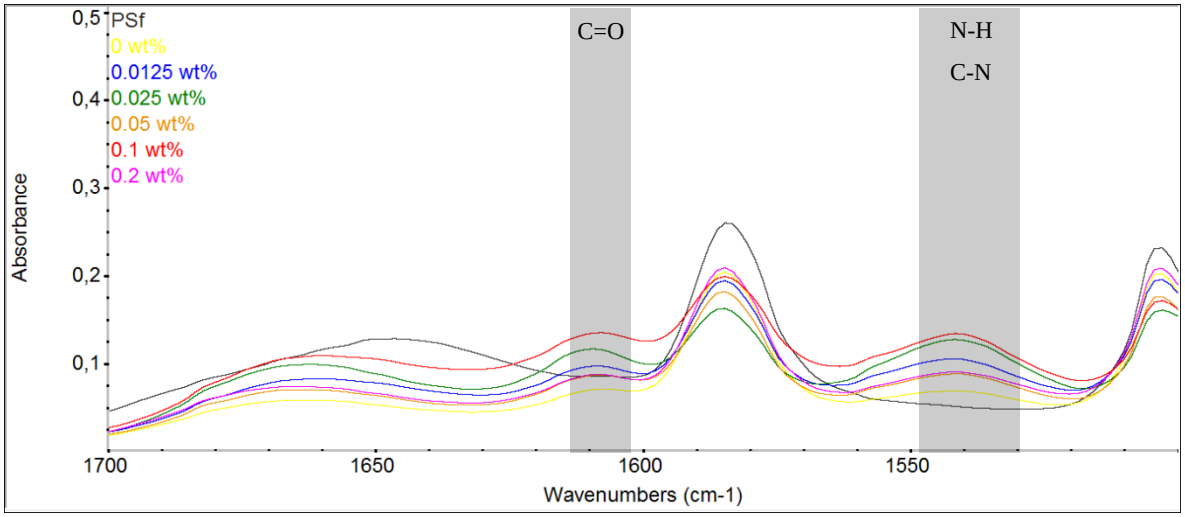

Supplementary Figure 2: ATR-IR spectra of all ECFP membranes, with sZIF-8 as filler. The typical C=O stretch is visible at around 1610 cm-1 and the N-H bend at 1540 cm-1 for all filler loadings.

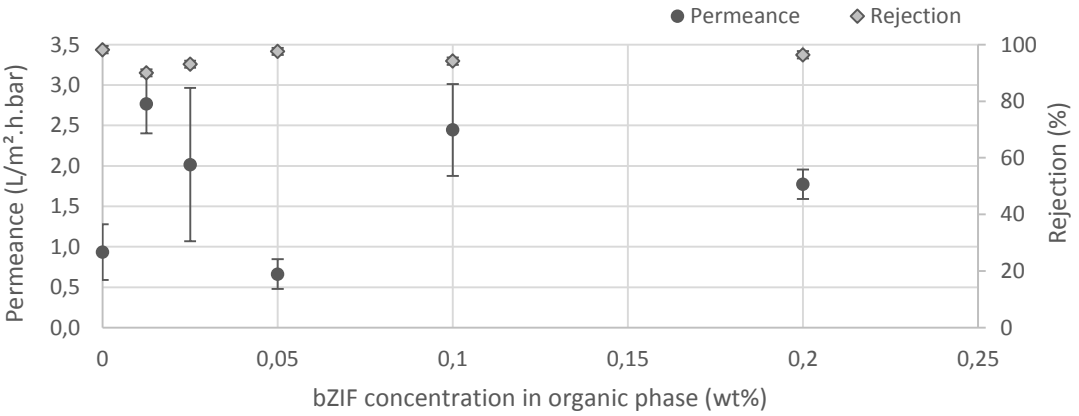

Supplementary Figure 3: Water permeance and RB rejection of ECFP membranes with bZIF-8 as filler. Filtration conditions: 35 μM in MQ-water, 10 bar.

ECFP bZIF

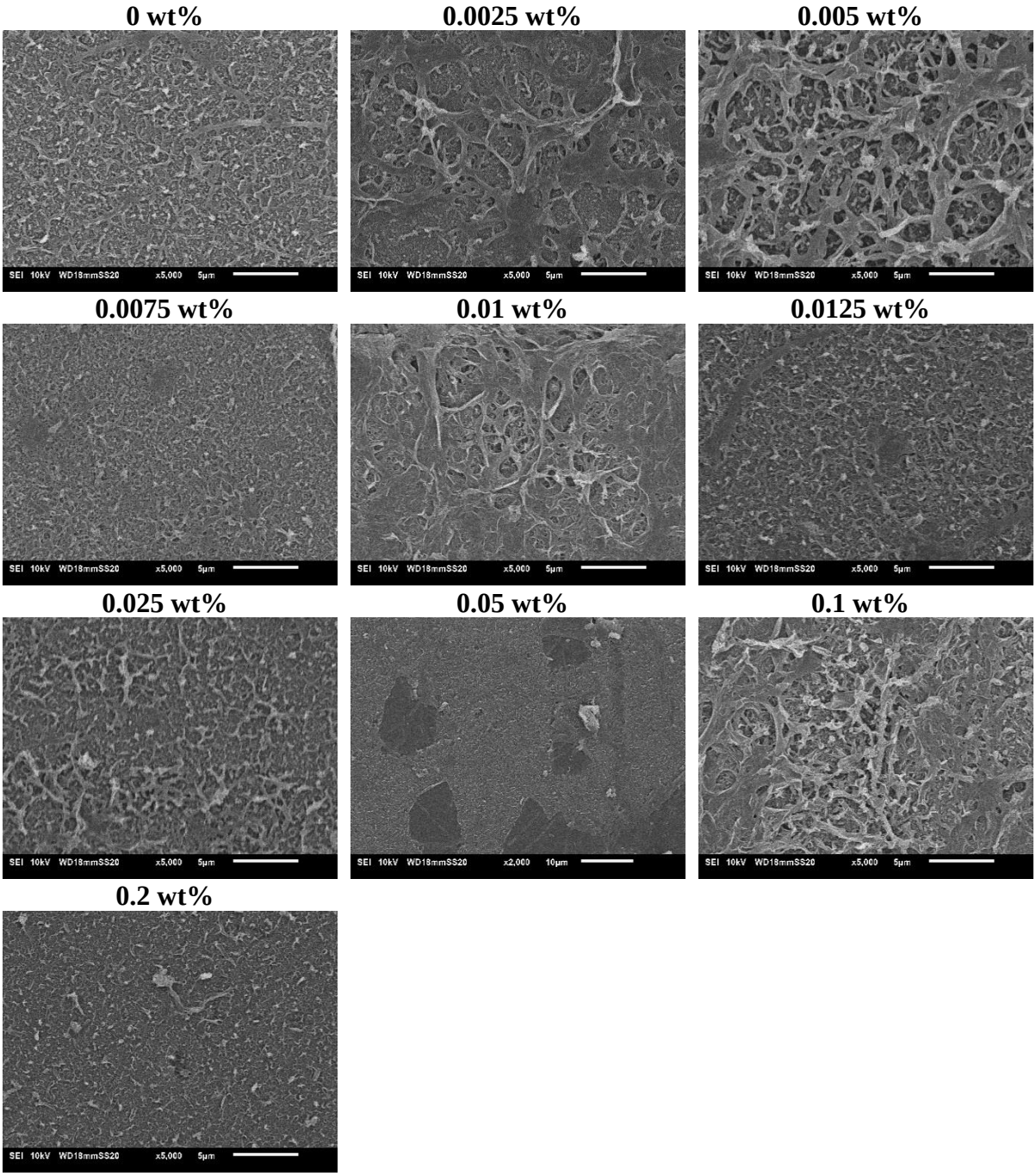

Supplementary Figure 4: SEM images of the ECFP membranes made with bZIF as filler, at a magnification of 5000x.

ECFP sZIF

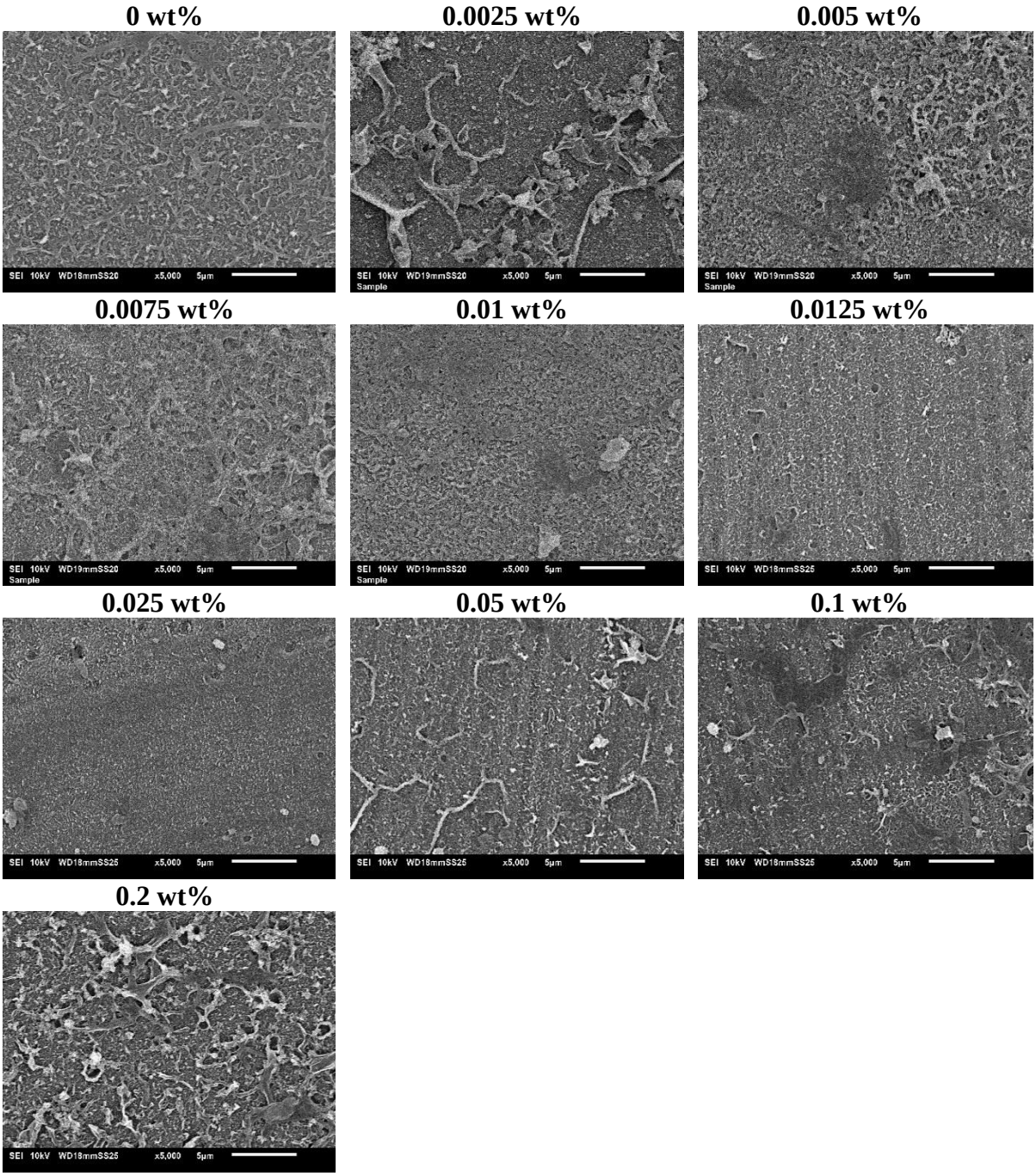

Supplementary Figure 5: SEM images of the ECFP membranes made with sZIF as filler, at a magnification of 5000x.

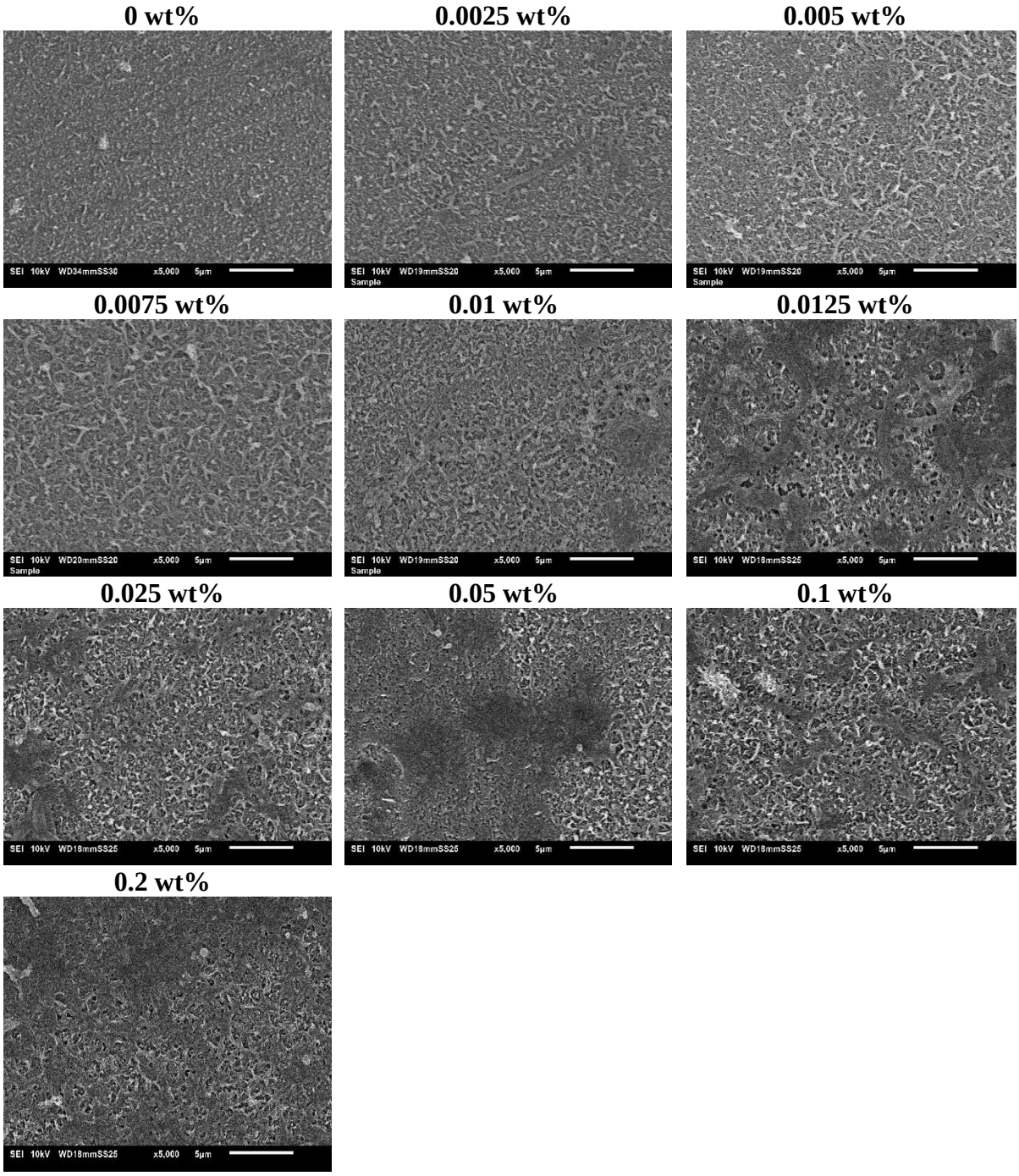

Supplementary Figure 6: SEM images of the TRAD membranes made with bZIF as filler, at a magnification of 5000x.

TRAD sZIF

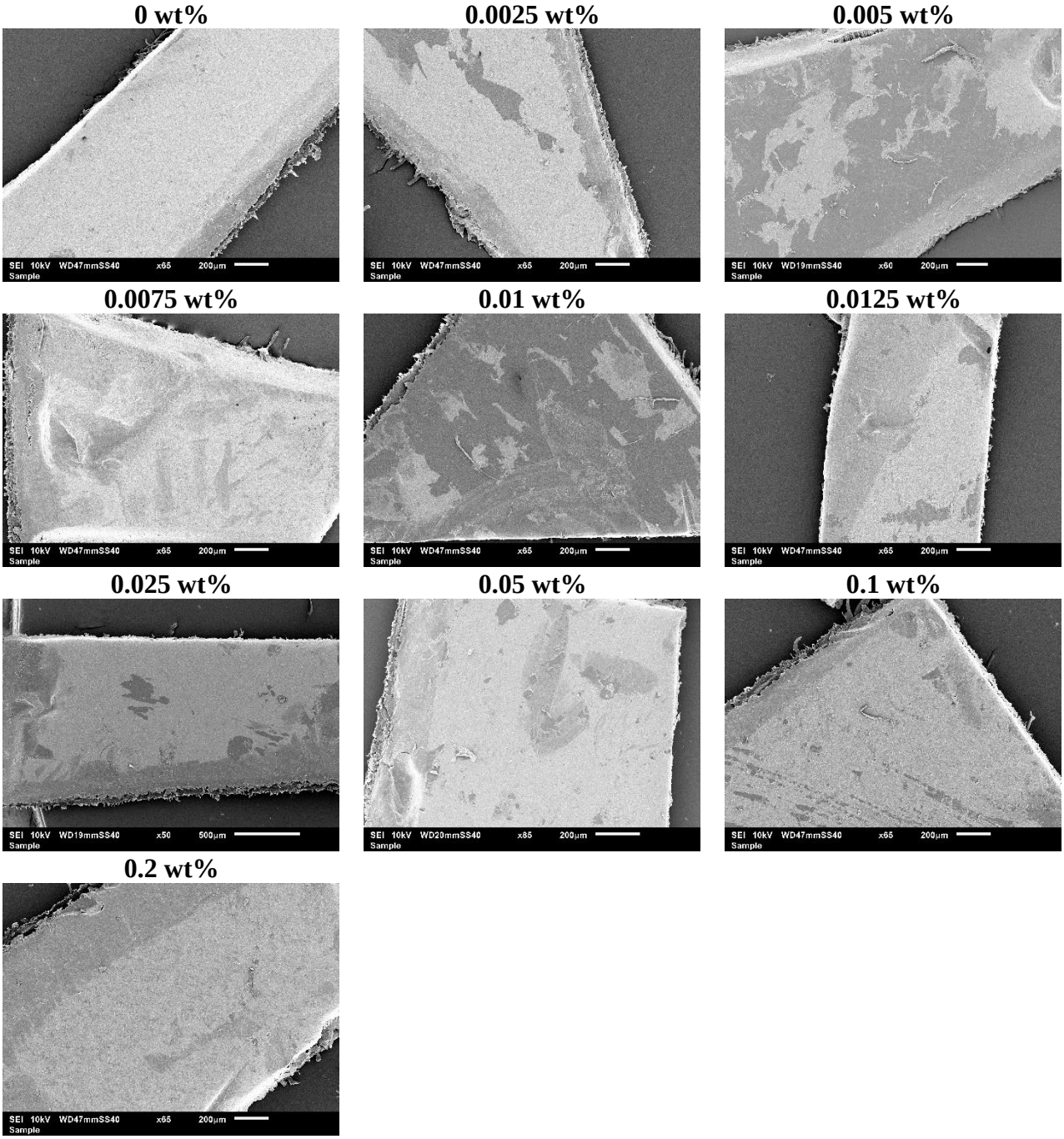

Supplementary Figure 7: SEM images of the TRAD membranes made with sZIF as filler, at a magnification of 65x.

TRAD sZIF

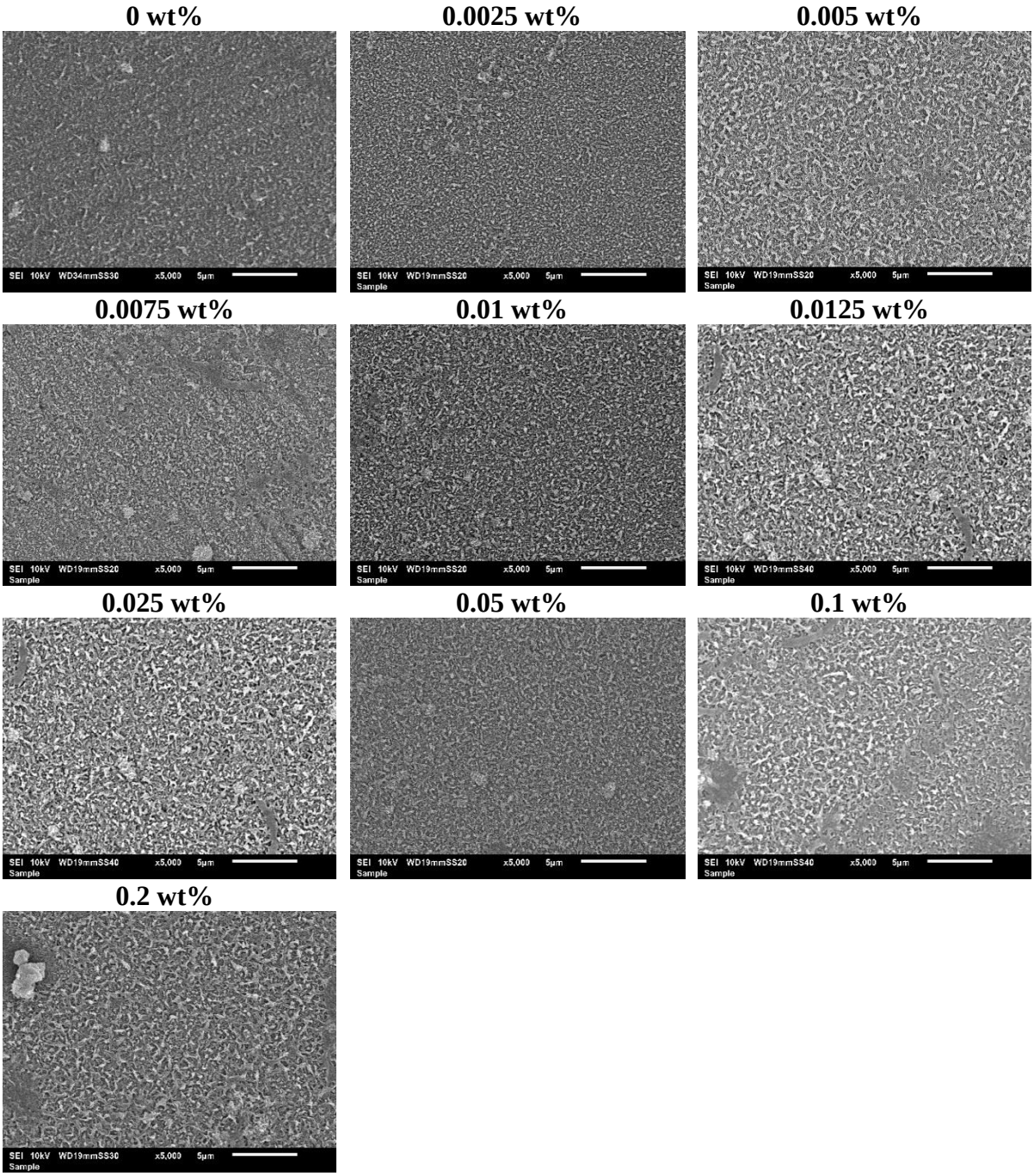

Supplementary Figure 8: SEM images of the TRAD membranes made with sZIF as filler, at a magnification of 5000x.

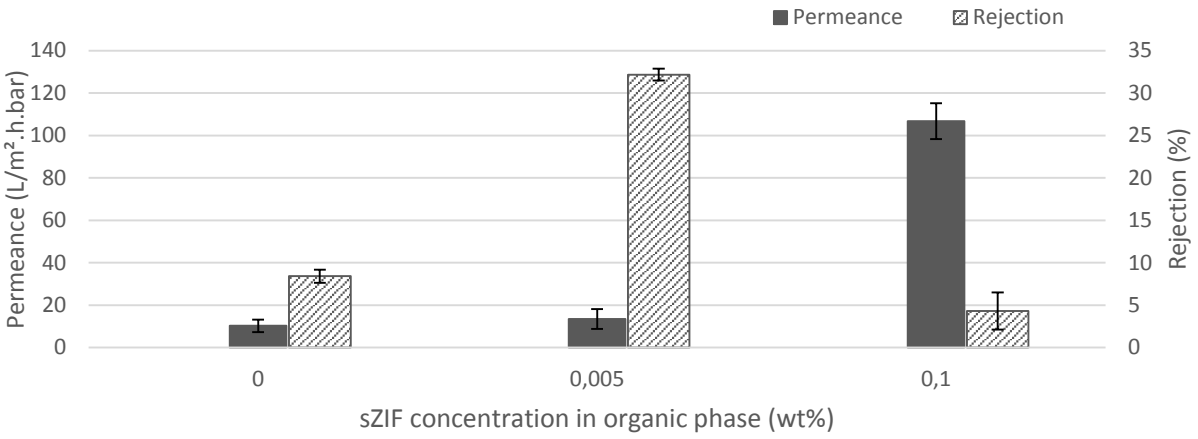

Supplementary Figure 9: NaCl permeance and rejection of ECFP CMPI membranes with sZIF-8 as filler. Filtration conditions: 1000 ppm NaCl in MQ-water, 10 bar.

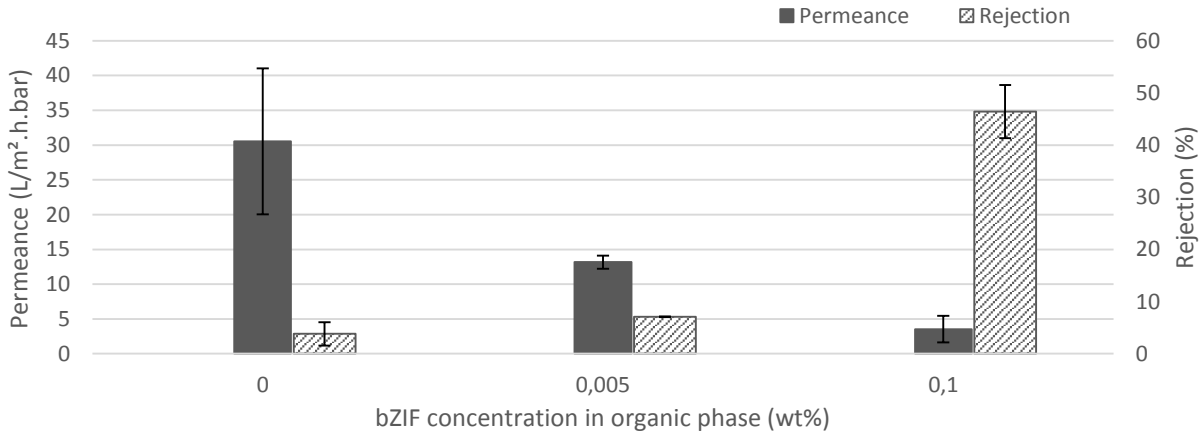

Supplementary Figure 10: NaCl permeance and rejection of TRAD CMPI membranes with bZIF-8 as filler. Filtration conditions: 1000 ppm NaCl in MQ-water, 10 bar.

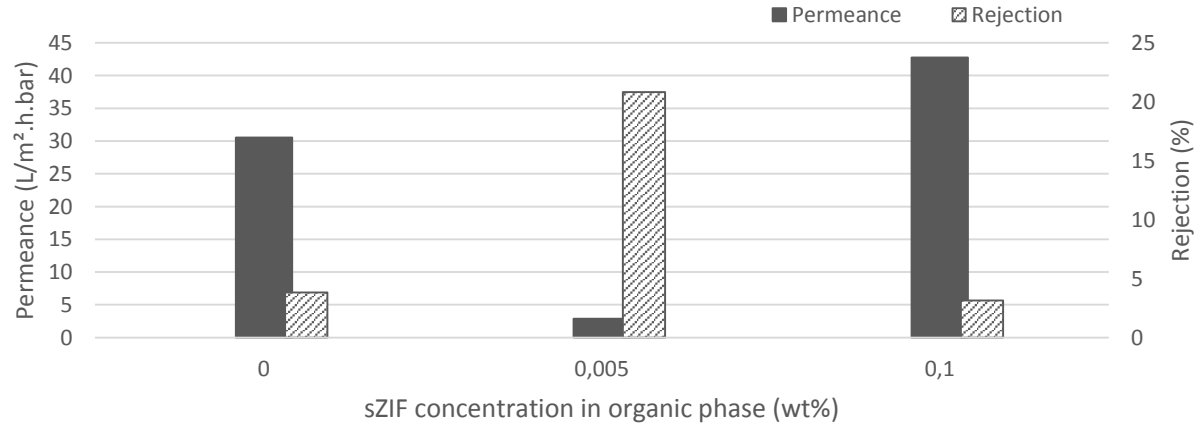

Supplementary Figure 11: NaCl permeance and rejection of TRAD CMPI membranes with sZIF-8 as filler. Filtration conditions: 1000 ppm NaCl in MQ-water, 10 bar.

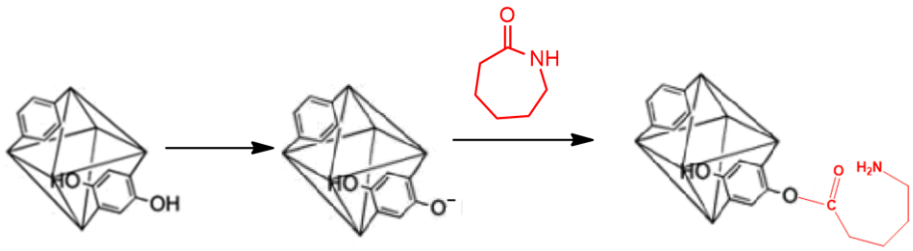

Supplementary Figure 12: Ring opening mechanism of caprolactam via the nucleophilic oxygen anion, present on a modified UiO-66 particles.

"An investment in knowledge always pays the best interest."

- B. Franklin

DIENSTEN ALGEMEEN BEHEER
DIRECTIE STAFDIENSTEN ALGEMEEN BEHEER
DIENST VGM
W. DE CROYLAAN 58 – BUS 5530, BE-3001 LEUVEN
TEL. + 32 16 32 20 24 FAX + 32 16 32 29 95
WWW.KULEUVEN.BE/VGM vgm@kuleuven.be

KATHOLIEKE
UNIVERSITEIT
LEUVEN

MELDINGSFORMULIER:
RISICOANALYSE VOOR EXPERIMENT MET CHEMISCHE PRODUCTEN VAN RISICOKLASSE E3 EN E4

Vul het formulier elektronisch in, in overleg met het VGM-antennelid chemische veiligheid.

1. Identificatie van de afdeling (gebruikers)

Aanvrager/contactpersoon: Sanne Hermans, Rhea Verbeke
Tel: 016/32 86 97
E-mail adres: sanne.hermans@biw.kuleuven.be

Afdeling: Centrum voor Oppervlaktechemie en Katalyse (COK)
Magazijncode[1]: INB1
Leidinggevende : Ivo Vankelecom

2. Identificatie experiment

Titel(benaming): Interfaciale polymerisatie membranen (maximaal 40 karakters)
Startdatum: 27/11/2014 Geplande einddatum: 01/06/2014

☐ Het betreft een nieuw experiment
☐ Het betreft een bestaand experiment zonder eerder opgestelde risicoanalyse
☒ Het betreft een wijziging/uitbreiding van een bestaand experiment met eerder opgestelde risicoanalyse
Deze wijziging/uitbreiding betreft (gelieve aan te duiden en verder in het formulier te beschrijven):
☒ personen
☐ lokalen waar het experiment plaatsvindt
☒ chemische producten
☐ andere risico's
☐ verlenging
Dossiernummer of referentienummer vorig advies: KG/2010.0017 (indien gekend)

☒ Indien VGM-DOSSIER beschikbaar:
☒ experiment in het kader van een bestaande activiteit
Geef nummer van de activiteiten: deelactiviteit 2 in vorige risicoanalyse
☐ experiment in het kader van een nieuwe activiteit (in overleg met VGM-antenne en Afdelingshoofd[1])
Geef naam van de nieuwe activiteit voor het VGM-dossier: (max. 40 karakters)

☐ Doorloopproeven (**onbewaakt** experiment binnen of buiten de diensturen)

[1] https://admin.kuleuven.be/vgm/intranet/doc/antenne/antennemagazijncodes.xlsx/view

Beschrijving van al de aangewende(of gevormde) chemische producten*

Productnaam	**Casnummer**	**Fysische toestand** (gas/vloei-baar/vast)	**Aangewende hoeveelheid**	**Aangewende concentratie**	**Chemische risicoklasse product (E4/E3/E2/E1)**
1. n-hexaan	110-54-3	vloeibaar	250 ml	Solvent for 4	E3
2. N-methylpyrrolidon	872-50-4	vloeibaar	90 g	Solvent for 7	E4
3. piperazine	110-85-0	vast	10 g	4 wt/v%	E3
4. 1,3,5-benzeentricarbonyltrichloride	4422-95-1	vast	0,25 g	0,1 wt/v%	E2
5. natrium dodecylsulfaat	151-21-3	vast	0.25 g	0,1 wt/v%	E1
6. triethylamine	121-44-8	vloeibaar	2.5 g	1 wt/v%	E3
7. polysulfon	25154-01-2	vast	16.2 g	18 wt%	E1
8. roos bengaal	632-69-9	vast	0.01779 g	35 µM	E1
9. 2-propanol	67-63-0	vloeibaar	500 ml	Solvent for 8	E3
10. m-fenyleendiamine	108-45-2	vast	5 g	2 wt/v%	E3

*** Indien mogelijk de zeer gevaarlijke producten of processen vervangen door minder gevaarlijke !**

Lokaalgegevens

Gebouw	**Lokaal**	**Omschrijving deelactiviteit** (bv. voorbereiding, experiment, nabehandeling, meting, …)	**Specificaties lokaal**
331.01	03.95	1. Synthese steunlaagmembraan	☒ eigen afdeling ☐ ruimte toegewezen aan andere afdeling
331.01	03.95	2. Synthese composietmembraan (interfaciale polymerisatie)	☒ eigen afdeling ☐ ruimte toegewezen aan andere afdeling
331.01	03.95	3. Klassieke filtratie-experimenten (metingen)	☒ eigen afdeling ☐ ruimte toegewezen aan andere afdeling
331.01	03.105	4. High-throughput filtratie-experimenten (metingen)	☒ eigen afdeling ☐ ruimte toegewezen aan andere afdeling

* indien manipulaties worden uitgevoerd in een ruimte toegewezen aan een andere afdeling dan moet het meldingsformulier ook naar dit afdelingshoofd gestuurd worden (in kopie).

Personen die het experiment zullen uitvoeren of voor een practicum het toezichthoudend personeel

Naam - voornaam	**Geboorte datum**	**Personeelsgroep**
Hermans Sanne	25/05/1986	☒ KU ☐ Student KU ☐ UZ ☐ VIB ☐ Externen:
Verbeke Rhea	30/11/1992	☐ KU ☒ Student KU ☐ UZ ☐ VIB ☐ Externen:

3. Beschrijving experiment en risicoanalyse

Beschrijving handelingen en aangewende technieken:

Nummer* **deel-activiteit**	**Beschrijving handelingen(manipulaties) en technieken**	**Gebruikte uitrusting**	**Nummers ** gebruikte producten**
1	Afwegen, mengen, casten polymeeroplossing	Geijkte weegschaal (331-01_03-95#BAL1), roerplaat (331-01_03-95#MSH001), automatische filmapplicator (331-01_03-95#COAT)	2, 3, 5, 6, 7
2	Afwegen, mengen, interfaciale polymerisatie	Geijkte weegschaal (331-01_03-95#BAL1), roerplaat (331-01_03-95#MSH001), glazen bekers	membraan uit deelexperiment 1; 1, 4
3	Voedingsmengsel en druk aanbrengen, filtreren	filtratiecel (331-01_03-95#SC001), stikstofleiding	membraan uit deelexperiment 1 en 2; 8, 9
4	Voedingsmengsel en druk aanbrengen, filtreren	High-throughput filtratiemodule (331-01_03-105#Spider3), stikstofleiding	membraan uit deelexperiment 1 en 2; 8, 9

* Nummer van het deelexperiment zoals weergegeven onder “Lokaalgegevens”

** Nummer chemische producten zoals weergegeven onder “Beschrijving aangewende(of gevormde) chemische producten”

Frequentie uitvoering experiment:

- ☒ Dagelijks
- ☒ Wekelijks
- ☐ Maandelijks
- ☐ Minder dan maandelijks

Indien gewenst, kan u hier meer informatie over het experiment toevoegen (bv. reactieschema) of verwijzen naar een bijlage

Deze stoffen zullen gebruikt worden voor interfaciale polymerisatie.
Werkingsprincipe van interfaciale polymerisatie (zie ook vorige risicoanalyse):
Bij deze techniek wordt een steunlaag geïmpregneerd, typisch met een waterige amineoplossing, en vervolgens in contact gebracht met een niet-mengbaar organisch solvent dat een tweede monomeer bevat, typisch een hexaangebaseerde acylchloride oplossing. Aan de interfase reageren beide monomeren dan tot een zeer dun polyamidelaagje.

Risico’s verbonden aan de chemische producten

Vóór het gebruik van de chemische producten dienen de gevaren, R- of H- en S of P-zinnen, gekend te zijn!

Op te zoeken in de KULeuven gevaarlijke stoffendatabank (via KULoket, algemeen, gevaarlijke stoffen) of op de veiligheidsinformatiebladen van de fabrikant.

Voor de producten van risicoklasse E3 en **E4** dienen de gevaren aangeduid te worden in onderstaande tabel.

Naam chemisch product	n-hexaan	2-propanol	N-methylpyrolidon	m-fenyleendiamine	triethylamine
Explosie- en brandgevaar					
Zeer licht of licht ontvlambaar (R11, **R12**)	☒	☐	☐	☐	☒
Explosief (**R1**, **R2**, **R3,** R5) +metalen (R4) +O2 (**R6**) +brandb.stoffen (R9) + afgesloten en T↑ (R44)	☐	☐	☐	☐	☐
Instabiel product (**R17**, R18, R19)	☐	☐	☐	☐	☐
Incompatibel met water (R14, R15)	☐	☐	☐	☐	☐
Incompatibel met oxiderende stoffen (R16)	☐	☐	☐	☐	☐
Acuut gevaar voor gezondheid					
Zeer giftig (**R26**, **R27**, **R28**) + zuur (**R32**) Giftig (R23, R24) + water (R29) + zuur (R31)	☐	☒	☒	☒	☒
Ernstige brandwonden (R35)	☐	☐	☐	☐	☒
Gevaar voor gezondheid op langere termijn					
Kankerverwekkend of kanker niet uitgesloten (**R40**, **R45, R49**)	☐	☐	☐	☐	☐
Teratogeen (R63, **R61**) en schade aan vruchtbaarheid (**R60**, R62)	☒	☒	☒	☐	☐
Mutageen (**R46**)	☐	☐	☐	☐	☐
Ernstige onherstelbare effecten (mogelijks) (R39, R68), Gezondheidsschade bij langdurige blootstelling (R48)	☒	☐	☐	☒	☐

Bijkomende opmerkingen voor bepaalde producten:

Andere risico's verbonden aan het experiment

☐ Verbranden, bevriezen (☐ hoge of lage temperaturen, ☐ cryogene stoffen, …)
☒ Implosie, explosie (☒ hoge drukken, ☐ lage drukken, ☐ onderdruk, …)
☐ Brand (☐ ovens, ☐ verwarmingsspiralen, ☐ bunzenbrander, ☐ oliebaden …)
☐ Niet-ioniserende straling (☐ NMR, ☐ lasers, ☐ UV-lampen, ...)
☐ Elektrocutie (☐ naakte contacten, ☐ vochtige omgeving, ☐ hoge vermogens, ...)
☐ Valgevaar (☐ opstellingen op hoogte, ☐ in de hoogte, ☐ moeilijk bereikbaar, ...)
☐ Biologisch risico (☐ pathogene µ-organismen, ☐ GGO, ☐ cellen, ☐ bloed, ☐ proefdieren, ...)
☐ Ioniserende straling (X-stralen, radio-isotopen, ...)
☐ De kans bestaat dat bij een ernstig incident **NIET** zelfstandig alarm kan gegeven worden (bv. gebruik van zeer toxische dampen of gassen, explosierisico, aanwezigheid verstikkend gas, …)

☐Andere:

Voorzorgsmaatregelen toe te passen

Nummer Deelexperiment*	1	2	3	4	5
Collectieve beschermingsmiddelen					
- Gesloten systeem	☐	☐	☐	☐	☐
- Zuurkast(trekkast)	☒	☒	☒	☒	☐
- Plaatselijke afzuiging	☐	☐	☐	☐	☐
- Ruimtelijke afzuiging	☐	☐	☐	☐	☐
- Veiligheidsscherm	☐	☐	☐	☐	☐
- Opvangbakken onder opstelling	☐	☐	☐	☐	☐
- Andere:	☐	☐	☐	☐	☐
Individuele beschermingsmiddelen					
- Laboschort	☒	☒	☒	☒	☒
- Veiligheidsbril	veiligheidsbril (artnr. 18042)	veiligheidsbril (artnr. 18042)	veiligheidsbril (artnr. 18042)	veiligheidsbril (artnr. 18042)	veiligheidsbril (artnr. 18042)
- Handschoenen:	wegwerpnitrile EN 374 (artnr. 58951)	wegwerpnitrile EN 374 (artnr. 58951)	wegwerpnitrile EN 374 (artnr. 58951)	wegwerpnitrile EN 374 (artnr. 58951)	wegwerpnitrile EN 374 (artnr. 58951)
- Maskers:	Kies een item.	Kies een item.	Kies een item.	Kies een item.	Kies een item.
- Wegwerp hygiëne haarnetje	☐	☐	☐	☐	☐
- Andere:	☐	☐	☐	☐	☐

Specifieke preventiemaatregelen

☒ controle werking zuurkast

☒ controle glaswerk op barsten

☐ bevestigen spanringen aan koelslangen

☐ automatisch uitschakelen verwarmingssysteem bij defecte koeling

☒ overdrukbeveiligingssysteem

☐ brandblusser voor metaalbranden (D-blusser) aanwezig

☐ zuurstofkit aanwezig (verplicht bij het werken met cyaniden)

☐ detector met alarm bij werken met giftige of brandbare gassen

☐ aanwezigheid gasmasker met specifieke filters (interventie)

☐ aanwezigheid calciumgluconaatzalf (werken met waterstoffluoride)

☒ interventiekit aanwezig

☐ specifiek neutralisatieproduct aanwezig nl.

☐ invullen en opsturen formulier doorloopproeven (zie https://admin.kuleuven.be/vgm/intranet/AntenneDoorloopproeven.html)

☒ aanwezigheid van een 2de persoon in de buurt vereist

☐ automatisch alarmsysteem (bv. dodemansalarm)

Andere:

Werkpraktijken

☒ Toepassen Code Goede Laboratoriumpraktijk https://admin.kuleuven.be/vgm/intranet/ChemischeVeiligheidCodeGoedeLabopraktijken.html)

☒ Interne opleiding en begeleiding
☒ Selectieve inzameling afval – chemisch afval

Bijzondere maatregelen bij storing/falen: beschrijf hoe een noodgeval wordt opgevangen (denk o.a. aan stroomuitval, ventilatie-uitval, uitval watertoevoer, uitval perslucht, uitval gastoevoer, …)

* Nummer van het deelexperiment zoals weergegeven onder "Lokaalgegevens"

Indien niet alle voorzorgsmaatregelen toegepast kunnen worden, mag het experiment niet starten!
Persoonlijke beschermingsmiddelen kunnen verkregen worden via het aanvraagformulier (https://admin.kuleuven.be/vgm/intranet/doc/personen/personenfaanvraagpbm.docx).

Chemisch afval
Per afvalfractie de categorie van het chemisch afval aangeven.

Afvalfractie	Afvalcategorie	Recipiënt aanwezig
Indien zuivere stoffen:		
gehalogeneerde organische afvalvloeistoffen	☐1 - ☐2 - ☐ 3 - ☒ 4 - ☐5 - ☐ 6 - ☐ Andere	☒
bijzondere afvalvloeistoffen (amines)	☐1 - ☐2 - ☐ 3 - ☐ 4 - ☒5 - ☐ 6 - ☐ Andere	☒
basische anorganische afvalvloeistoffen	☐1 - ☒2 - ☐ 3 - ☐ 4 - ☐5 - ☐ 6 - ☐ Andere	☒
niet-gehalogeneerde organische afvalvloeistoffen	☐1 - ☐2 - ☒ 3 - ☐ 4 - ☐5 - ☐ 6 - ☐ Andere	☒
Indien mengsels:		
Hoofdcomponent :	☐1 - ☐2 - ☐ 3 - ☐ 4 - ☐5 - ☐ 6 - ☐ Andere	☐
Hoofdcomponent : met	☐1 - ☐2 - ☐ 3 - ☐ 4 - ☐5 - ☐ 6 - ☐ Andere	☐
Hoofdcomponent : met	☐1 - ☐2 - ☐ 3 - ☐ 4 - ☐5 - ☐ 6 - ☐ Andere	☐
Hoofdcomponent : met	☐1 - ☐2 - ☐ 3 - ☐ 4 - ☐5 - ☐ 6 - ☐ Andere	☐
Hoofdcomponent : met	☐1 - ☐2 - ☐ 3 - ☐ 4 - ☐5 - ☐ 6 - ☐ Andere	☐
Hoofdcomponent : met	☐1 - ☐2 - ☐ 3 - ☐ 4 - ☐5 - ☐ 6 - ☐ Andere	☐
Andere:		
	☐1 - ☐2 - ☐ 3 - ☐ 4 - ☐5 - ☐ 6 - ☐ Andere	☐
	☐1 - ☐2 - ☐ 3 - ☐ 4 - ☐5 - ☐ 6 - ☐ Andere	☐

Opmerkingen / vragen: Uitbreiding van vorige risicoanalyse (KG/2010.0017) met chemische producten en een nieuwe uitvoerder (student)

Bezorg dit formulier aan uw VGM-antennecoördinator en leidinggevende . De VGM-antennecoördinator bezorgt deze melding aan de Dienst VGM indien producten van klasse E4 met vrijgave voorkomen.

DIENSTEN ALGEMEEN BEHEER
DIRECTIE STAFDIENSTEN ALGEMEEN BEHEER
DIENST VGM
W. DE CROYLAAN 58 – BUS 5530, BE-3001 LEUVEN
TEL. + 32 16 32 20 24 FAX + 32 16 32 29 95
WWW.KULEUVEN.BE/VGM vgm@kuleuven.be

KATHOLIEKE
UNIVERSITEIT
LEUVEN

MELDINGSFORMULIER:
RISICOANALYSE VOOR EXPERIMENT MET CHEMISCHE PRODUCTEN VAN RISICOKLASSE E3 EN E4

Vul het formulier elektronisch in, in overleg met het VGM-antennelid chemische veiligheid.

1. Identificatie van de afdeling (gebruikers)

Aanvrager/contactpersoon: Cédric Van Goethem, Rhea Verbeke
Tel: 016 37 93 43
E-mail adres: cedric.vangoethem@biw.kuleuven.be

Afdeling: COK
Magazijncode[1]: INB1
Leidinggevende : Prof. Vankelecom

2. Identificatie experiment

Titel(benaming): ECFP membranen (maximaal 40 karakters)
Startdatum: 27/11//2014 Geplande einddatum: 01/06/2017

☒ Het betreft een nieuw experiment
☐ Het betreft een bestaand experiment zonder eerder opgestelde risicoanalyse
☒ Het betreft een wijziging/uitbreiding van een bestaand experiment met eerder opgestelde risicoanalyse
Deze wijziging/uitbreiding betreft (gelieve aan te duiden en verder in het formulier te beschrijven):
☒ personen
☒ lokalen waar het experiment plaatsvindt
☒ chemische producten
☒ andere risico's
☐ verlenging
Dossiernummer of referentienummer vorig advies: KG/2010.0017 (indien gekend)

☒ Indien VGM-DOSSIER beschikbaar:
☒ experiment in het kader van een bestaande activiteit
Geef nummer van de activiteiten: deelactiviteit 2 in vorige risicoanalyse
☐ experiment in het kader van een nieuwe activiteit (in overleg met VGM-antenne en Afdelingshoofd[1])
Geef naam van de nieuwe activiteit voor het VGM-dossier: (max. 40 karakters)

☐ Doorloopproeven (**onbewaakt** experiment binnen of buiten de diensturen)

[1] https://admin.kuleuven.be/vgm/intranet/doc/antenne/antennemagazijncodes.xlsx/view

Beschrijving van al de aangewende(of gevormde) chemische producten*

Productnaam	**Casnummer**	**Fysische toestand** (gas/vloei-baar/vast)	**Aangewende hoeveelheid**	**Aangewende concentratie**	**Chemische risicoklasse product (E4/E3/E2/E1)**
1. n-hexaan	110-54-3	vloeibaar	250 ml	>99% : solvent for 6, 7 and 2	E3
2. 1,3,5-benzeentricarbonyltrichloride	4422-95-1	vast	0.25 g	0.1 wt/v%	E2
3. m-fenyleendiamine	108-45-2	vast	5g	2 wt/v%	E3
4. polysulfon	25154-01-2	vast	16.2 g	18 wt%	E1
5. N-methylpyrrolidon	872-50-4	vloeibaar	90 g	solvent for 4	E4
6. 2-propanol	67-63-0	vloeibaar	500 ml	solvent	E3
7. ZIF-8	/	vast	1 g	tot 0.4 wt% in 1	/
8.					
9.					
10.					

*** Indien mogelijk de zeer gevaarlijke producten of processen vervangen door minder gevaarlijke !**

Lokaalgegevens

Gebouw	**Lokaal**	**Omschrijving deelexperiment** (bv. voorbereiding, eigenlijk experiment, nabehandeling, meting, …)	**Specificaties lokaal**
LBI	03.95	1. Synthese steunlaag membranen	☒ eigen afdeling ☐ ruimte toegewezen aan andere afdeling*
LBI	03.95	2. Synthese composietmembraan (interfaciale polymerisatie)	☒ eigen afdeling ☐ ruimte toegewezen aan andere afdeling*
LBI	03.105	3. High-throughput filtratie-experimenten (metingen)	☒ eigen afdeling ☐ ruimte toegewezen aan andere afdeling*
		4.	☐ eigen afdeling ☐ ruimte toegewezen aan andere afdeling*
		5.	☐ eigen afdeling ☐ ruimte toegewezen aan andere afdeling*

* indien manipulaties worden uitgevoerd in een ruimte toegewezen aan een andere afdeling dan moet het meldingsformulier ook naar dit afdelingshoofd gestuurd worden (in kopie).

Personen die het experiment zullen uitvoeren of voor een practicum het toezichthoudend personeel

Naam - voornaam	**Geboorte-datum**	**Personeelsgroep**
Verbeke Rhea	**30/11/1992**	☐ KU ☒ Student KU ☐ UZ ☐ VIB ☐ Externen:
Van Goethem Cédric	**22/10/1991**	☒ KU ☒ Student KU ☐ UZ ☐ VIB ☐ Externen:
		☐ KU ☐ Student KU ☐ UZ ☐ VIB ☐ Externen:
		☐ KU ☐ Student KU ☐ UZ ☐ VIB ☐ Externen:
		☐ KU ☐ Student KU ☐ UZ ☐ VIB ☐ Externen:
		☐ KU ☐ Student KU ☐ UZ ☐ VIB ☐ Externen:
		☐ KU ☐ Student KU ☐ UZ ☐ VIB ☐ Externen:

		☐ KU ☐ Student KU ☐ UZ ☐ VIB ☐ Externen:
		☐ KU ☐ Student KU ☐ UZ ☐ VIB ☐ Externen:

3. Beschrijving experiment en risicoanalyse

Beschrijving handelingen en aangewende technieken:

Nummer* deel-experiment	**Beschrijving handelingen en technieken**	**Gebruikte uitrusting**	**Nummers ** gebruikte producten**
1	Afwegen, mengen, casten polymeeroplossing	Geijkte weegschaal, roerplaat, automatische filmapplicator	4,5
2	Afwegen, mengen, interfaciale polymerisatie	Geijkte weegschaal, roerplaat, glazen bekers	membraan uit deelexperiment 1; 2, 3
3	Voedingsmengsel en druk aanbrengen, filtreren	High-throughput filtratiemodule, stikstofleiding	membraan uit deelexperiment 2; 6-7
4			
5			

* Nummer van het deelexperiment zoals weergegeven onder “Lokaalgegevens”

** Nummer chemische producten zoals weergegeven onder “Beschrijving aangewende(of gevormde) chemische producten”

Frequentie uitvoering experiment:

- ☐ Dagelijks
- ☒ Wekelijks
- ☐ Maandelijks
- ☐ Minder dan maandelijks

Indien gewenst, kan u hier meer informatie over het experiment toevoegen (bv. reactieschema) of verwijzen naar een bijlage

Risico’s verbonden aan de chemische producten

Vóór het gebruik van de chemische producten dienen de gevaren, R- of H- en S of P-zinnen, gekend te zijn!

Op te zoeken in de KULeuven gevaarlijke stoffendatabank (via KULoket, algemeen, gevaarlijke stoffen) of op de veiligheidsinformatiebladen van de fabrikant.

Voor de producten van risicoklasse E3 en **E4** dienen de gevaren aangeduid te worden in onderstaande tabel.

Naam chemisch product	n-hexane	m-fenyleendiamine	N-methylpyrrolidon	2-methyl imidazool	dimethylformamide	
Explosie- en brandgevaar						
Zeer licht of licht ontvlambaar (**H220, H222,224, H228,** H225) / (R11**, R12**)	☒	☐	☐	☐	☐	☐
Ontvlambaar gas, aerosol, vaste stof(H221, H223**, H228**)	☐	☐	☐	☐	☐	☐

Ontvlambaar door zelfverhitting **(H251,H252)**	☐	☐	☐	☐	☐	☐
Brand, ontploffing met scherfwerking (H204, **H202**, **H203**), massa-explosie bij brand (H205)	☐	☐	☐	☐	☐	☐
Explosief (**EUH001, EUH006, H200, H201**) /(**R1,R2,R3**,R5) +brandb.stoffen (H271, H272)/(R9) + T↑(H240, H241), afgesloten en T↑ (EUH044) /(R44)	☐	☐	☐	☐	☐	☐
Ontvlamb damp/lucht mengsel (EUH018)	☐	☐	☐	☐	☐	☐
Ontplofbare peroxiden (EUH019)	☐	☐	☐	☐	☐	☐
Incompatibel met water (EUH014, H260) /(R14,R15)	☐	☐	☐	☐	☐	☐
Vat spontaan vlam in contact met lucht **(H250)**	☐	☐	☐	☐	☐	☐
Explosief + metalen (R4) + O2 **(R6**)	☐	☐	☐	☐	☐	☐
Incompatibel met oxiderende stoffen (R16)	☐	☐	☐	☐	☐	☐
Instabiel product (**R17**, R18, R19)	☐	☐	☐	☐	☐	☐
Acuut gevaar voor gezondheid						
Zeer giftig (**H300, H330, H310**) / (**R26, R27, R28**) + zuur (EUH032)/ (R32) Giftig (H311, H331, EUH070) / (R23, R24) + water (EUH029) / (R29) + zuur (EUH031) / (R31)	☐	☒	☒	☐	☐	☐
Ernstige brandwonden (H314) / (R35)	☐	☐	☐	☒	☐	☐
Gevaar voor gezondheid op langere termijn						
Kankerverwekkend of kanker niet uitgesloten (**H350, H350i, H351**) / (**R40, R45, R49**)	☐	☐	☐	☐	☐	☐
Teratogeen (H361d, **H360D**) / (**R61**, R63) en schade aan vruchtbaarheid (H361f, **H360F**) / (**R60**, R62) , beide (H361fd, **H360FD, H360Df**, **H360Fd)**	☒	☐	☐	☐	☒	☐
Mutageen (H341, **H340**) / (**R46**)	☐	☒	☐	☐	☐	☐
Schade aan bep organen (H371, H372, **H370**) bij herh of langd. blootstelling (H373)	☐	☐	☐	☐	☐	☐
Ernstige onherstelbare effecten (mogelijks) (R39, R68), Gezondheidsschade bij langdurige blootstelling (R48)	☒	☐	☐	☐	☐	☐

Bijkomende opmerkingen voor bepaalde producten:

Andere risico's verbonden aan het experiment

☐ Verbranden, bevriezen (☐ hoge of lage temperaturen, ☐ cryogene stoffen, …)
☐ Implosie, explosie (☐ hoge drukken, ☐ lage drukken, ☐ onderdruk, …)
☐ Brand (☐ ovens, ☐ verwarmingsspiralen, ☐ bunzenbrander, ☐ oliebaden …)
☐ Niet-ioniserende straling (☐ NMR, ☐ lasers, ☐ UV-lampen, ...)
☐ Elektrocutie (☐ naakte contacten, ☐ vochtige omgeving, ☐ hoge vermogens, ...)
☐ Valgevaar (☐ opstellingen op hoogte, ☐ in de hoogte, ☐ moeilijk bereikbaar, ...)
☐ Biologisch risico (☐ pathogene µ-organismen, ☐ GGO, ☐ cellen, ☐ bloed, ☐ proefdieren, ...)
☐ Ioniserende straling (X-stralen, radio-isotopen, ...)
☐ De kans bestaat dat bij een ernstig incident **NIET** zelfstandig alarm kan gegeven worden (bv. gebruik van zeer toxische dampen of gassen, explosierisico, aanwezigheid verstikkend gas, …)
☐Andere:

Voorzorgsmaatregelen toe te passen

Nummer Deelexperiment*	**1**	**2**	**3**	**4**	**5**
Collectieve beschermingsmiddelen					

- Gesloten systeem	☐	☐	☐	☐	☐
- Zuurkast(trekkast)	☒	☒	☒	☐	☐
- Plaatselijke afzuiging	☒	☒	☒	☐	☐
- Ruimtelijke afzuiging	☒	☒	☒	☐	☐
- Veiligheidsscherm	☐	☐	☐	☐	☐
- Opvangbakken onder opstelling	☐	☐	☐	☐	☐
- Andere:	☐	☐	☐	☐	☐
Individuele beschermingsmiddelen					
- Laboschort	☒	☒	☒	☐	☐
- Veiligheidsbril	veiligheidsbril (artnr. 18042)	veiligheidsbril (artnr. 18042)	veiligheidsbril (artnr. 18042)	veiligheidsbril (artnr. 18042)	veiligheidsbril (artnr. 18042)
- Handschoenen:	wegwerpnitrile EN 374 (artnr. 58951)	wegwerpnitrile EN 374 (artnr. 58951)	wegwerpnitrile EN 374 (artnr. 58951)	wegwerpnitrile EN 374 (artnr. 58951)	wegwerpnitrile EN 374 (artnr. 58951)
- Maskers:	Kies een item.	Kies een item.	Kies een item.	Kies een item.	Kies een item.
- Wegwerp hygiëne haarnetje	☐	☐	☐	☐	☐
- Andere:	☐	☐	☐	☐	☐

Specifieke preventiemaatregelen

☒ controle werking zuurkast
☐ controle glaswerk op barsten
☐ bevestigen spanringen aan koelslangen
☐ automatisch uitschakelen verwarmingssysteem bij defecte koeling
☐ overdrukbeveiligingssysteem
☐ brandblusser voor metaalbranden (D-blusser) aanwezig
☐ zuurstofkit aanwezig (verplicht bij het werken met cyaniden)
☐ detector met alarm bij werken met giftige of brandbare gassen
☐ aanwezigheid gasmasker met specifieke filters (interventie)
☐ aanwezigheid calciumgluconaatzalf (werken met waterstoffluoride)
☒ interventiekit aanwezig
☐ specifiek neutralisatieproduct aanwezig nl.
☐ invullen en opsturen formulier doorloopproeven (zie https://admin.kuleuven.be/vgm/intranet/AntenneDoorloopproeven.html)
☐ aanwezigheid van een 2de persoon in de buurt vereist
☐ automatisch alarmsysteem (bv. dodemansalarm)
Andere:

Werkpraktijken

☒ Toepassen Code Goede Laboratoriumpraktijk https://admin.kuleuven.be/vgm/intranet/ChemischeVeiligheidCodeGoedeLabopraktijken.html)
☐ Interne opleiding en begeleiding
☒ Selectieve inzameling afval – chemisch afval

Bijzondere maatregelen bij storing/falen: beschrijf hoe een noodgeval wordt opgevangen (denk o.a. aan stroomuitval, ventilatie-uitval, uitval watertoevoer, uitval perslucht, uitval gastoevoer, …)

* Nummer van het deelexperiment zoals weergegeven onder “Lokaalgegevens”

Indien niet alle voorzorgsmaatregelen toegepast kunnen worden, mag het experiment niet starten!
Persoonlijke beschermingsmiddelen kunnen verkregen worden via het aanvraagformulier (https://admin.kuleuven.be/vgm/intranet/doc/personen/personenfaanvraagpbm.docx).

Chemisch afval
Per afvalfractie de categorie van het chemisch afval aangeven.

KATHOLIEKE
UNIVERSITEIT
LEUVEN

Afvalfractie	Afvalcategorie	Recipiënt aanwezig
Indien zuivere stoffen:		
9	☐1 - ☐2 - ☒ 3 - ☐ 4 - ☐5 - ☐ 6 - ☐ Andere	☒
1	☐1 - ☐2 - ☒ 3 - ☐ 4 - ☐5 - ☐ 6 - ☐ Andere	☒
	☐1 - ☐2 - ☐ 3 - ☐ 4 - ☐5 - ☐ 6 - ☐ Andere	☐
	☐1 - ☐2 - ☐ 3 - ☐ 4 - ☐5 - ☐ 6 - ☐ Andere	☐
	☐1 - ☐2 - ☐ 3 - ☐ 4 - ☐5 - ☐ 6 - ☐ Andere	☐
	☐1 - ☐2 - ☐ 3 - ☐ 4 - ☐5 - ☐ 6 - ☐ Andere	☐
Indien mengsels:		
Hoofdcomponent :1 met 2	☐1 - ☐2 - ☐ 3 - ☒ 4 - ☐5 - ☐ 6 - ☐ Andere	☒
Hoofdcomponent :3 met water	☐1 - ☐2 - ☐ 3 - ☐ 4 - ☐5 - ☐ 6 - ☒ Andereamines	☒
Hoofdcomponent :1 met 3	☐1 - ☐2 - ☒ 3 - ☐ 4 - ☐5 - ☐ 6 - ☒ Andereamines	☒
Hoofdcomponent : met	☐1 - ☐2 - ☐ 3 - ☐ 4 - ☐5 - ☐ 6 - ☐ Andere	☐
Hoofdcomponent : met	☐1 - ☐2 - ☐ 3 - ☐ 4 - ☐5 - ☐ 6 - ☐ Andere	☐
Hoofdcomponent : met	☐1 - ☐2 - ☐ 3 - ☐ 4 - ☐5 - ☐ 6 - ☐ Andere	☐
Andere:		
	☐1 - ☐2 - ☐ 3 - ☐ 4 - ☐5 - ☐ 6 - ☐ Andere	☐
	☐1 - ☐2 - ☐ 3 - ☐ 4 - ☐5 - ☐ 6 - ☐ Andere	☐

Opmerkingen / vragen:

Bezorg dit formulier aan uw VGM-antennecoördinator en leidinggevende .
De VGM-antennecoördinator bezorgt deze melding aan de Dienst VGM indien producten van klasse E4 met vrijgave voorkomen.

Advies Dienst VGM

DIENSTEN ALGEMEEN BEHEER
DIRECTIE STAFDIENSTEN ALGEMEEN BEHEER
DIENST VGM
W. DE CROYLAAN 58 – BUS 5530, BE-3001 LEUVEN
TEL. + 32 16 32 20 24 FAX + 32 16 32 29 95
WWW.KULEUVEN.BE/VGM vgm@kuleuven.be

KATHOLIEKE
UNIVERSITEIT
LEUVEN

MELDINGSFORMULIER:
RISICOANALYSE VOOR EXPERIMENT MET CHEMISCHE PRODUCTEN VAN RISICOKLASSE E3 EN E4

Vul het formulier elektronisch in, in overleg met het VGM-antennelid chemische veiligheid.

1. Identificatie van de afdeling (gebruikers)

Aanvrager/contactpersoon: Cédric Van Goethem, Rhea Verbeke
Tel: 0472 467 465
E-mail adres: cedric.vangoethem@biw.kuleuven.be

Afdeling: COK
Magazijncode[1]: INB1
Leidinggevende : Prof. Ivo Vankelecom

2. Identificatie experiment

Titel(benaming): Polyimide membrane functionalization (maximaal 40 karakters)
Startdatum: 17 nov 2014 Geplande einddatum: 31 jun 2014

☒ Het betreft een nieuw experiment
☐ Het betreft een bestaand experiment zonder eerder opgestelde risicoanalyse
☐ Het betreft een wijziging/uitbreiding van een bestaand experiment met eerder opgestelde risicoanalyse
Deze wijziging/uitbreiding betreft (gelieve aan te duiden en verder in het formulier te beschrijven):
- ☐ personen
- ☐ lokalen waar het experiment plaatsvindt
- ☐ chemische producten
- ☐ andere risico's
- ☐ verlenging

Dossiernummer of referentienummer vorig advies: ☐ (indien gekend)

☐ Indien VGM-DOSSIER beschikbaar:
- ☐ experiment in het kader van een bestaande activiteit
  Geef nummer van de activiteiten:
- ☐ experiment in het kader van een nieuwe activiteit (in overleg met VGM-antenne en Afdelingshoofd[1])
  Geef naam van de nieuwe activiteit voor het VGM-dossier: (max. 40 karakters)

☐ Doorloopproeven (**onbewaakt** experiment binnen of buiten de diensturen)

[1] https://admin.kuleuven.be/vgm/intranet/doc/antenne/antennemagazijncodes.xlsx/view

Beschrijving van al de aangewende(of gevormde) chemische producten*

Productnaam	**Casnummer**	**Fysische toestand** (gas/vloei-baar/vast)	**Aangewende hoeveelheid**	**Aangewende concentratie**	**Chemische risicoklasse product (E4/E3/E2/E1)**
1. methanol	67-56-1	vloeibaar	50ml	solvent for 2 and 3	E4
2. 4-aminobenzoëzuur	150-13-0	vast	2.5g	2.5 wt/v%	E1
3. 6-aminohexaanzuur	60-32-2	vast	2.5g	2.5 wt/v%	unknown, E1 based on similar risks and H/P numbers as for chemical 2 (based on manufacturer MSDS)
4. Tri-ethylamine	121-24-8	vloeibaar	1.25 g	5 wt/v%	E3
5.					
6.					
7.					
8.					
9.					
10.					

*** Indien mogelijk de zeer gevaarlijke producten of processen vervangen door minder gevaarlijke !**

Lokaalgegevens

Gebouw	**Lokaal**	**Omschrijving deelexperiment** (bv. voorbereiding, eigenlijk experiment, nabehandeling, meting, …)	**Specificaties lokaal**
LBI	03.95	1. voorbereiding en experiment	☒ eigen afdeling ☐ ruimte toegewezen aan andere afdeling*
		2.	☐ eigen afdeling ☐ ruimte toegewezen aan andere afdeling*
		3.	☐ eigen afdeling ☐ ruimte toegewezen aan andere afdeling*
		4.	☐ eigen afdeling ☐ ruimte toegewezen aan andere afdeling*
		5.	☐ eigen afdeling ☐ ruimte toegewezen aan andere afdeling*

* indien manipulaties worden uitgevoerd in een ruimte toegewezen aan een andere afdeling dan moet het meldingsformulier ook naar dit afdelingshoofd gestuurd worden (in kopie).

Personen die het experiment zullen uitvoeren of voor een practicum het toezichthoudend personeel

Naam - voornaam	**Geboorte-datum**	**Personeelsgroep**
Van Goethem Cédric	**22-10-1991**	☒ KU ☐ Student KU ☐ UZ ☐ VIB ☐ Externen:
Verbeke Rhea	**30-11-1992**	☐ KU ☒ Student KU ☐ UZ ☐ VIB ☐ Externen:
		☐ KU ☐ Student KU ☐ UZ ☐ VIB ☐ Externen:
		☐ KU ☐ Student KU ☐ UZ ☐ VIB ☐ Externen:

		☐ KU ☐ Student KU ☐ UZ ☐ VIB ☐ Externen:
		☐ KU ☐ Student KU ☐ UZ ☐ VIB ☐ Externen:
		☐ KU ☐ Student KU ☐ UZ ☐ VIB ☐ Externen:
		☐ KU ☐ Student KU ☐ UZ ☐ VIB ☐ Externen:
		☐ KU ☐ Student KU ☐ UZ ☐ VIB ☐ Externen:

3. Beschrijving experiment en risicoanalyse

Beschrijving handelingen en aangewende technieken:

Nummer* deel-experiment	**Beschrijving handelingen en technieken**	**Gebruikte uitrusting**	**Nummers ** gebruikte producten**
1	afwegen, mengen, immersie in oplossing van 2/3/4 in 1	Geijkte weegschaal,	1,2,3
2			
3			
4			
5			

* Nummer van het deelexperiment zoals weergegeven onder "Lokaalgegevens"

** Nummer chemische producten zoals weergegeven onder "Beschrijving aangewende(of gevormde) chemische producten"

Frequentie uitvoering experiment:

- ☐ Dagelijks
- ☐ Wekelijks
- ☒ Maandelijks
- ☐ Minder dan maandelijks

Indien gewenst, kan u hier meer informatie over het experiment toevoegen (bv. reactieschema) of verwijzen naar een bijlage

Risico's verbonden aan de chemische producten

Vóór het gebruik van de chemische producten dienen de gevaren, R- of H- en S of P-zinnen, gekend te zijn!

Op te zoeken in de KULeuven gevaarlijke stoffendatabank (via KULoket, algemeen, gevaarlijke stoffen) of op de veiligheidsinformatiebladen van de fabrikant.

Voor de producten van risicoklasse E3 en **E4** dienen de gevaren aangeduid te worden in onderstaande tabel.

Naam chemisch product	methanol	triethylamine				
Explosie- en brandgevaar						
Zeer licht of licht ontvlambaar (**H220, H222,224, H228,** H225) / (R11**, R12**)	☒	☒	☐	☐	☐	☐
Ontvlambaar gas, aerosol, vaste stof(H221, H223**, H228**)	☐	☐	☐	☐	☐	☐
Ontvlambaar door zelfverhitting **(H251,H252)**	☐	☐	☐	☐	☐	☐
Brand, ontploffing met scherfwerking (H204, **H202**, **H203**), massa-explosie bij brand (H205)	☐	☐	☐	☐	☐	☐
Explosief (**EUH001, EUH006, H200, H201**) /(**R1,R2,R3**,R5) +brandb.stoffen (H271, H272)/(R9) + T↑(H240, H241), afgesloten en T↑ (EUH044) /(R44)	☐	☐	☐	☐	☐	☐
Ontvlamb damp/lucht mengsel (EUH018)	☐	☐	☐	☐	☐	☐

Ontplofbare peroxiden (EUH019)	☐	☐	☐	☐	☐	☐
Incompatibel met water (EUH014, H260) /(R14,R15)	☐	☐	☐	☐	☐	☐
Vat spontaan vlam in contact met lucht **(H250)**	☐	☐	☐	☐	☐	☐
Explosief + metalen (R4) + O2 **(R6**)	☐	☐	☐	☐	☐	☐
Incompatibel met oxiderende stoffen (R16)	☐	☐	☐	☐	☐	☐
Instabiel product (**R17**, R18, R19)	☐	☐	☐	☐	☐	☐
Acuut gevaar voor gezondheid						
Zeer giftig (**H300, H330, H310**) / (**R26, R27, R28**) + zuur (EUH032)/ (R32) Giftig (H311, H331, EUH070) / (R23, R24) + water (EUH029) / (R29) + zuur (EUH031) / (R31)	☒	☒	☐	☐	☐	☐
Ernstige brandwonden (H314) / (R35)	☐	☒	☐	☐	☐	☐
Gevaar voor gezondheid op langere termijn						
Kankerverwekkend of kanker niet uitgesloten (**H350, H350i, H351**) / (**R40, R45, R49**)	☐	☐	☐	☐	☐	☐
Teratogeen (H361d, **H360D**) / (**R61**, R63) en schade aan vruchtbaarheid (H361f, **H360F**) / (**R60**, R62) , beide (H361fd, **H360FD, H360Df**, **H360Fd)**	☐	☐	☐	☐	☐	☐
Mutageen (H341, **H340**) / (**R46**)	☐	☐	☐	☐	☐	☐
Schade aan bep organen (H371, H372, **H370**) bij herh of langd. blootstelling (H373)	☒	☐	☐	☐	☐	☐
Ernstige onherstelbare effecten (mogelijks) (R39, R68), Gezondheidsschade bij langdurige blootstelling (R48)	☐	☐	☐	☐	☐	☐

Bijkomende opmerkingen voor bepaalde producten:

Andere risico's verbonden aan het experiment

☐ Verbranden, bevriezen (☐ hoge of lage temperaturen, ☐ cryogene stoffen, …)
☐ Implosie, explosie (☐ hoge drukken, ☐ lage drukken, ☐ onderdruk, …)
☐ Brand (☐ ovens, ☐ verwarmingsspiralen, ☐ bunzenbrander, ☐ oliebaden …)
☐ Niet-ioniserende straling (☐ NMR, ☐ lasers, ☐ UV-lampen, ...)
☐ Elektrocutie (☐ naakte contacten, ☐ vochtige omgeving, ☐ hoge vermogens, ...)
☐ Valgevaar (☐ opstellingen op hoogte, ☐ in de hoogte, ☐ moeilijk bereikbaar, ...)
☐ Biologisch risico (☐ pathogene µ-organismen, ☐ GGO, ☐ cellen, ☐ bloed, ☐ proefdieren, ...)
☐ Ioniserende straling (X-stralen, radio-isotopen, ...)
☐ De kans bestaat dat bij een ernstig incident **NIET** zelfstandig alarm kan gegeven worden (bv. gebruik van zeer toxische dampen of gassen, explosierisico, aanwezigheid verstikkend gas, …)
☐Andere:

Voorzorgsmaatregelen toe te passen

Nummer Deelexperiment*	**1**	**2**	**3**	**4**	**5**
Collectieve beschermingsmiddelen					
- Gesloten systeem	☐	☐	☐	☐	☐
- Zuurkast(trekkast)	☒	☐	☐	☐	☐
- Plaatselijke afzuiging	☐	☐	☐	☐	☐
- Ruimtelijke afzuiging	☐	☐	☐	☐	☐
- Veiligheidsscherm	☐	☐	☐	☐	☐
- Opvangbakken onder opstelling	☐	☐	☐	☐	☐
- Andere:	☐	☐	☐	☐	☐

Individuele beschermingsmiddelen

- Laboschort	☒	☐	☐	☐	☐
- Veiligheidsbril	veiligheidsbril (artnr. 18042)	Kies een item.	Kies een item.	Kies een item.	Kies een item.
- Handschoenen:	wegwerpnitrile EN 374 (artnr. 58951)	Kies een item.	Kies een item.	Kies een item.	Kies een item.
- Maskers:	Kies een item.	Kies een item.	Kies een item.	Kies een item.	Kies een item.
- Wegwerp hygiëne haarnetje	☐	☐	☐	☐	☐
- Andere:	☐	☐	☐	☐	☐

Specifieke preventiemaatregelen

- ☒ controle werking zuurkast
- ☐ controle glaswerk op barsten
- ☐ bevestigen spanringen aan koelslangen
- ☐ automatisch uitschakelen verwarmingssysteem bij defecte koeling
- ☐ overdrukbeveiligingssysteem
- ☐ brandblusser voor metaalbranden (D-blusser) aanwezig
- ☐ zuurstofkit aanwezig (verplicht bij het werken met cyaniden)
- ☐ detector met alarm bij werken met giftige of brandbare gassen
- ☐ aanwezigheid gasmasker met specifieke filters (interventie)
- ☐ aanwezigheid calciumgluconaatzalf (werken met waterstoffluoride)
- ☒ interventiekit aanwezig
- ☐ specifiek neutralisatieproduct aanwezig nl.
- ☐ invullen en opsturen formulier doorloopproeven (zie https://admin.kuleuven.be/vgm/intranet/AntenneDoorloopproeven.html)
- ☐ aanwezigheid van een 2de persoon in de buurt vereist
- ☐ automatisch alarmsysteem (bv. dodemansalarm)

Andere:

Werkpraktijken

- ☒ Toepassen Code Goede Laboratoriumpraktijk https://admin.kuleuven.be/vgm/intranet/ChemischeVeiligheidCodeGoedeLabopraktijken.html)
- ☐ Interne opleiding en begeleiding
- ☒ Selectieve inzameling afval – chemisch afval

Bijzondere maatregelen bij storing/falen: beschrijf hoe een noodgeval wordt opgevangen (denk o.a. aan stroomuitval, ventilatie-uitval, uitval watertoevoer, uitval perslucht, uitval gastoevoer, …)
In geval van een ventillatie-uitval mag de fles met de aminozuur in MeOH oplossing in geen geval geopend worden tot de ventillatie terug hersteld is.

* Nummer van het deelexperiment zoals weergegeven onder “Lokaalgegevens”

Indien niet alle voorzorgsmaatregelen toegepast kunnen worden, mag het experiment niet starten!
Persoonlijke beschermingsmiddelen kunnen verkregen worden via het aanvraagformulier (https://admin.kuleuven.be/vgm/intranet/doc/personen/personenfaanvraagpbm.docx).

Chemisch afval
Per afvalfractie de categorie van het chemisch afval aangeven.

KATHOLIEKE
UNIVERSITEIT
LEUVEN

Afvalfractie	**Afvalcategorie**	**Recipiënt aanwezig**
Indien zuivere stoffen:		
	☐1 - ☐2 - ☐ 3 - ☐ 4 - ☐5 - ☐ 6 - ☐ Andere	☐
	☐1 - ☐2 - ☐ 3 - ☐ 4 - ☐5 - ☐ 6 - ☐ Andere	☐
	☐1 - ☐2 - ☐ 3 - ☐ 4 - ☐5 - ☐ 6 - ☐ Andere	☐
	☐1 - ☐2 - ☐ 3 - ☐ 4 - ☐5 - ☐ 6 - ☐ Andere	☐
	☐1 - ☐2 - ☐ 3 - ☐ 4 - ☐5 - ☐ 6 - ☐ Andere	☐
	☐1 - ☐2 - ☐ 3 - ☐ 4 - ☐5 - ☐ 6 - ☐ Andere	☐
Indien mengsels:		
Hoofdcomponent :1 met 2	☐1 - ☐2 - ☐ 3 - ☐ 4 - ☒5 - ☐ 6 - ☐ Andere	☒
Hoofdcomponent :1 met 3	☐1 - ☐2 - ☐ 3 - ☐ 4 - ☒5 - ☐ 6 - ☐ Andere	☒
Hoofdcomponent :1 met 2/3 +4	☐1 - ☐2 - ☐ 3 - ☐ 4 - ☐5 - ☐ 6 - ☒ AndereAmines	☒
Hoofdcomponent : met	☐1 - ☐2 - ☐ 3 - ☐ 4 - ☐5 - ☐ 6 - ☐ Andere	☐
Hoofdcomponent : met	☐1 - ☐2 - ☐ 3 - ☐ 4 - ☐5 - ☐ 6 - ☐ Andere	☐
Hoofdcomponent : met	☐1 - ☐2 - ☐ 3 - ☐ 4 - ☐5 - ☐ 6 - ☐ Andere	☐
Andere:		
	☐1 - ☐2 - ☐ 3 - ☐ 4 - ☐5 - ☐ 6 - ☐ Andere	☐
	☐1 - ☐2 - ☐ 3 - ☐ 4 - ☐5 - ☐ 6 - ☐ Andere	☐

Opmerkingen / vragen:

Bezorg dit formulier aan uw VGM-antennecoördinator en leidinggevende .
De VGM-antennecoördinator bezorgt deze melding aan de Dienst VGM indien producten van klasse E4 met vrijgave voorkomen.

Advies Dienst VGM